Study of HVDC Transmission Based Grid for Green Energy Harvesting

THESIS

Submitted in partial fulfilment

of the requirements for the degree of

DOCTOR OF PHILOSOPHY

by

HARIPRIYA T.

ID No. 2011PHXF0430H

Under the Supervision of

Prof. Alivelu M. Parimi

BIRLA INSTITUTE OF TECHNOLOGY AND SCIENCE, PILANI

2018

BIRLA INSTITUTE OF TECHNOLOGY AND SCIENCE, PILANI

CERTIFICATE

This is to certify that the thesis entitled, **Study of HVDC Transmission Based Grid for Green Energy Harvesting** submitted by **HARIPRIYA T.** ID.No **2011PHXF0430H** for award of Ph.D. of the institute embodies original work done by her under my supervision.

Signature of the Supervisor

Dr. ALIVELU M. PARIMI
Associate Professor, Dept. of EEE,
BITS-Pilani, Hyderabad Campus

Date:

Acknowledgements

As I am reaching the end of a long journey with ups and downs, I wish to acknowledge the remarkable individuals who stood with me in my ups and downs. I want to give thanks to God for sustaining me and guiding me through this arduous journey.

At an outset, I would like to express my deep sense of gratitude and thanks to **Prof. Alivelu M. Parimi,** Associate Professor, Department of Electrical Engineering, BITS, Pilani-Hyderabad Campus, my thesis supervisor. I will always be indebted to her for her valuable guidance, constant encouragement and moral support. It has been a privilege for me to work under her valuable guidance.

I owe special thanks to my Doctoral Advisory Committee members, **Prof. BVVSN Prabhakar Rao**, **Prof. Sanket Goel, Prof. Y Yoganandam and Prof. Bhuvaneswari** for their inspiring support and invaluable scientific suggestions from time to time. They always extended helpful hands towards me whenever I needed them.

I express my sincere thanks to **Prof. U.M. Rao** for his guidance and support. I am thankful to **Dr. Prasant Kumar Pattnaik,** DRC Convener for his support. I am thankful to all the faculty members of Department of Electrical Engineering, BITS Pilani, Hyderabad campus for their kind help and encouragement in carrying out my research work. Constant moral support extended to me by my friends and well wishers are gratefully acknowledged.

I am grateful to **Prof. Souvik Bhattacharya**, Vice Chancellor, BITS, Pilani for permitting me to pursue research work in the institute. I would like to thank **Prof. G. Sundar,** Director, BITS-Pilani, Hyderabad Campus for providing necessary infrastructure and support.

Words are inadequate to express my thanks to my parents **Prof. T.Narayana** and **Smt. T. Lakshmi Devi** for all their love, support and constant encouragement when I was irritable and depressed. I would like to thank my sister, **Ms. T.Chandrakala** and brother, **Mr. T.Y.Vamsi Krishna** for their constant love and support.

I am greatly indebted to my husband **Dr. Sabapathy Sankarpandi** for his moral support, understanding and co-operation throughout the period of this work. My heartfelt regards goes to

my father in law and my mother in law, **Sh. Sankar Pandi S** and **Smt. Raghupathy S** for their love and support.

I owe special thanks to Management, Principal, Head of EEE Department and all faculty members of **VNRVJIET** for their support during my work.

I would like to thank all those who helped me in my myriad ways throughout the course of this work.

Haripriya T.

ABSTRACT

Renewable energies are making a strong foothold to fulfil rapidly growing energy demands in this decade. In recent years, large solar farms, onshore and offshore wind farms are widely injecting power into AC grids. Local small PV power agents and wind turbines on these farms will create frequency deviations leading to operational instability, if there is inefficient coordinated control strategy. In addition to its technical challenges like control and compensation of active and reactive power, voltage instability, poor power quality and storage issues etc., are being faced during AC grid integration. To overcome these issues PV and wind farm outputs are connected to a DC grid using high voltage DC transmission.

The main differences between AC and DC system result from the fact that in DC there is no reactive current, reactive power, frequency and phase angle. The attractiveness of DC transmission increases further due to the reasons like; 1) remote location of hydro, solar and wind farms from urban centers makes the DC transmission more flexible than AC, 2) DC power generation of renewable energy sources (RES) like solar and fuel cells make DC transmission and utilization more efficient than AC due to the improved conversion efficiency of DC-DC converters over inverters, 3) rapid growth in power electronics technology lead to fall in prices with improved power ratings. Due to these reasons DC grid integration is becoming attractive for renewable energy sources.

To integrate RES to DC grid efficiently many architecture topologies are proposed in the literature. A new topology for integrating RES like solar and wind to the high voltage DC grid is proposed in this work. The proposed DC grid-connected model is economical, efficient, reliable in its operation and simple in its construction due to reduced size and weight of the DC conductor and simple paralleling procedures. While integrating RES to DC grid DC-DC boost converters are

needed. The performance of boost converter in open loop and closed loop operation is studied using small signal mathematical modelling. The influence of change in load on the converter performance is examined. To step up the voltage from low voltage to medium voltage and medium to high voltage, multilevel boost converter (MLBC) and LCL boost converter are chosen. A comparative study is performed between two medium voltage DC-DC converters namely transformer less high gain boost converter and MLBC.

Few major challenges faced by RES during DC grid integration are unpredictable input due to the dependency on weather conditions, voltage imbalance due to grid side disturbances and influence of grid side faults on to the DC link. To overcome this problem hybrid controller is proposed, it aids in extracting the maximum power operating point from PV and wind in addition to achieving stable DC output according to grid requirements. The hybrid controller proposed here consists of random dearch method (RSM) based MPPT controller along with voltage droop controller which uses RSM based two loop average current control technique. The MPPT controller helps in harnessing the maximum power at varying weather conditions whereas the voltage controller helps in reducing the distortion in output voltage. The voltage droop controller has inner current control loop and outer voltage control loop, considering both grid side and input side perturbations.

RSM method is chosen here for the design of controllers, as it has simple computational steps, derivative free, guarantees global convergence and requires less memory. The performance of the proposed system is studied in continuous conduction mode. A comparative study is performed among different MPPT techniques like incremental conductance, perturb and observe fuzzy logic and random search methods to determine the efficient MPP tracker. Likewise, the performance of the proposed RSM based two loop average current controller is compared with linear Proportional and Integral controller to evaluate its droop control action. The proposed

voltage controller is able to generate stable DC output according to the grid requirement without any delay or deviation from its referred value.

Different configurations are proposed to integrate solar photo voltaic installations to DC grid. The performance of the proposed configurations is evaluated under different combinations of input and output variations. The stability of TLAC controlled DC-DC boost converter is evaluated.

The performance of proposed topology, integrating solar PV and wind farms to high voltage DC grid using hybrid controller is evaluated. The specifications of the proposed topology are attained using Nanhui wind project, in China. The hybrid controller used here extracts the maximum power operating point from PV and wind in addition to achieving stable DC output voltage at low voltage DC grid. To maintain constant voltage in HVDC link during unsymmetrical faults on the AC grid side and also to satisfy grid codes an efficient fault ride through (FRT) protection scheme is implemented using chopper protection circuit. Simulation studies are performed to demonstrate the performance of the proposed configuration under varying weather conditions and grid side disturbances, using MATLAB/ Simulink.

Contents

List of Figures

List of Tables

Abbreviations

AC	Alternating Current
DC	Direct Current
DG	Distributed Generation
DER	Distributed Energy Resources
GTO	Gate Turn Off
RES	Renewable Energy Source
IGBT	Insulated Gate Bipolar Transistor
MOSFET	Metal Oxide Semiconductor Field Effect Transistor
PI	Proportional Integral
PV	Photo Voltaic
PMSG	Permanent Magnet Synchronous Generator
DFIG	Double Fed Induction Generator
PWM	Pulse Width Modulation
RES	Renewable Energy Sources
VSC	Voltage Source Converter
MLBC	Multilevel Boost Converter
TFHBC	Transformerless High Gain Boost Converter
WECS	Wind Energy Conversion System
MPPT	Maximum Power Point Tracking
P&O	Perturb and Observe
IC	Incremental Conductance

ANN	Artificial Neural Network
FLC	Fuzzy Logic Control
RSM	Random Search Method
TLAC	Two Loop Average Current Controller
HVDC	High Voltage Direct Current
MG	Micro Grid
FRT	Fault Ride Through

CHAPTER-1

Introduction

This chapter describes background of the problem, motivation of the work, followed by objectives and the outline of the thesis**.**

1.1. Background of Study

The world today is facing environmental, economic and political consequences due to increase in the dependency on fossil fuels that lead to search for alternative sources of energy production. Energy generation using renewable energy sources (RES) is becoming prevalent due to their larger time horizon and environmental concerns. Increase in air pollution; fall in the prices due to rapid growth in renewable energy technologies; long term energy security and commitment to international bodies has lead to the growth in renewable energy sources, [1].

The overall share of renewable energy sources in total energy consumption is shown in Fig. 1.1, [2]. Despite the enormous growth in the renewable energy sector, there is a moderate change in the share of RES as shown in Fig.1.2. A major reason for this is the persistent growth in overall energy demand that counter acts the forward momentum of renewable energy technologies. By the end of the year 2016, RES has contributed to an estimated 30% of the world's power generating capacity that could supply an estimated 24.5% of global electricity demand, with hydropower providing about 16.6%.

Globally, approximately 5.9 TWh of modern renewable energy was produced, which includes hydropower, solar, wind, geothermal and modern biofuel production in 2016, as shown in Fig. 1.2, [3]. This represents a 5 to 6-fold increase since the 1960s.

From the figure it is observed that almost 70 percent of renewable energy consumption is from hydropower. Despite absolute growth in energy production, the share of hydropower is declining in comparison with other renewable energy technologies like solar and wind. Due to the increase in renewable energy technology and decrease in manufacturing cost as shown in Fig. 1.3 and 1.4 there is an increase in growth rate of solar and wind power generation.

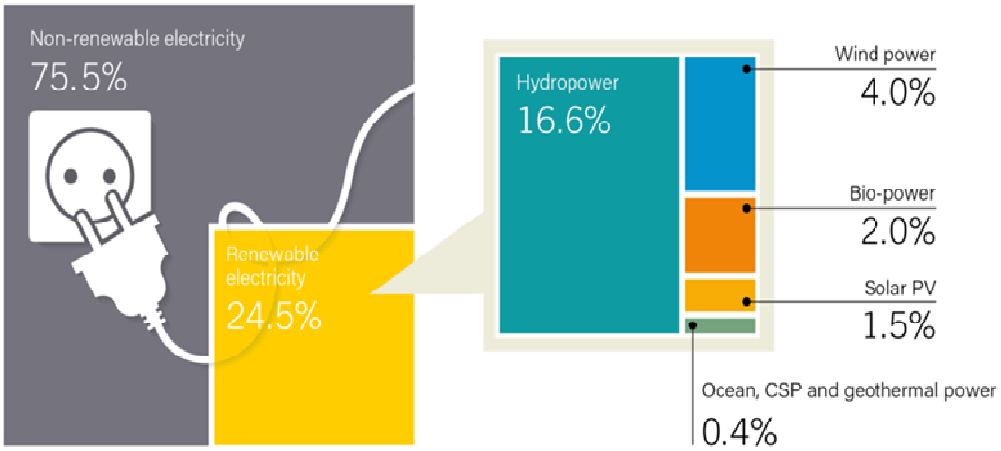

Fig.1.1: Share of renewable energy in global electricity production in 2017, Renewable 2017 Global Status Report [2]

Fig. 1.5 shows the cumulative installed capacity of wind energy all over the world over the past 50 years. The installed capacity of wind and its consumption rate in few major countries are shown in Fig. 1.6 and 1.7. From the projected data, it is observed that there is a tremendous growth in the utilization of wind energy all over the world, in particularly developing countries, where the growth rate is higher.

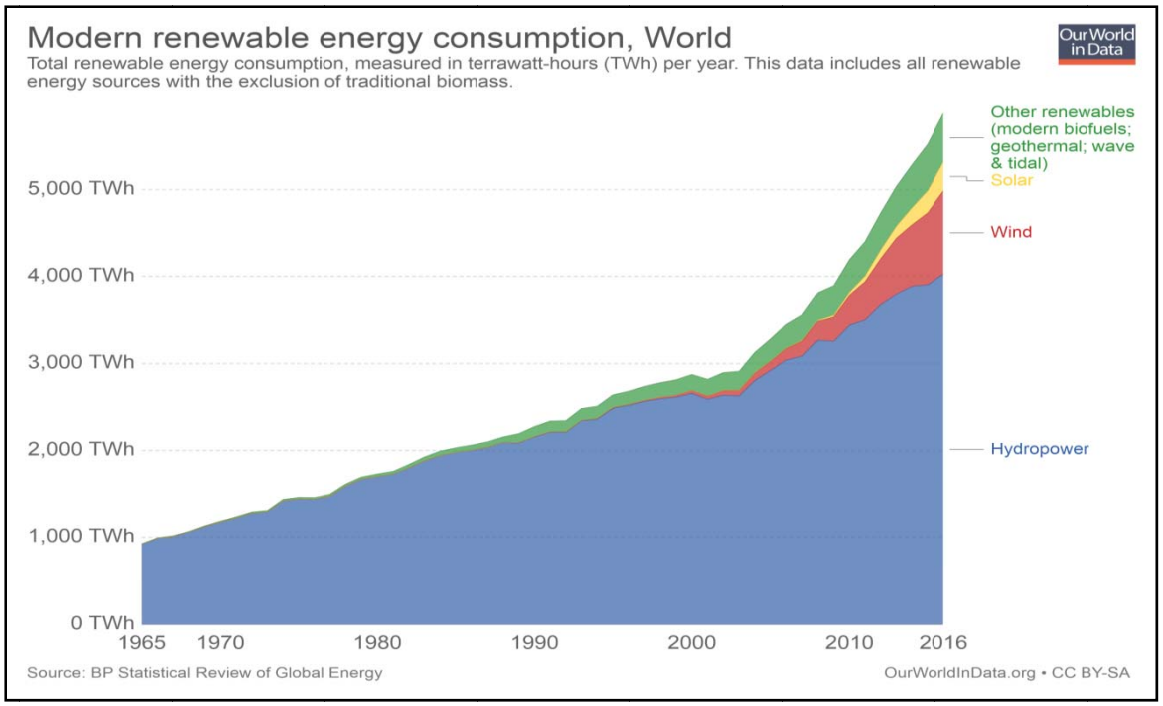

Fig.1. 2: Modern renewable energy consumption for past 50 years, Renewables report 2018 [3]

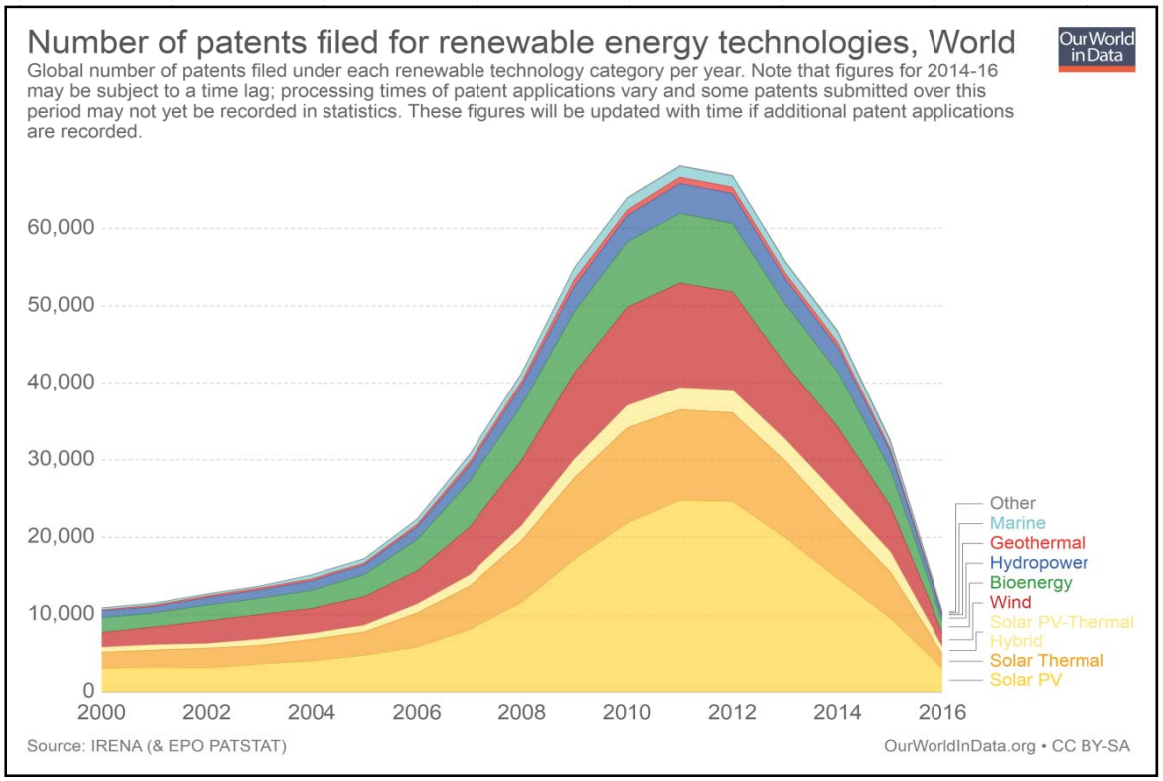

Fig.1. 3: Patents filed, Renewables report 2018 [3]

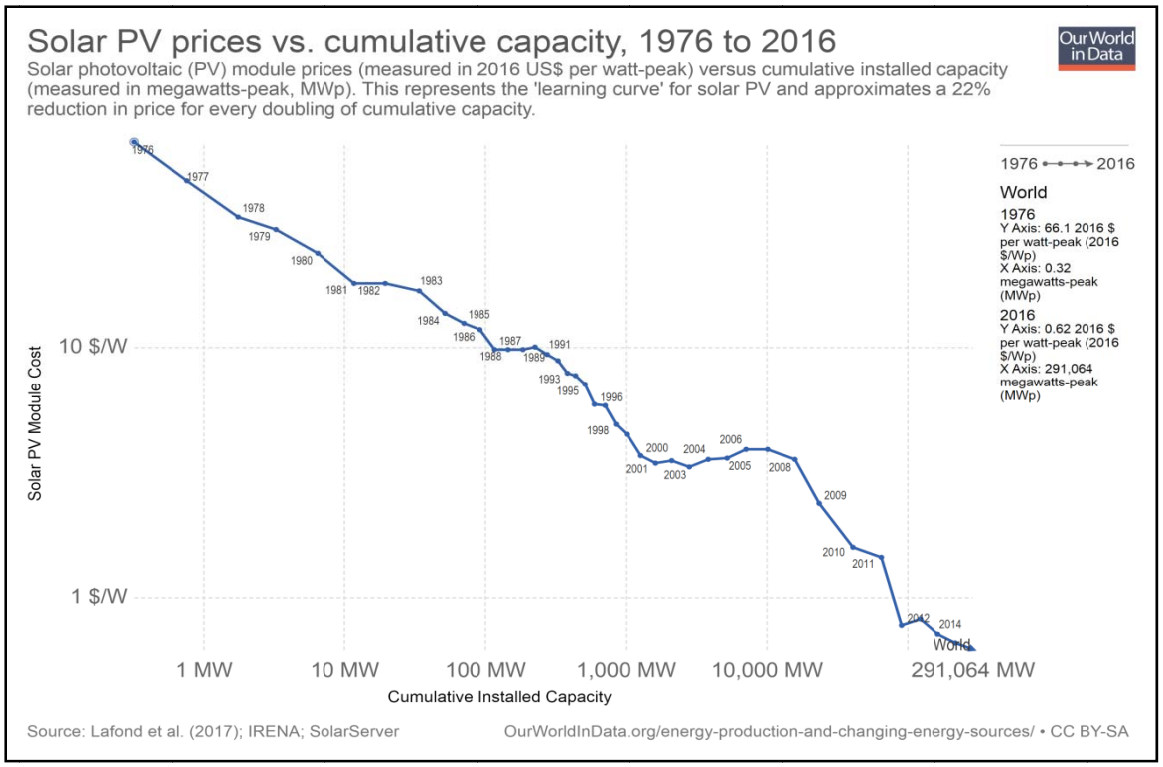

Fig.1. 4: Solar PV module cost versus cumulative installed capacity, Renewables report 2018 [3]

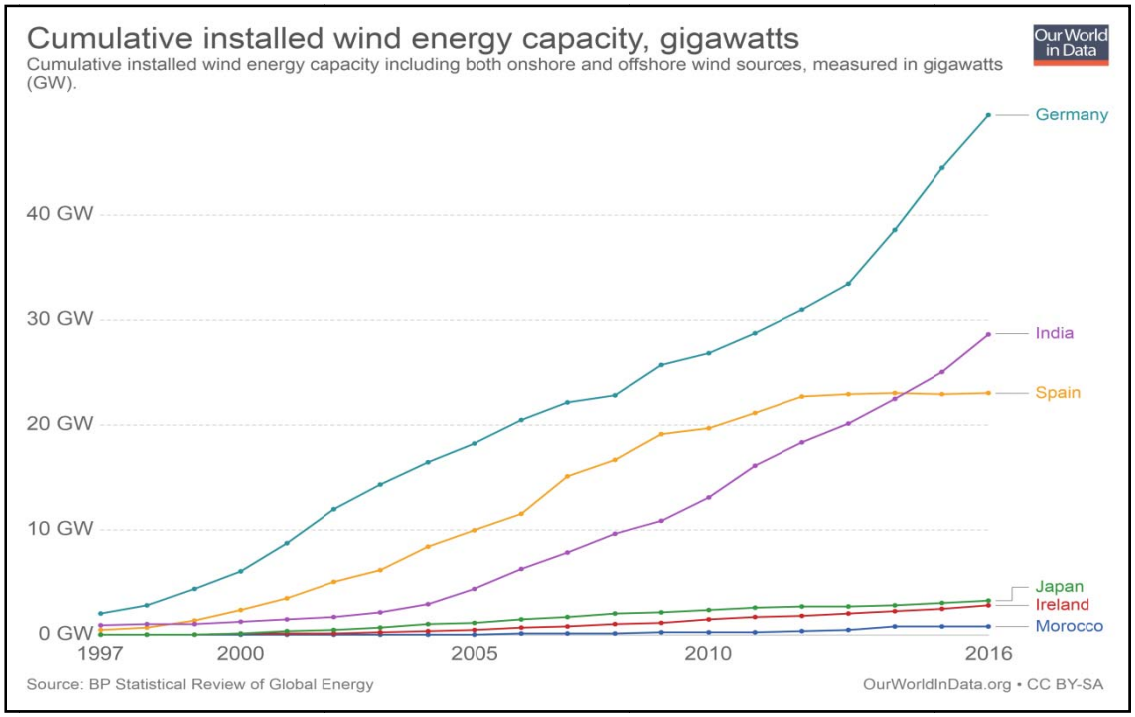

Fig.1. 5: Cumulative Installed wind energy capacity, Renewables report 2018 [3]

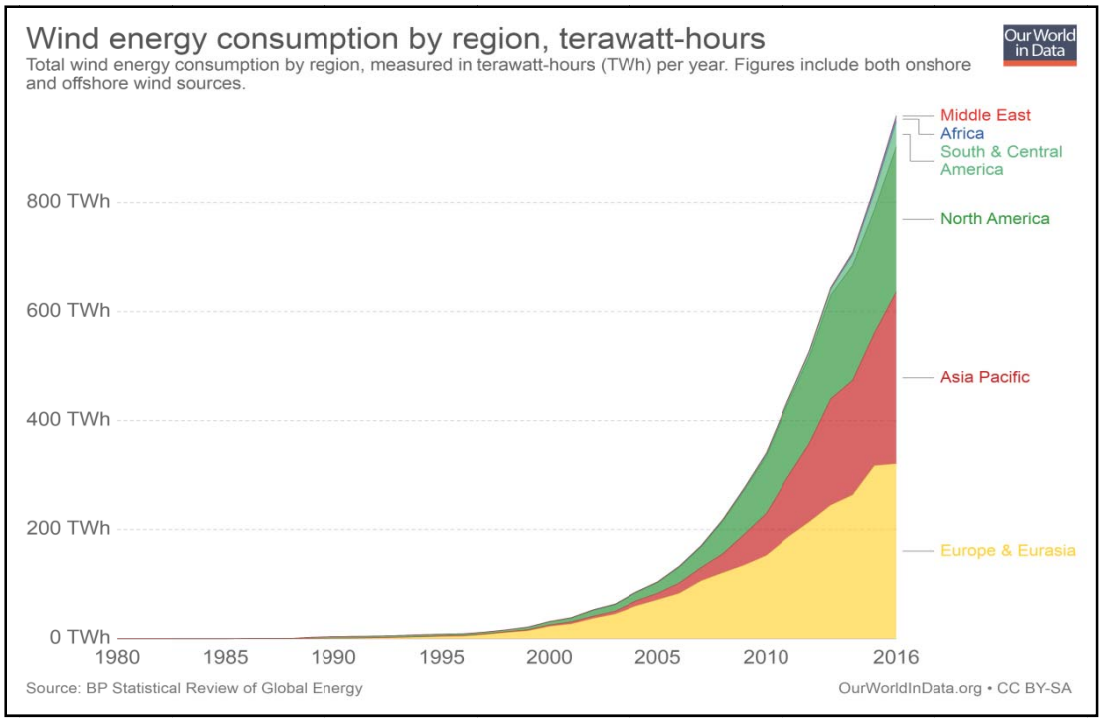

Fig.1. 6: Wind energy consumption by region, Renewables report 2018 [3]

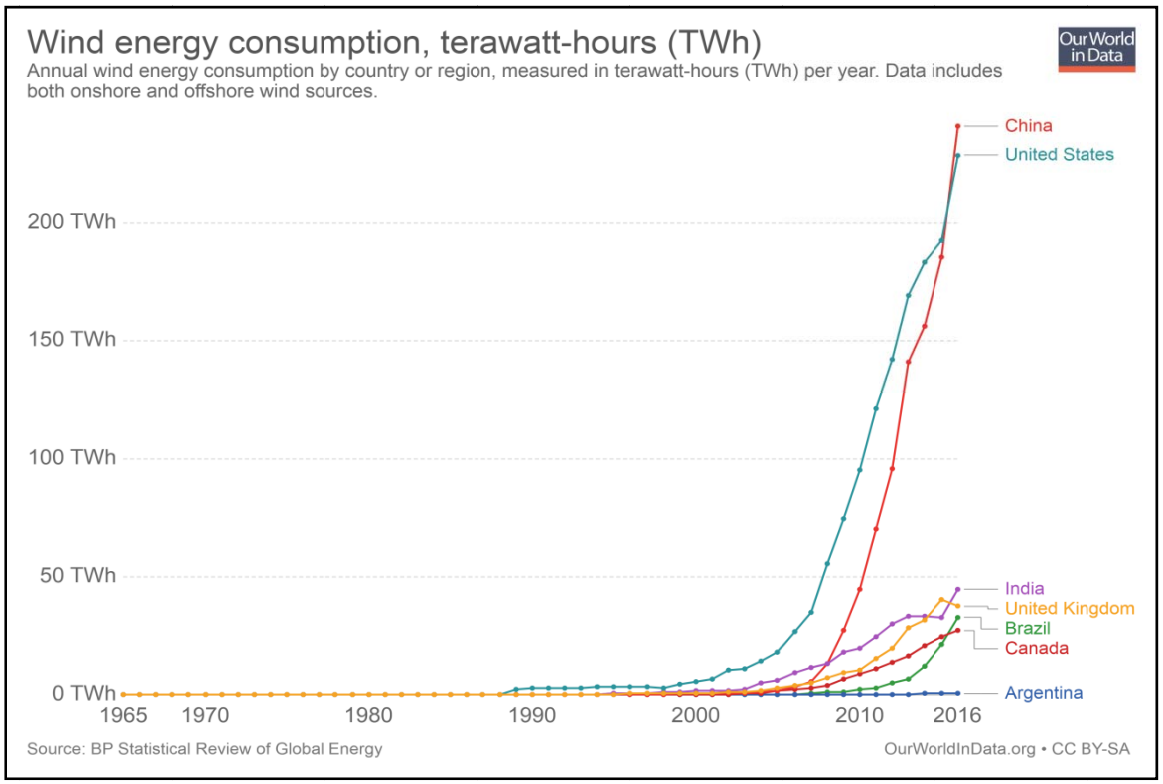

Fig.1. 7: Wind energy consumption by country, Renewables report 2018 [3]

At present, photovoltaic (PV) solar generation is assuming increased importance because of its distinctive advantages such as simplicity of allocation, high dependability, and absence of fuel cost, low maintenance and lack of noise due to the absence of moving parts. Furthermore, it is clean, pollution-free and inexhaustible energy source [4]. In addition to the above the cost of PV modules has fallen more than 100-fold since 1976 as projected in Fig. 1.4 with improved efficiency. This trend is expected to increase even more by the development of new power electronic technologies, new circuit topologies and control strategies. The utilization of solar energy by region and by different countries is shown in Fig. 1.8 and 1.9.

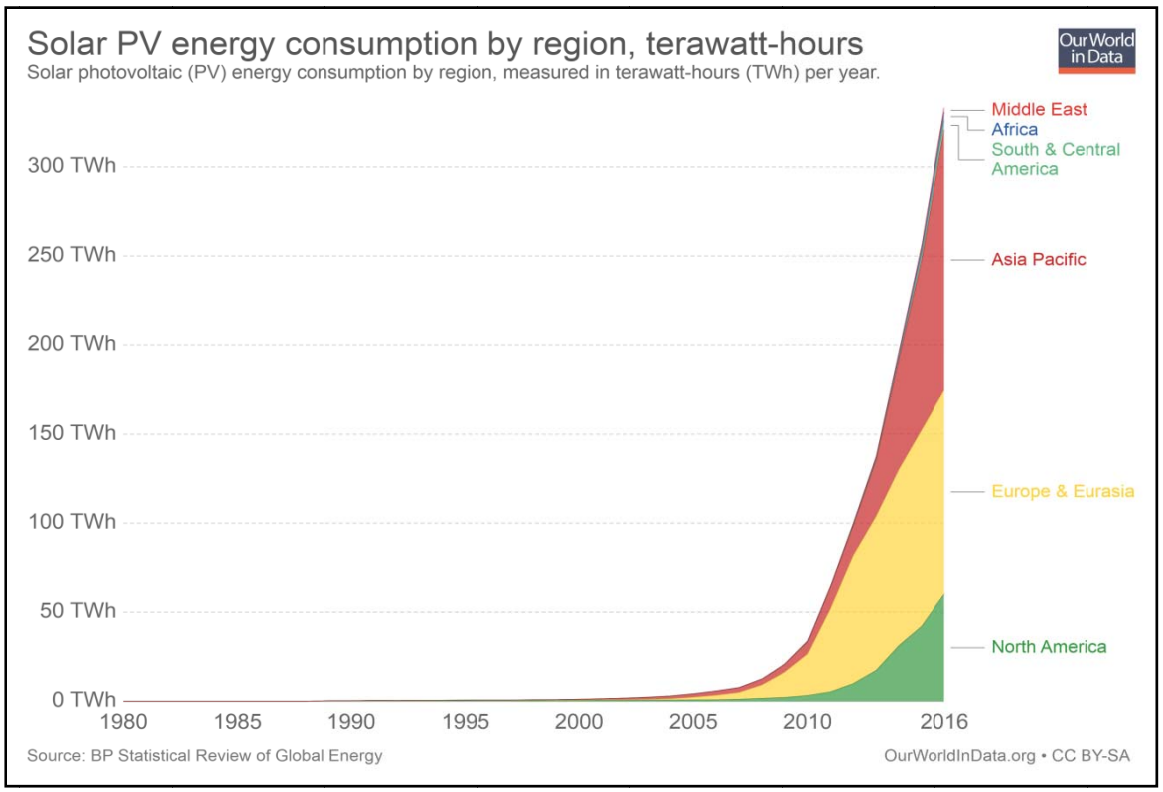

Fig.1. 8: Solar PV energy consumption by region, Renewables report 2018 [3]

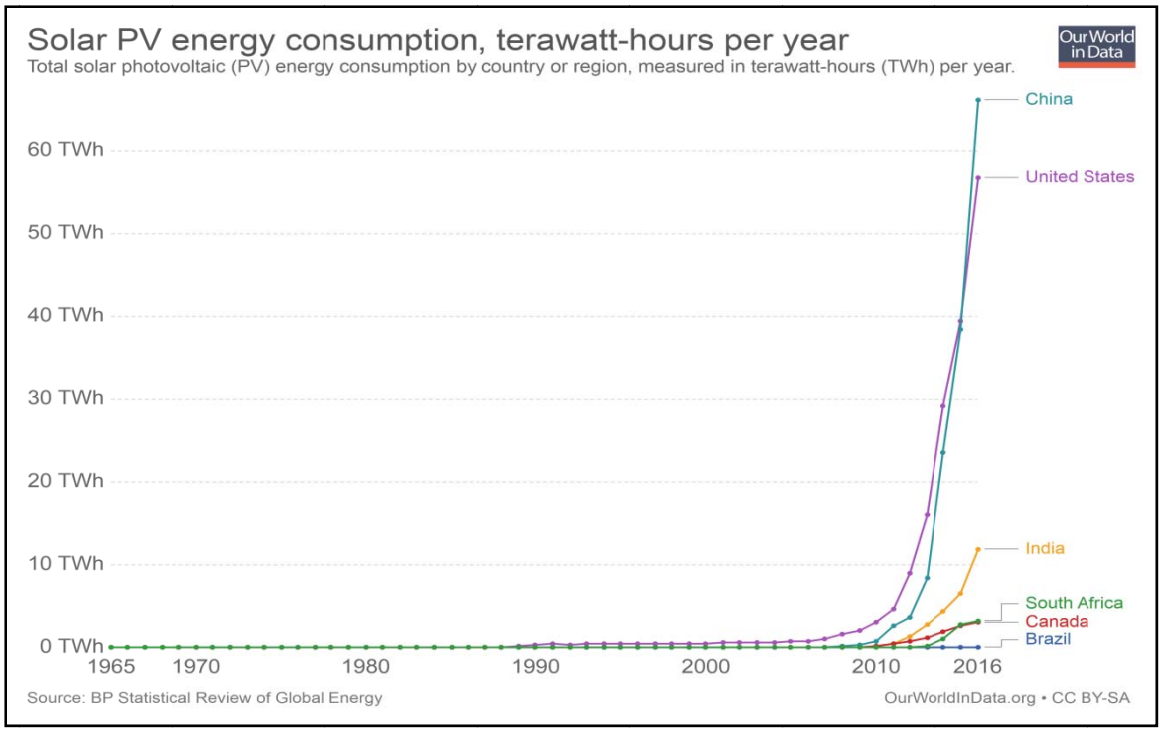

Fig.1. 9: Solar PV consumption by country, Renewables report 2018 [3]

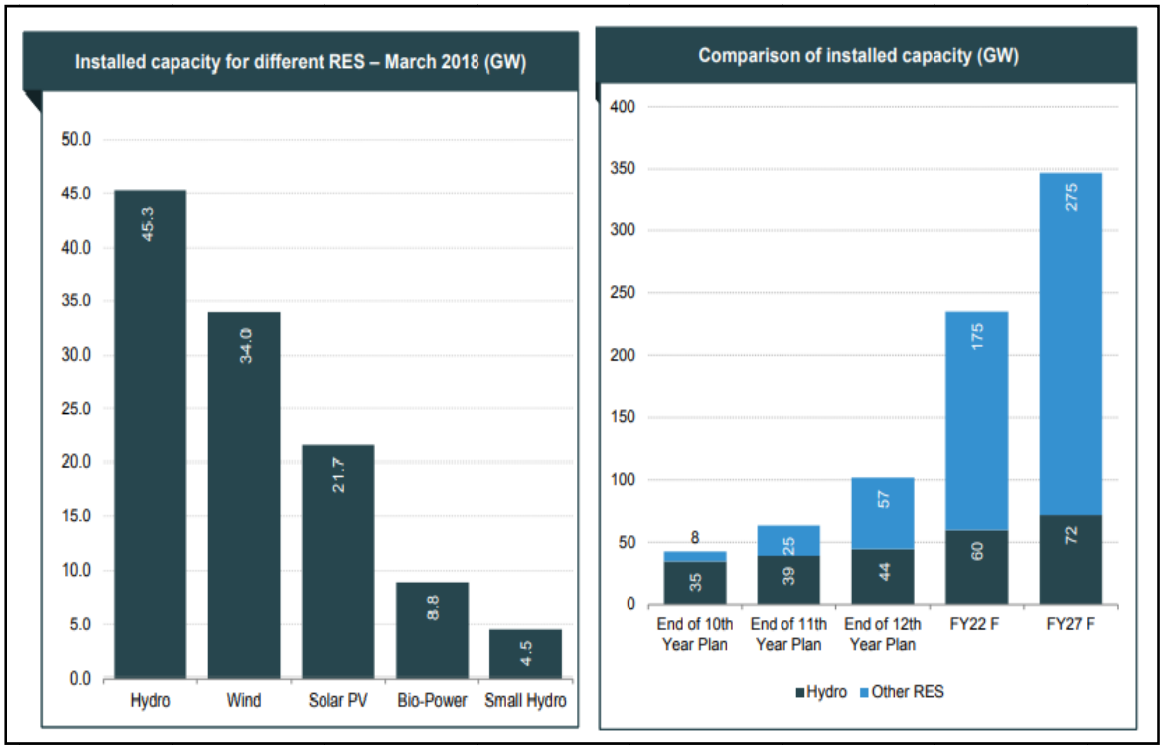

Fig.1. 10: Renewable energy share in India, MNRE 2018 report [5]

As of March 2018, the total RES installed capacity in India is 114.32 GW out of the total installed capacity 344 GW, which is 33.23 percent of overall installation, [5]. Out of which, the share of wind and solar are 34.05 GW and 21.65 GW, bio-power is 8.84 GW and small hydro power share is 4.49 GW as shown in Fig.1.10. From Fig. 1.10, it is observed that though hydro is dominating the growth rate is minimal in it when compared to other renewable energy sources.

Considering the potential of RES, 175 GW of power is targeted to extract from renewable energy sources by the year 2022 in India, [5]. It is estimated that India has renewable energy potential of 900GW from commercially exploitable sources of which 750 GW is from solar, 102 GW from wind, 25 GW from bio-energy and 20 GW from small hydro as shown in Fig.1.11.

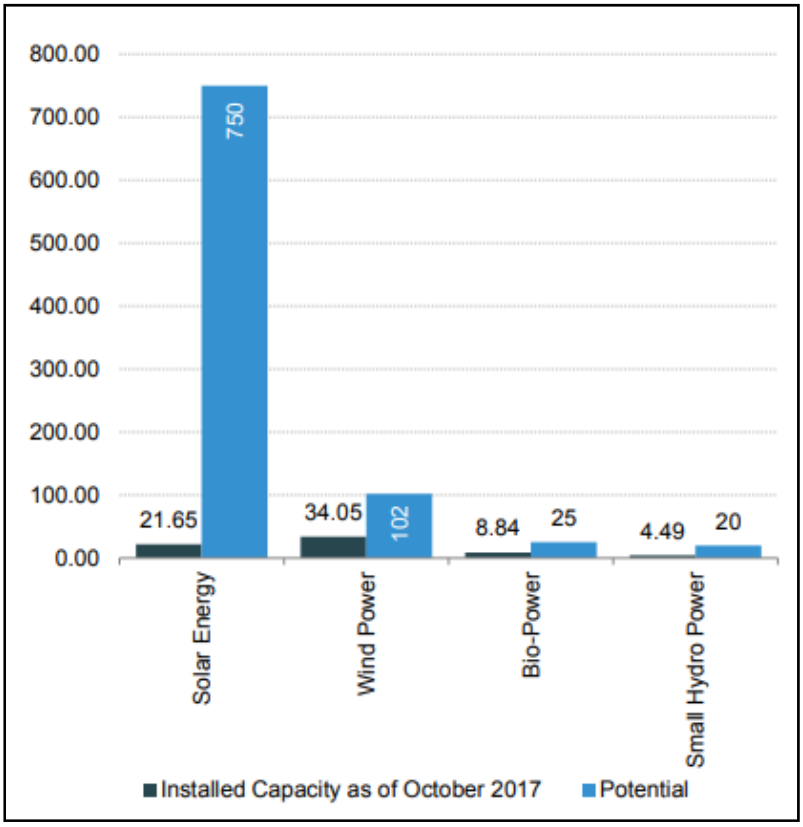

Fig.1. 11: Estimated Renewable energy share in India for year 2022, MNRE report [5]

1.2. Motivation of the Work

The integration of renewable energy sources such as wind and solar, adds to the many troubles of today's grid [6]. As the price of wind and PV generators continues to decline with improved technology, their penetration into the grid is increasing day by day challenging the grid operation and its stability.

But this process of integrating large solar PV installations and wind farms into the AC grid will largely affect the performance of transmission and distribution systems [7]. Technical challenges like voltage instability, frequency instability, dynamic reactive power compensation, poor power quality, synchronization issues and storage issues are being faced during the process of AC grid integration [8-10]. Frequency and voltage fluctuations include, grid-derived voltage fluctuations, imbalance in voltage and reversal of power flow direction etc. [11-12]. Devices like compensators and controllers are needed to improve the system performance, which increases the cost of investment [15]. RES like solar and fuel cells generate DC but connected to AC grid using an inverter, which offers poor conversion efficiency when compared to DC-DC converter circuit [16]. These inverters will introduce harmonics into the grid. Due to the presence of ripples at the output of inverter the power quality is degraded, using a filter at its output the harmonic content is removed [17]. In addition to that the current that the inverter feeds into the grid must be clean and in phase with the grid.

1.3. Problem Identification

Though there are some voltage control, frequency regulation and anti-islanding schemes that are realized through inverters but the control is not optimal and the efficiency is poor. Generally, energy storage systems enhance the performance of

distributed renewable generation systems and increase the efficiency of the entire power system but it is not economically viable for large scale integration of renewable energy sources. Use of compensators, controllers, converters and energy storage systems will increase the investment cost.

Many of these challenges faced during AC grid integration of RES can be overcome by integrating RES to DC grid. Challenges like frequency instability, reactive power compensation, poor power quality, harmonics during inversion and power factor will be mitigated by integrating RES to DC grid.

1.4. Objectives of the Thesis

Having carried out an intensified literature survey on challenges faced by the renewable energy sources during the grid integration; it is found that an attractive alternative to overcome these issues is required. In this concern, the objectives of the present work are summarized as follows.

- To study various factors influencing DC grid integration of RES and to identify various challenges faced by RES during DC grid integration
- To propose a novel topology for high voltage DC grid integration of RES
- To design a hybrid controller to addess two major challenges in DC grid integration namely extracting maximum power from time varying input and to supply stable DC voltage according to the grid demands.
- To integrate solar PV and wind farms to high voltage DC grid using simulation-based tool
- To protect high voltage DC link from overvoltages

1.5. Proposed Methodology

To identify the challenges faced by the present AC grid during the grid integration of renewable energy sources, a literature review was conducted. The solution to overcome these challenges is DC Grid integration of RES. The technical and economical advantages offered by DC system over AC system are discussed.

A literature review is conducted on different AC and DC collection topologies and a novel topology to integrate renewable energy sources to high voltage DC grid is proposed. Few major challenges faced by RES during DC grid integration are identified namely, time varying input due to the dependency on weather conditions, voltage imbalance due to grid side disturbances and influence of grid side faults on to the DC link. To address the first two challenges a hybrid controller is proposed here, which aids in extracting the maximum power operating point from PV and wind in addition to achieving stable DC output according to grid requirements.

To track the maximum power at varying weather conditions, RSM based controller is chosen and RSM based two loop average current controller is designed for voltage regulation. To protect the DC link from over voltages caused due to the presence of unsymmetrical faults on grid side and also to satisfy grid codes, an efficient FRT protection scheme is implemented using DC chopper protection circuit.

1.6. Outline of the Thesis

This thesis is organized in the following manner.

Chapter 1 deals with the Introduction, Motivation of the Work, Problem Identification with Proposed Methodology, Objectives and the Outline of the Thesis.

In **Chapter 2**, an overview of problems faced by the present AC grid due to the penetration of renewable energy sources are discussed from the literature study. Different factors influencing DC grid integration of renewable energy sources are discussed. Various topologies proposed in literature for AC grid integration and DC grid integration of renewable energy sources (RES) are discussed. In addition to this the challenges faced during HVDC grid integration of RES are discussed here.

In **Chapter 3**, different DC-DC boost converter configurations are discussed. The operation and working of converter circuits like DC-DC Boost converter, transformer less high gain boost converter, multilevel DC-DC Boost converter and LCL boost converter are discussed. In addition, the small signal modeling of boost converter, the open loop operation and closed loop operation of boost converter with a fuzzy controller are discussed. A comparative study is performed between two medium voltage converters namely transformer less high gain boost converter and multilevel DC-DC Boost converter using simulation.

A novel topology to integrate solar and wind farms to high voltage DC grid is proposed in **Chapter 4**. The need for hybrid controller and its configuration are discussed in this chapter. The hybrid controller consists of Maximum Power Point Tracking (MPPT) controller along with voltage regulator, the MPPT controller helps in harnessing the maximum power at varying weather conditions whereas the voltage controller helps in reducing the distortion in output voltage. Different MPPT techniques in literature are discussed, a comparative study is performed among these techniques to determine the efficient MPP tracker. A random search method based two loop average current controller is proposed in this chapter for voltage regulation. To evaluate the performance

of proposed voltage controller the response of it is compared with linear proportional integral controller.

Chapter 5 initially discusses about the modeling of PV module. Different configurations, to integrate solar photo voltaic installations to DC grid are discussed. The impact of hybrid controller on the proposed system performance is evaluated under different combinations of varying input and fluctuating output. The stability analysis of boost converter with TLAC controller is discussed in this chapter.

Chapter 6 includes modeling of wind turbine, drive train model and permanent magenet synchronous generator. Simulation of the proposed topology connecting solar PV and wind farm installations to high voltage DC grid using DC transmission.is performed in this chapter. To maintain constant DC link voltage during unsymmetrical faults and also to satisfy grid codes an efficient Fault Ride Through (FRT) protection is offered by DC chopper circuit. The fault ride through protection offered by DC chopper circuit on the proposed system is evaluated using simulation.

The **Chapter 7** concludes the thesis and the major contributions. The recommendations for future work are also suggested in the chapter.

CHAPTER-2

Literature Review

2.1. Introduction

The problems faced by the present AC grid due to the penetration of renewable energy sources (RES) are discussed in this chapter. Literature review is conducted on large scale integration of onshore, offshore wind and solar PV farms to DC grid. The factors influencing high voltage DC grid integration of RES are discussed, in addition to the advantages offered by DC transmission over AC transmission. Different topologies proposed in the literature for AC and DC grid integration of RES are discussed. The major challenges faced during DC grid integration are identified.

2.2. Technical challenges faced by PV and wind energy sources during AC grid integration

The operation and management of interconnected power system is a complex task and it faces significant voltage and frequency fluctuations as well as blackouts. These issues are further complicated by the large scale integration of renewable energy sources in the transmission and distribution systems. Depending up on the topology and size of the grid, the impact of RES on it will vary. RES when connected to low power grid might not have any impact on power quality and its reliability; however, if the injected power of grid-connected RES increases, the overall reliability of the system and power quality will be reduced. The degradation in power quality can be measured in terms of voltage flickers, voltage rise, and harmonics. The decrease in reliability can be observed from the

sustained interruptions. Some of the key issues faced by the grid during AC grid integration of RES are provided below.

2.2.1. Frequency Instability

The frequency of grid is unstable due to various reasons like time varying input and varying load demand. The generation and distribution companies have been deviating from their agreement or injection schedule resulting in deviations in the supply frequency [12].

To achieve frequency stability, fast acting primary reserves like hydro or gas are used; tertiary reserves that can sustain and support the actions of the secondary reserve are activated [13, 14]. At present there are no such reserve capacities, to maintain the frequency with in the safe limits, in the absence of a functional capacity market. As there are no incentives given to conventional or RES generators to keep their spare capacity for reserve purposes, the generators will generate power at their maximum capacity to increase their revenue. In addition to this, the availability of secondary reserves is significantly constrained by shortage of gas supply in gas power plants and seasonal unavailability of hydro plants.

2.2.2. Grid Derived Voltage Stability

Due to time varying nature of solar and wind energy, difficulties will arise in maintaining a balance between generation and demand, affecting the voltage stability due to changing demand for reactive power [15]. Since most of the wind generators, namely squirrel cage induction generator and double fed induction generator being inductive in nature, will absorb substantial reactive power from grid during starting and some during normal operation. Due to variable wind speed characteristics, generator start up occurs

multiple times in a day, resulting in huge quantum of reactive power absorption from the grid, creating voltage instability [16].

To overcome this issue, inverters used in grid interface are configured to operate in 'voltage-following' mode and they are set to disconnect RES connected to the grid when the grid voltage moves beyond the set parameters, [17] This ensures the system to maintain power quality as well as helps to protect the system against unintentional islanding. When large number of RES are connected to a particular feeder, their automatic disconnection from the grid when the grid voltage violates the limits can be problematic since the other generators on the network will suddenly have to supply the additional power to the grid [18].

2.2.3. Synchronizations Issues

Voltage imbalance occurs when the voltage amplitude in each phase is different from the other phases or when the phase angle difference between any two phase is not exactly 120°. Disproportionate installation of single phase systems will cause severely unbalanced networks leading to damage of DG, motors, controls, transformers, and power electronic devices. Thus, for high PV and wind farm penetrations, the cumulative size of all systems connected in each phase should be maintained the same [19].

2.2.4. Variability

Variability is the main hurdle for integrating RES into the AC grid, with inaccurate forecasting techniques the output power generated is variable in nature that results in poor frequency and voltage control [20-22].

2.2.5. Voltage Rise

Voltage rise is one of the challenges that would arise due to the increase in the penetration of RES into the grid during low demand season. It can be controlled by using power factor control devices, reducing the voltage setting of high-voltage/medium-voltage substation, and using ring-operated distribution network with respect to the RES interconnection [23]. Voltage regulators can also be used to compensate voltage drop and maintain the voltage in the designated range along the line.

2.2.6. Oscillations

In modern power systems, RES like solar and wind are integrated to AC grid in large scale using power electronic converters like inverters [24, 25]. Due to which, the interaction between the converter and the grid has changed the system dynamics significantly creating new oscillation issues. For example, sub/super synchronous oscillations at wind farms [26], high frequency harmonic oscillations in micro grids [27] and low-frequency oscillations created by constant power loads. These oscillations generated would impact the stable operation of the system and the efficient penetration of RES.

2.2.7. Poor power quality

Renewable energy sources such as solar and fuel cells rely on voltage source based inverters to integrate with an AC grid. These inverters will introduce harmonics into the grid. Likewise, the output power generated by wind farms, rely on variable wind speed which is uncontrollable affecting the power quality of generated power. Voltage and current harmonics are highly expected due to grid integration of RES [28, 29].

Connectivity standards proposed by CE in 2013 (2013) indicate that harmonic current injections and flicker introduced by solar and wind generating stations shall

not be beyond the limits specified in IEC 61000 and IEEE 519 Standard respectively, [30]. The DC current injected into the grid should not be greater than 0.5% of the full rated output.

2.2.8. Dynamically varying reactive power support

The wind generating stations should be capable of supplying dynamically varying reactive power support, in order to maintain the power factor between the limits 0.95 lagging and 0.95 leading [30]. If the power factor maintained on the grid is poor it will increase the losses in the line and hence instability in voltage due to improper voltage regulation. By using inverters and operating them in "voltage-following mode" and "voltage-regulating mode" power factor correction can be done [31, 32]. But various factors need to be considered while using inverters for power factor correction namely.

- The size of the inverter should be increased to accommodate both reactive power support and maximum active power to the grid.
- The allocation of reactive power support comes at the cost of energy.
- FACTS devices like STATCOM or SVCs can provide reactive power support in a cost-effective manner [33, 34], with minimum losses, whereas VAR compensation offered by inverters takes rapid response time and is infinitely variable. In applications where rapid and frequent changes in voltage takes place because of large transients in load then VAR compensation by inverter may be justified.

From the studies, it is observed that the use of inverters for voltage regulation of network at high PV penetrations need centralized control in order to achieve optimal operation of the network as a whole.

2.2.9. Poor Forecasting

Forecasting the power is one of the major aspects in managing power for grid system planning, it ensures the reliability and stability of grid. Unlike conventional system where load forecasting is done in case of renewable energy technologies, forecasting studies are conducted at the generation side, [35]. In RES the source of generation are variable and uncontrollable due to which grid integration becomes more difficult to ensure grid stability, henceforth, there is a need for forecasting study at generator side. The characteristics of each renewable energy generation technology are different from other and hence the forecasting techniques. There are different forecasting techniques for each of the technologies like short and long term forecasts. Short term forecasting study is conducted in hours and it doesn't creates any problem during integration, where as long term forecasting study is not accurate and impacts the operation of the grid [36,37].

2.2.10. Location of RE Plants

In general, RE plants of large scale are being connected to the grid, so the area occupied by such plants is considerable. For each technology, there are several factors that will influence its location. Identifying a location to install and operate RE plant involves various factors that will make Grid integration more challenging. Few factors that influence are, all RE sources are not available in the region we chose, the distance between generating plant and the grid is a major factor in terms of efficiency and cost. Dependency on weather, climate, and geographical locations are few other deciding factors. [38-39].

2.2.11. Voltage Flicker

Voltage flicker problem arises due to change in environmental and surrounding conditions, which would show a significant impact on voltage change on the feeder. In case of solar and wind energy systems, the output changes as a function of wind speed and sun's radiations [40]. These voltage flickers are also produced due to switching operations usually during starting or shutdown operation of equipment. Rapid change in voltage occurs within 10 min averaging interval, typically on a time scale between half a period (10 ms at 50 Hz) and a few seconds [41]. Supervisory schemes are used to monitor the voltage magnitude and change in voltage per unit time and to maintain them within the desired limits [42].

2.3. Literature review on large scale integration of offshore wind farms and PV farms to DC grid

Many of the challenges faced during AC grid integration of RES can be overcome by integrating RES to DC grid. Challenges like frequency instability, reactive power compensation, poor power quality, harmonics during inversion and power factor will be mitigated by integrating RES to DC grid. The factors influencing large scale integration of PV and wind farms to DC grid are given below [50-56]:

- To overcome the frequency instability issue integrating conventional AC power with HVDC grid was investigated by various researchers to ensure huge penetration of RES into the DC grid as well as to maintain a stable operation of grid [50, 51].
- Due to higher capital cost of large solar farms, the investors and designers will try to extract the maximum possible power output from the installed plant. The

traditional AC collector grid concept is not the optimum choice for solar farms, as the power generated by PV modules is DC and it is inherently flexible and easier to couple multiple DC sources than coupling AC sources. The DC collector grid concept for large onshore and offshore wind farms has already been investigated in [52].

- HVAC transmission between onshore load centres and offshore wind farms is not a feasible option in case of wind farms since the active current carrying capability of long AC cables is less when compared to DC due to the presence of "high charging capacitance" in AC cables. Thus, long distance HVAC transmission will create high cable losses, reduced efficiency and requires compensation of reactive power [53]. These challenges can be overcome by HVDC systems, which provides better transmission efficiency, higher power transmission capacity, improved system stability, reduced losses and no reactive power control, [54].
- Improved conversion efficiency of DC-DC converters over inverters [55]
- Rapid growth in power electronics technology leads to fall in prices with improved power ratings, [56].

Some of the other reasons to choose electrical DC Grid Architecture in future applications are given below. The advantages offered by HVDC transmission over EHVAC transmission are also discussed below [57-64]:

- Use of DC transmission will improve the transmission efficiency as a result; many HVDC transmission systems are built around the world.

- DC system offers greater flexibility, using DC buses of different voltage ratings, grid integration of battery storage systems and renewable generation systems can be made easier.
- Using DC Micro grid, the power supplied by DC production for applications like lightning, charging of DC vehicles will be increased which influences the utilization of renewable energy.
- Security and reliability of power supply will be improved due to increase in the use of distributed power system, example: DC micro- grid and smart grid technology.
- Use of VSCs-HVDC and converter station will improve the bidirectional power transfer capability of AC power grids.
- HVDC transmission systems can be operated in islanded and weak AC systems. Reversal of power flow is possible in DC without affecting the polarity of DC supply
- Using DC Bus of different voltage ratings, power conversion from AC to DC or DC to AC can be minimized.
- DC cable cost is lesser in comparison with AC cable considering same power flow due to the absence of skin effect and optimal use of cable.
- Absence of capacitive currents in DC cable which is in contrast to AC long cable that produces high values of capacitive currents.

In addition to above, DC technology offers advantages like improved power flow control, reduced right-of-way and reduced infrastructure, etc., [64,65]. In the present work different topologies for integrating renewable energy sources to high voltage DC grid are discussed. Many topologies are available in literature to integrate offshore wind

farms to the onshore grid. These collection topologies are proposed considering the distance of the farm from the shore, voltage levels, number of wind turbines and technological choices, [70]. In this work, a new topology is proposed to integrate PV and wind farm installations to high voltage DC grid.

2.4. Topologies proposed in literature for AC and DC grid integration of renewable energy sources

2.4.1 Configuration of Offshore Wind Power Plants with AC collection System

An "offshore wind power plant" configuration with AC collection system can be constructed in radial, ring and star connection schemes. The radial collection system is the most commonly used and economical due to its simplicity. The turbines when connected in string configuration are shown in Fig. 2.1(a) but it has a drawback that the system is unreliable. The ring collection system as shown in Fig. 2.1(b) offers better reliability compared to radial system, but there is increase in investment cost. The star collection system as shown in Fig. 2.1(c) reduces the ratings of the cable that are used to connect the wind turbine and collector point, thus reducing the investment cost [65].

2.4.2 Configuration of Offshore Wind Power Plant with DC Collection System

There are three different DC collection systems proposed in literature for offshore wind power plant configurations based on the type of connections, namely parallel, series and hybrid [66-70]. In the first configuration, voltage of the turbine is maintained constant, whereas in the second configuration, the turbine current is maintained constant while in hybrid configuration a mix of parallel and series is implemented [67]. In general both series and hybrid topologies face technical challenges

like increase in insulation with increase in voltage level and over sizing of wind plants to overcome over voltages etc. [68]. For the parallel configuration, three DC offshore wind power plant (OWPP) configuration schemes are proposed in literature based on converter requirements and offshore collector platforms existence [69, 70]. In addition to that, a new hybrid topology is proposed in this work that offers better efficiency and reliability than the previous topologies.

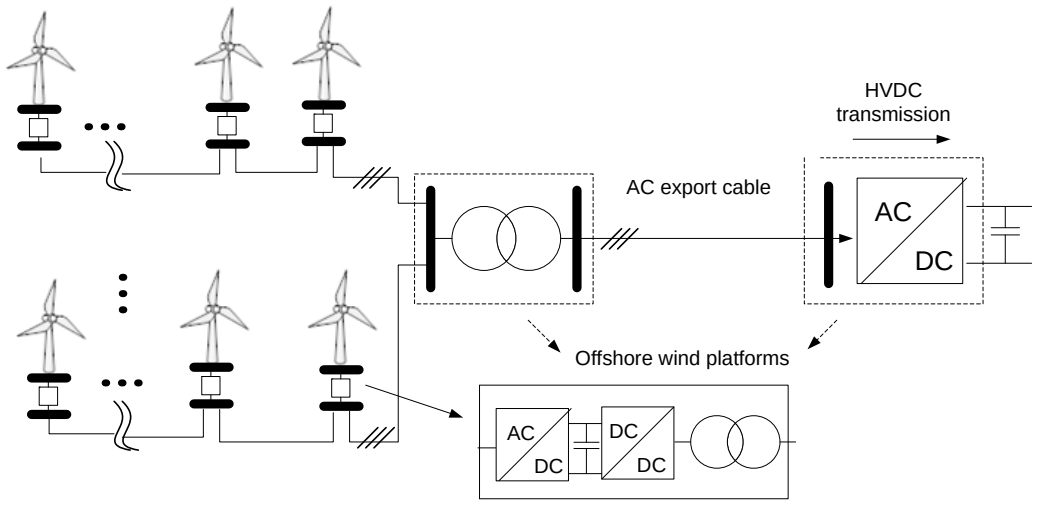

(a)

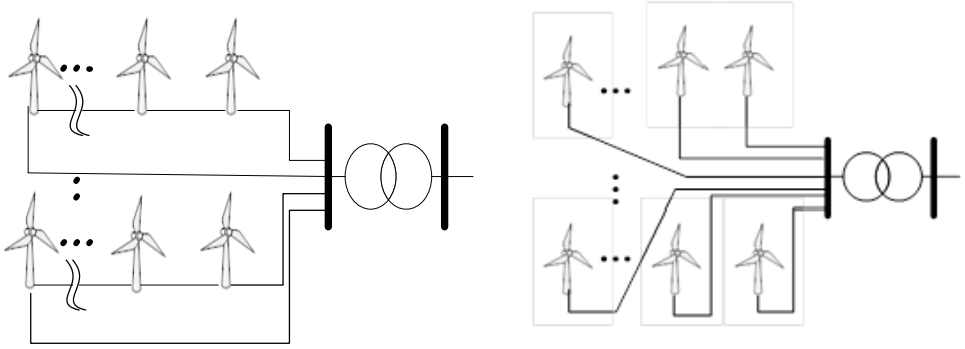

(b) (c)

Fig 2. 1: (a) layout of radial collection (b) ring collection and (c) star collection configuration of the ac offshore wind power plant.

The scheme of DC configuration 1 is shown in Fig. 2.2 (a). In this case, wind turbines are connected directly to the HVDC main substation through feeders. To improve the voltage profile and to transfer the power to the onshore grid using HVDC transmission a DC-DC Converter is used, [67]. The major advantage of this topology is the absence of intermediate collector platform thus saving the capital costs.

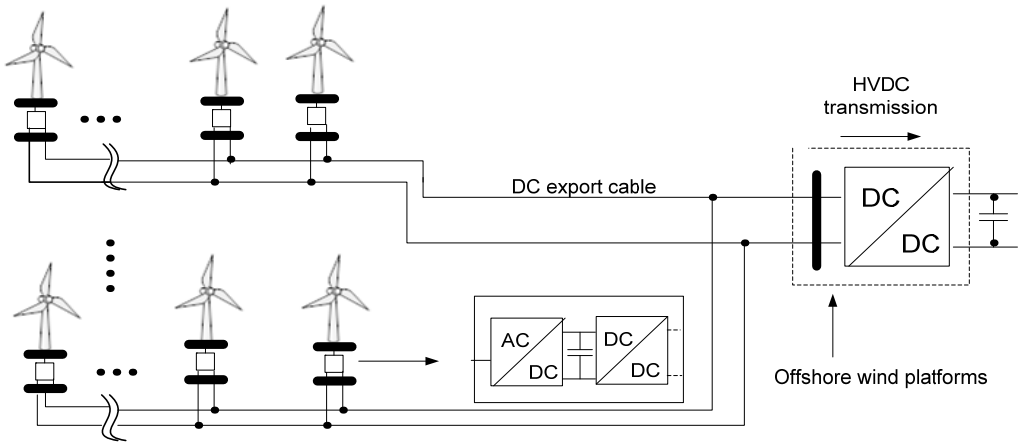

(a)

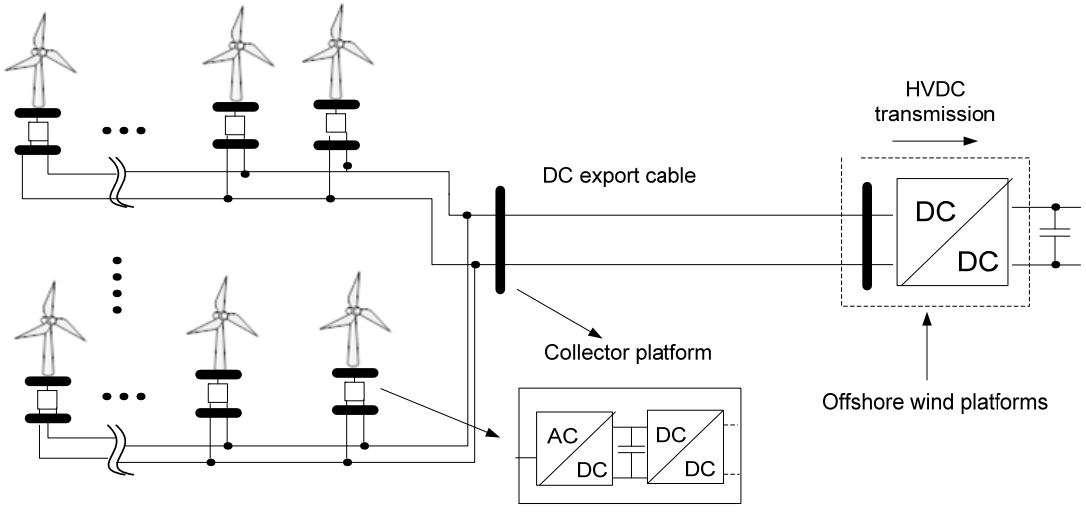

(b)

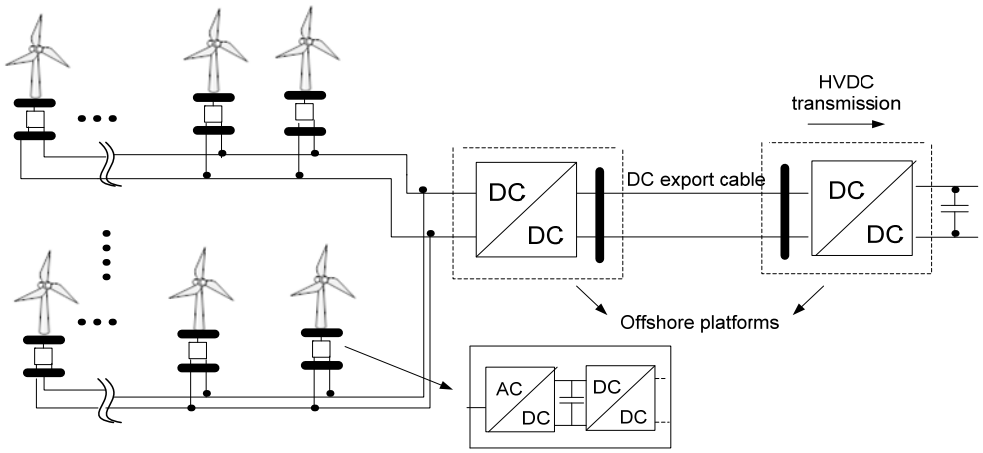

(c)

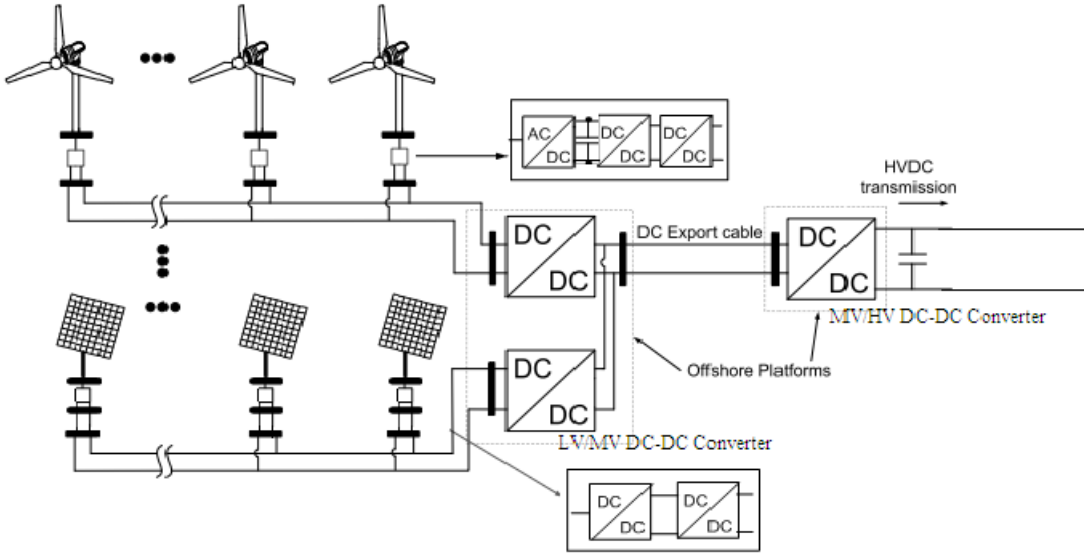

(d)

Fig 2. 2: (a) DC offshore wind power plant configuration 1, (b) DC Offshore Wind Power Plant Configuration 2, (c) DC Offshore Wind Power Plant Configuration 3, (d) Proposed DC Offshore Wind Power Plant Configuration.

The second DC OWPP configuration is shown in Fig. 2.2(b), which consists of offshore collection point to which turbine strings are connected. This scheme differs from the first due to the presence of intermediate platform that connects inter-array

cables to the feeders. The major advantage of this scheme is the absence of DC-DC converter, which is replaced with export cables of larger cross sectional area, saving the investment cost and reducing the energy losses, but it has the drawback of dissipating excess power in export cable.

The schematic diagram of third DC OWPP is shown in Fig. 2.2(c), it consists of DC-DC step-up Converters, one at the end of the wind farm and the other one before HVDC transmission link, are used to improve the voltage profile and to deliver the power to shore. The major advantage of this scheme is the reduction of export cable power loss, which will be dominant if distance between the main HVDC offshore platform and the collector is large. Due to lack of redundancy, this system is unreliable, incase if the converter fails to operate, then there is discontinuity in power delivered to the grid.

The schematic diagram of the proposed system for connecting OWPP and solar power plants to DC grid using DC Collection system is shown in Fig. 2.2 (d). It consists of a string of PV and Wind farms connected to low voltage DC grid. Each PV string consists of solar PV farm connected to low voltage DC grid using two series connected DC-DC Converters where as in offshore wind string consists of wind turbine fed PMSG connected to low voltage DC Grid using rectifier and two series connected DC-DC Converters.

The first converter is a conventional boost circuit that is used to extract maximum power using MPPT technique and the second converter is a multilevel boost converter that is used to maintain the stable DC output considering grid side and input side nonlinearities. In addition to that, they will improve the voltage profile and helps in delivering the power to the grid. Many such strings consisting of PV and wind farms are connected to low voltage DC grid, which is connected to DC offshore collection platform

using DC cables. At low voltage DC grid using MLBC the voltage level is improved from low voltage to medium voltage. To achieve the high voltage gain and to transmit the power through HVDC transmission, LCC coupled step-up DC-DC Converter is installed at offshore platform, it boosts up the voltage from medium voltage to high voltage.

The proposed system offers better reliability in comparison with the configurations of the previous system configurations, as there are two different sources, there is continuity in power supply. In the proposed configuration, though the capital expenditure is high due to increase in the number of converters, but the system performance, reliability and flexibility will improve.

2.5. Factors affecting the integration of RES to HVDC Grid

Few major challenges faced by RES during DC grid integration are unpredictable input due to the dependency on weather conditions, voltage imbalance due to grid side disturbances and influence of grid side faults on to the DC link. To address the first two challenges, a hybrid controller is proposed here, which aids in extracting the maximum power operating point from PV and wind in addition to achieving stable DC output according to grid requirements. The hybrid controller proposed here consists of Random Search Method (RSM) based MPPT controller along with RSM based two loop average current controller, the MPPT controller helps in harnessing the maximum power at varying weather conditions whereas the voltage controller helps in reducing the distortion in output voltage. RSM method is chosen here for the design of controllers, as it has simple computational steps, derivative free, guarantees global convergence and requires less memory.

Another major issue is fault ride through (FRT) when RES are connected to a DC grid, some grid codes need to be satisfied to overcome fault ride through issue. If three phase fault occurs on AC side of the system, then the imbalance between power delivered and power utilized will create a voltage imbalance which charges the capacitor of DC link to more than its capacity, affecting the equipments nearby. To maintain constant DC link voltage during unsymmetrical faults and also to satisfy grid codes an efficient FRT protection scheme is implemented using converter circuit. Detailed simulation studies are performed to demonstrate the performance of the proposed configuration under different test conditions using MATLAB/ Simulink.

2.6. Summary

Due to increase in the potential market for wind and solar energy generation, their penetration to the grid is increasing with time. Due to which the present AC grid faces technical challenges like operational instability, control and compensation of active and reactive power, voltage and frequency instability and storage issues. It is observed from the literature review majority of these issues can be overcome by integrating to DC grid which seems to be a promising solution, when compared to AC Grid due to its technical and economical benefits. To integrate these RES to DC Grid a literature survey is conducted on different topologies architecture topologies for high voltage DC grid integration, these topologies are discussed here. A new topology for integrating RES to high voltage DC grid is proposed here. The major factors influencing DC grid integration of RES are discussed here in brief.

CHAPTER-3

DC-DC Boost Converters for DC Grid Integration

3.1. Introduction

To integrate solar and wind farms to DC grid DC-DC converter of different voltage and power ratings are needed at low, medium and high voltage DC grids. In this chapter different converters needed for DC grid integration of RES are identified and their performance is validated. Due to wide range of applications for high-voltage (HV) high power DC–DC converters in large on shore and offshore wind farms and large solar farms, an intensive research is being conducted on them [71]. Nevertheless, power electronics faces a big challenge in the design of these converters due to extreme blocking voltage faced by the semiconductor switches [72].

Semiconductor switches like integrated gate-commutated thyristor (IGCT) and the HV insulated gate bipolar transistor (IGBT) are widely used for HV application but they offer high switching losses hence their switching frequency is limited to about 1 kHz [73]. For high frequency switching operation (>10 kHz), the most attractive switches are the MOSFET and IGBT. But they have the drawback that they cannot withstand high voltage stress when used in circuits like conventional DC-DC converters for high-power application. Hence conventional DC–DC converters are not the best choice for high-frequency, high voltage operation [74]. Some common solutions described in the literature on DC–DC converters for high-frequency and high voltage applications are discussed below.

Conventional boost converters, interleaved and cascaded boost converter topologies when used to obtain the required high voltage gain [75-77] have the inherent issues like high ripple current, extreme maintenance of duty cycle and relatively higher losses affecting the efficiency. Converters with transformers and coupled inductors have the limitation on switching frequency. The size of the converter becomes bulky and expensive in such converters since the losses in transformer vary as a function of switching frequency. In addition, there is increase in voltage stress across the switch due to high current flow through the boost inductor. Coupled inductor switched capacitor, coupled inductor with voltage multiplier cell techniques were proposed in [78-80], to achieve desired high voltage gain but the complexity in operation and component count and component size, voltage stress will increase with the increase in gain factor.

An isolated converter circuit consisting of full-bridge converter circuit with two legs connected in series in primary circuit is proposed in [81, [82]. The voltage stress across each switch is less and it can be further reduced by increasing the number of levels but the complexity will increase with the increase in the number of series connected full-bridge legs in the primary side.

Converters like dual active bridge (DAB) DC-DC converter, flyback converter are frequently used in the low and medium voltage applications [83], [84]. These topologies when used for HVDC applications, the number of series connected semiconductor switches in a switch string are increased to sustain such high DC voltage. With this arrangement, the voltage stress across each semiconductor switch will come down but it needs an additional voltage balancing circuit; otherwise, it will lead to unequal voltage distribution across the switches in static and dynamic states, creating damage due to

overvoltage to one or many [85]. A Transformer less high gain Boost Converter (TFHBC) is proposed in [86], it offers better efficiency and high gain factor, But is has the drawback that it can be used for medium voltage applications as the gain factor increases the voltage stress across the switch increases..

In the later days, the concept of multilevel based DC-DC power conversion attracted the attention of researchers and proven to be a suitable solution to obtain the required high voltage gain at high power level [87]. The main advantages of this topology are continuous input current, low voltage stress, self-voltage balancing, high efficiency, low EMI noise and harmonic distortion, ability to achieve high voltage with low voltage component, single switch structure and large conversion ratio without extreme duty cycle or transformer, which allows for high switching frequency. Further, multiple sources can also be connected to the converter, which makes this as an attractive topology for renewable energy conversion. But the major drawback of this topology is the complexity will increase with the increase in the number of levels for high voltage applications so its application is limited to medium and low voltage applications. An LCL DC-DC converter circuit for high voltage and high power applications offers high-gain factor without an intermediate AC transformer is proposed in [88]. This converter circuit consists of internal passive LCL circuits; that eliminates the issues with high-frequency transformers.

In this chapter, the operation and working of converter circuits like DC-DC boost converter, transformer less high gain boost converter, multilevel DC-DC boost converter and LCL boost converter are discussed. Using small signal mathematical modeling of boost converter, its open loop and closed loop performance is validated for different

loads. A comparative study is performed between two medium voltage DC-DC converters namely transformer less high gain boost converter and multilevel DC-DC boost converter.

3.2. Modeling of Conventional DC-DC Boost Converters

The DC-DC boost converter circuit consisting of a solar PV cell as its DC input voltage source V_{in}, controllable MOSFET switch, filter inductor L and capacitor C, load resistor R, and a PWM block is shown in Fig. 3.1, [89]. A current generator represented by symbol 'I_z' is connected in parallel to the load to examine the response of the system for the corresponding load changes. The voltage across the capacitor and current through the inductor and duty cycle of the converter are represented by V_o, I_L and d. The proposed scheme is considered to operate in continuous conduction mode (CCM).

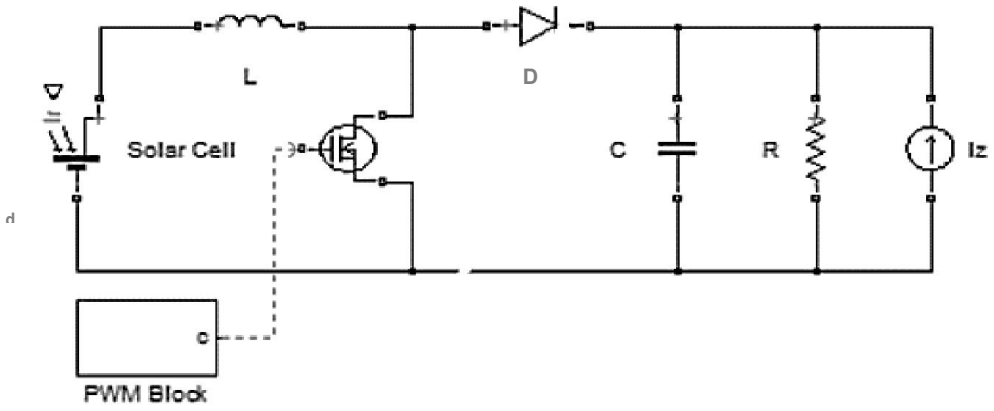

Fig. 3. 1: DC-DC Boost converter, [89].

When the MOSFET switch is turned ON, diode is turned OFF and the inductor coil gets charged through the source. When the switch is turned OFF, energy from both the inductor and input is fed to the load. It is assumed that the switch chosen here is ideal

and the losses in the capacitance and inductance are negligible. The output voltage of the converter expressed in terms of input voltage and duty cycle is,

$$V_o = \frac{V_{in}}{(1-d)} \tag{3.1}$$

3.2.1. Mathematical Modeling of DC-DC Boost Converter

The ideal dynamics of the conventional boost converter circuit can be obtained by applying the state space averaging method [89], which would help in designing the controller. When the switch is closed, the corresponding circuit is shown in Fig. 3.2(a). By applying Kirchhoff's voltage law to the loop, consisting of the inductor and source and Kirchhoff's current law to the node connecting the capacitor branch the following relations are obtained.

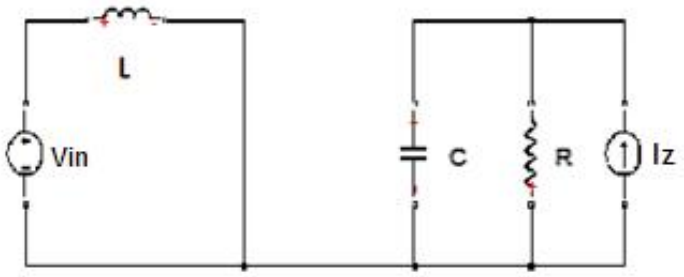

(a)

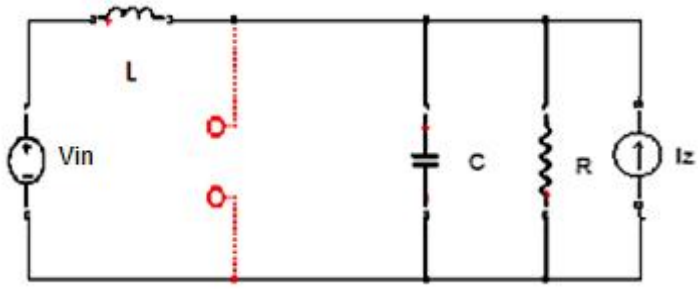

(b)

Fig. 3. 2: (a) Boost converter circuit during on state, (b) Boost converter circuit during off state, [89].

$$\frac{di_L}{dt} = \frac{1}{L} V_{in} \tag{3.2}$$

$$\frac{dv}{dt} = \frac{1}{C}(i_z - \frac{V}{R}) \tag{3.3}$$

During OFF state, when the switch is OFF and the diode is ON the corresponding circuit is as shown in Fig.3.2 (b). By applying the Kirchhoff's voltage and Kirchhoff's current law to the circuit, the equations of OFF state are obtained as in (3.4) and (3.5). The inductor current is represented by i_L and V is the voltage across the capacitor.

$$\frac{di_L}{dt} = \frac{1}{L}(V_{in} - V) \tag{3.4}$$

$$\frac{dv}{dt} = \frac{1}{C}(i_L - i_Z - \frac{V}{R}) \tag{3.5}$$

3.2.2. Small Signal Modeling

In this work DC-DC boost Converter shown in Fig. 3.1 is modeled using "Small signal state-space averaging technique". A set of differential equations representing the ON and OFF state operation of boost Converter in "continuous conduction modes" are used to represent "state space representation", [89].

The current through the inductor current i_L and voltage across the capacitor V are given by,

$$x(t) = [i_L(t), V(t)]^T$$

where $x(t)$ is the state vector.

The continuous state-space equations of the system during ON state are

$$\dot{x} = Ax + Bu \tag{3.6}$$

where,

$$A = dA_{on} + (1-d)A_{off}$$

$$B = dB_{on} + (1-d)B_{off} \tag{3.7}$$

Let $x_1 = i_L$ and $x_2 = V$

The equations (3.2) and (3.3) in terms of input and state variables are given by,

$$\dot{x}_1 = \frac{1}{L}V_{in} \tag{3.8}$$

$$\dot{x}_2 = \frac{1}{C}(i_Z - \frac{x_2}{R}) \tag{3.9}$$

In state space form:

$$\dot{x}(t) = [i_L(t).V(t)]^T \begin{bmatrix} \dot{x}_1 \\ \dot{x}_2 \end{bmatrix} = \begin{bmatrix} 0 & 0 \\ 0 & -1/RC \end{bmatrix} \begin{bmatrix} x_1 \\ x_2 \end{bmatrix} + \begin{bmatrix} 1/L & 0 \\ 0 & 1/C \end{bmatrix} \begin{bmatrix} V_{in} \\ I_Z \end{bmatrix} \tag{3.10}$$

The state space equation for (3.4) and (3.5) will become,

$$\dot{x}_1 = \frac{1}{L}(V_{in} - x_2) \tag{3.11}$$

$$\dot{x}_2 = \frac{1}{C}(i_L + i_Z - \frac{x_2}{R}) \tag{3.12}$$

In state space form:

$$\begin{bmatrix} \dot{x}_1 \\ \dot{x}_2 \end{bmatrix} = \begin{bmatrix} 0 & -1/L \\ 1/C & -1/RC \end{bmatrix} \begin{bmatrix} x_1 \\ x_2 \end{bmatrix} + \begin{bmatrix} 1/L & 0 \\ 0 & 1/C \end{bmatrix} \begin{bmatrix} V_{in} \\ I_Z \end{bmatrix} \tag{3.13}$$

Using perturbation technique linearization of the time varying system given in equation (3.6) is performed by introducing small AC perturbations in DC steady state quantities.

$$x(t) = X + \hat{x}(t) \tag{3.14}$$

$$v_o(t) = V_O + \hat{v}_o(t) \tag{3.15}$$

$$d(t) = D + \hat{d}(t) \tag{3.16}$$

These variables when substituted in (6) give,

$$\frac{d[X+\hat{x}(t)]}{dt}=\{[D+\hat{d}(t)]A_1+[D'+\hat{d}'(t)]A_2\}[X+\hat{x}(t)]+\{[D+\hat{d}(t)]B_1+[D'+\hat{d}'(t)]B_2\}U \quad (3.17)$$

$$V_o+\hat{v}_o(t)=\{[D+\hat{d}(t)]C_1+[D'+\hat{d}'(t)]C_2\}[X+\hat{x}(t)] \quad (3.18)$$

Small signal analysis starts by recognizing that the derivative of steady state component *dx/dt* is zero. By collecting term

$$\frac{d\hat{x}(t)}{dt}=(AX+BV_g)+A\hat{x}(t)+\{[A_1-A_2]X+[B_1-B_2]V_g\}U)+(A_1-A_2)\hat{x}(t)\hat{d}(t) \quad (3.19)$$

$$V_o+\hat{v}_o(t)=CX+C\hat{x}(t)+\{[C_1-C_2]X\}\hat{d}(t) \quad (3.20)$$

where,

$$\begin{aligned} A &= A_1d + A_2d' \\ B &= B_1d + B_2d' \\ C &= C_1d + C_2d' \end{aligned} \quad (3.21)$$

A linear equation is obtained with small changes in the variables as shown below:

$$\dot{\tilde{x}}(t) = A\tilde{x} + B\tilde{u} + E\tilde{d} \quad (3.22)$$

By substituting the above equation in (3.6), the matrices A and B can be obtained.

$$0 = AX + BV_g \quad (3.23)$$

$$V_o = CX \quad (3.24)$$

The final representation using averaging method is given by,

$$\frac{d\hat{x}(t)}{dt} = A\hat{x}(t) + [(A_1 - A_2)X + (B_1 - B_2)U)\hat{d}(t) \quad (3.25)$$

$$\hat{v}_o(t) = C\hat{x}(t) + [(C_1 - C_2)X]\hat{d}(t) \quad (3.26)$$

Thus Equations (3.23), (3.24), (3.25) and (3.26) represent small-signal modeling of DC-DC converter operated in the CCM.

3.2.3. Fuzzy Logic Controller

Fuzzy logic gives the solution for controlling non-linear processes and it is derived from fuzzy set theory [90]. The fuzzy control for the converter chosen is developed using input membership functions for error '*e*' and change in error '*ce'* and the output membership function for Duty cycle, D of the DC-DC boost converter.

$$e = V_r - V_o$$

$$ce = e_k - e_{k-1}$$

where V_r is the desired output voltage and V_o is the actual output voltage measured. The subscript '*k'* denotes values at the beginning of k^{th} sampling cycle, [90].

The fuzzy inference system used here will determine the duty cycle of the boost converter. For instance, if the output voltage fed to the load continues to increase gradually, the fuzzy logic controller will increase the duty cycle of the boost converter accordingly to reach the set point. The resolution of fuzzy logic control depends upon the "fuzziness" of the control variables while the fuzziness of the control variables varies with the "fuzziness" of their membership functions. Fuzzy logic control involves three different stages of evaluation namely: "fuzzification, inference or rule evaluation and defuzzification".

The fuzzy variables '*e*', '*ce*' are taken as input to the fuzzy controller and '*D*' acts as output of fuzzy controller. Table 3.1 gives the fuzzy rule base created in the present work

based on intuitive reasoning and experience. Fuzzy memberships NB, NS, ZE, PS and PB are defined as 'negative big', 'negative small', 'zero', 'positive small' and 'positive big'.

Table 3. 1: Fuzzy Rule Base.

ΔV / ΔP	NB	NM	NS	ZE	PS	PM	PB
NB	NB	NB	NB	NB	NM	NS	PS
NM	NB	NB	NB	NM	NS	PS	PM
NS	NB	NB	NM	NS	PS	PM	PB
ZE	NB	NM	NS	PS	PM	PB	PB
PS	NM	NS	PS	PM	PB	PB	PB
PM	NS	PS	PM	PB	PB	PB	PB
PB	ZE	PM	PB	PB	PB	PB	PB

Table 3. 2: Specifications of DC-DC Boost Converter

S.No	Parameter	Value
1.	Input voltage, V_{in}	12 V
2.	Output Voltage, V_o	24 V
3.	Inductance of L	200 μH
4.	Capacitance of C	10 μF
5.	Resistor, R_L	120 Ω, 360 Ω, 330 kΩ

3.2.4. Design and Simulation

The Simulink model of open loop DC-DC boost converter developed by using set of "state space equations" is shown in Fig. 3.3. The specifications of the converter are given in Table 3.2. The influence of load resistance value on to the output is analyzed

here considering the performance parameters like rise time, peak time, overshoot voltage, steady state error and, and settling time.

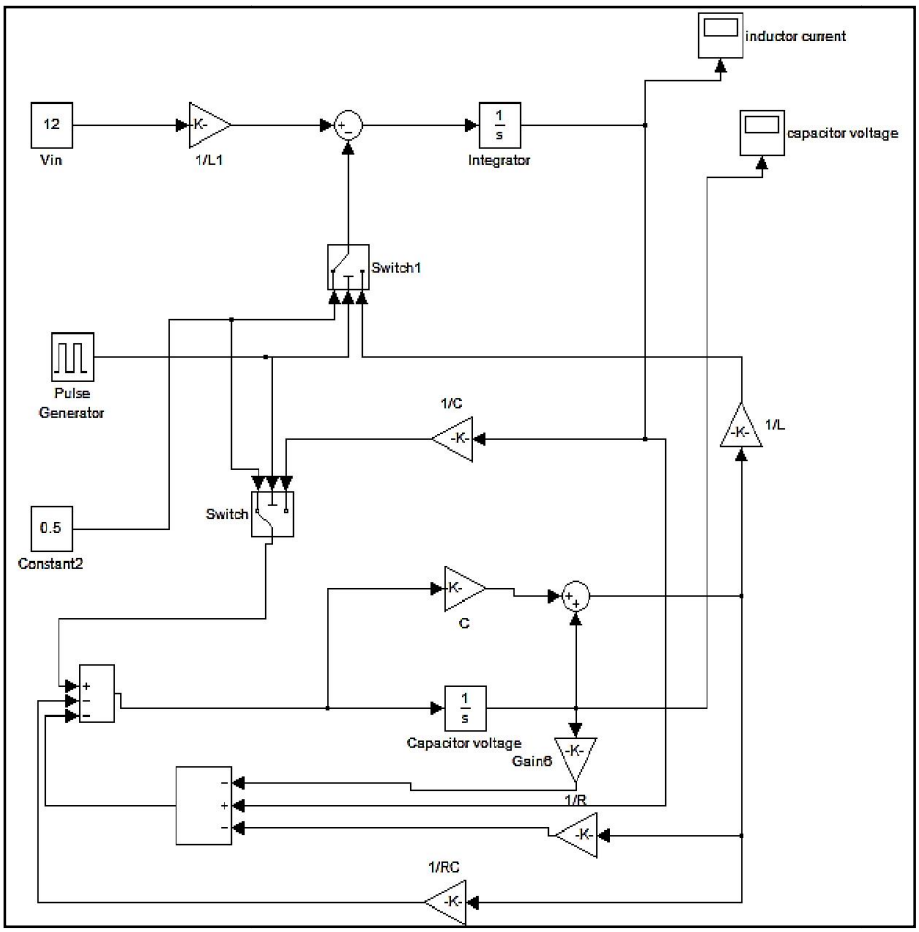

Fig. 3. 3: Open loop model of DC-DC boost converter.

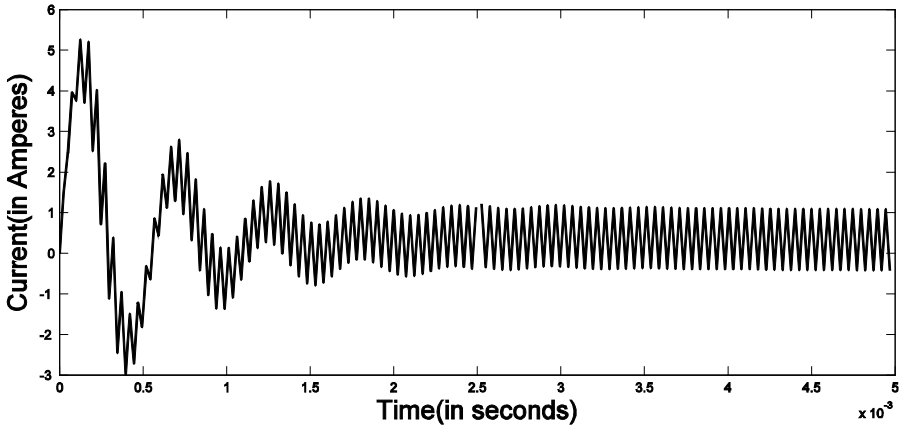

(a)

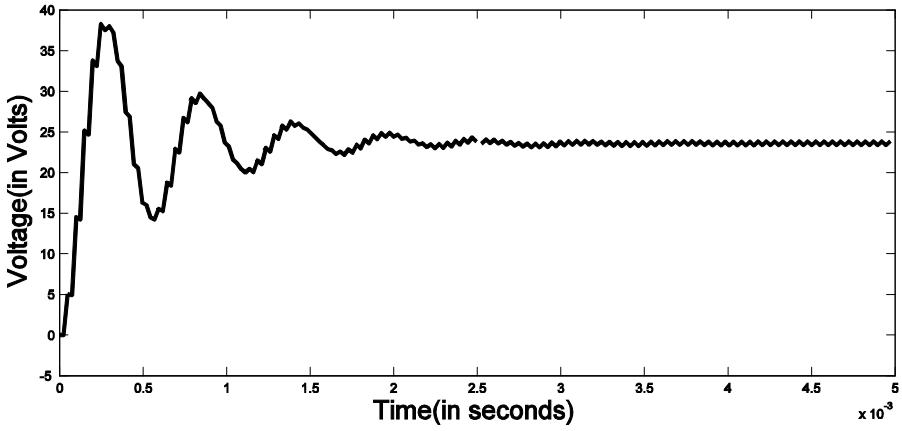

(b)

Fig. 3. 4: Open-loop response of boost converter when load resistance, R_L is 120 Ω

(a) Inductor current (b) output voltage.

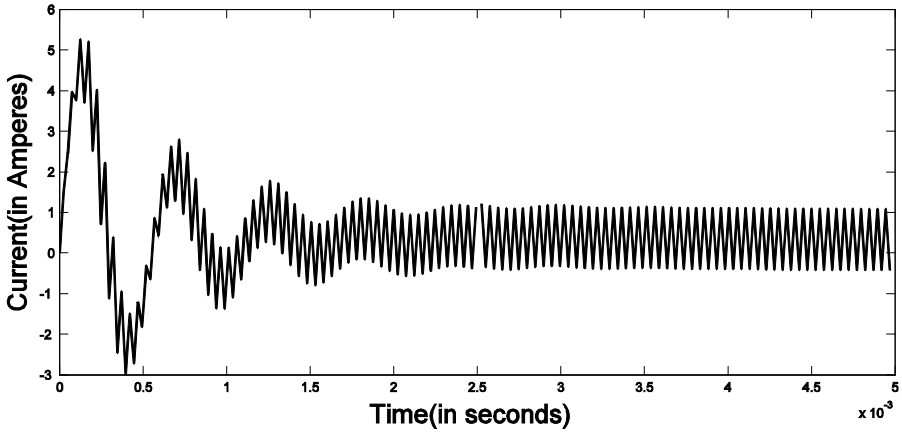

(a)

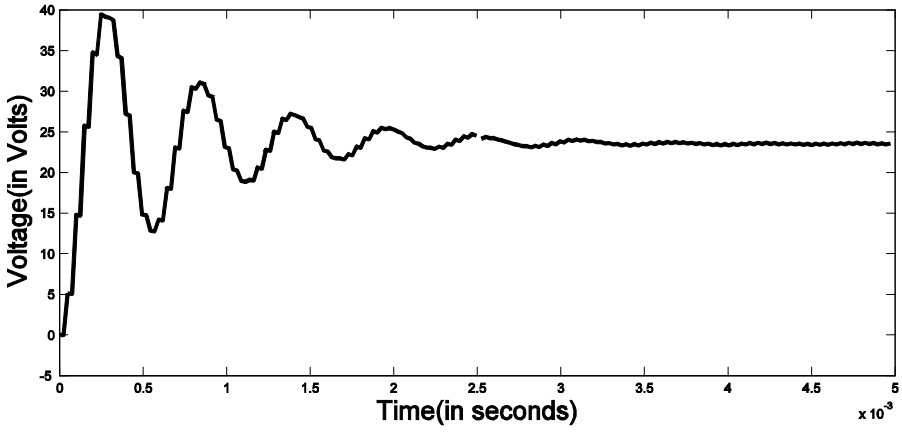

(b)

Fig. 3. 5: Open-loop response of boost converter when load resistance, R_L is 360 Ω

(a) Inductor current (b) output voltage.

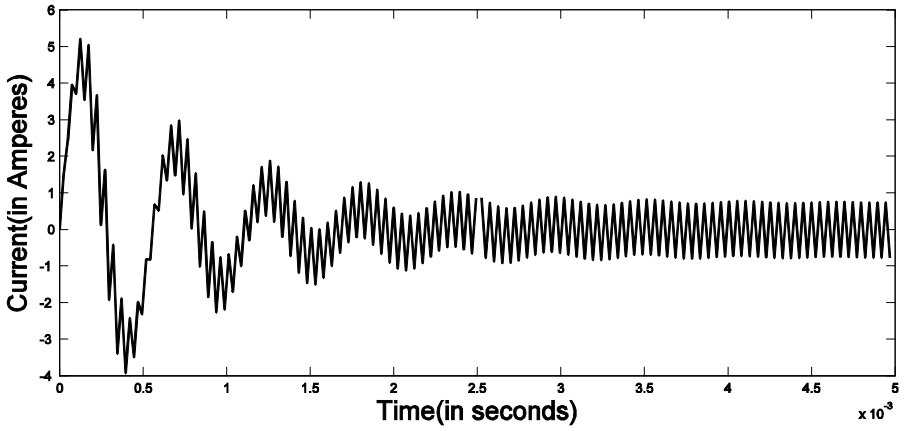

(a)

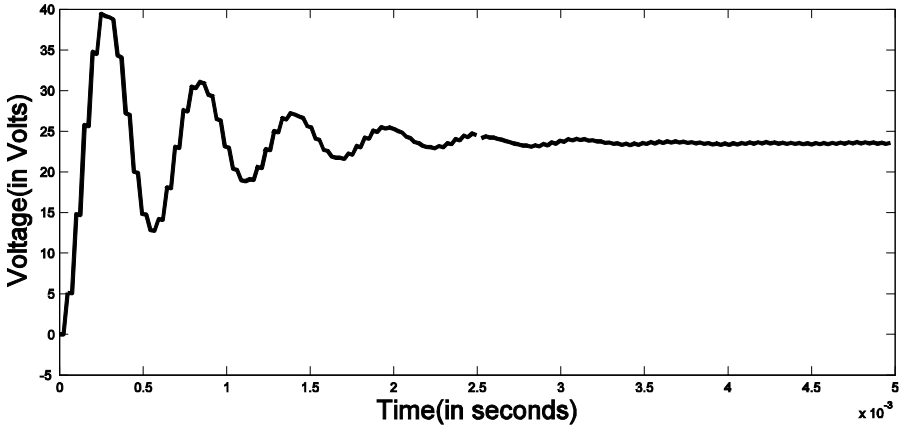

(b)

Fig. 3. 6: Open-loop response of boost converter when load resistance, R_L is 330 Ω

(a) Inductor current (b) output voltage.

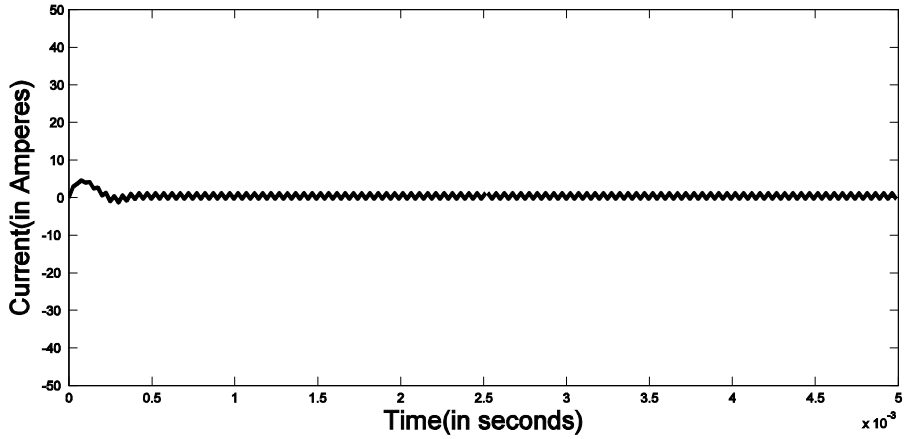

(a)

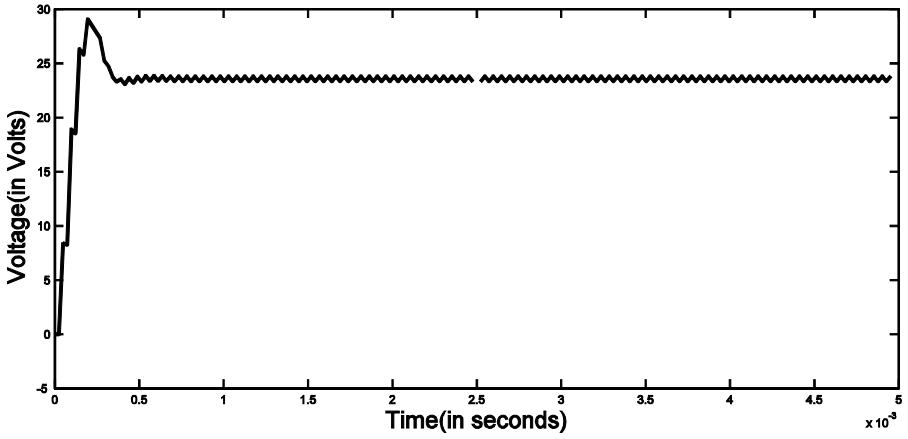

(b)

Fig. 3. 7: Closed loop response of boost converter when load resistance, R_L is 120 Ω

(a) Current through the inductor and (b) Voltage across capacitor

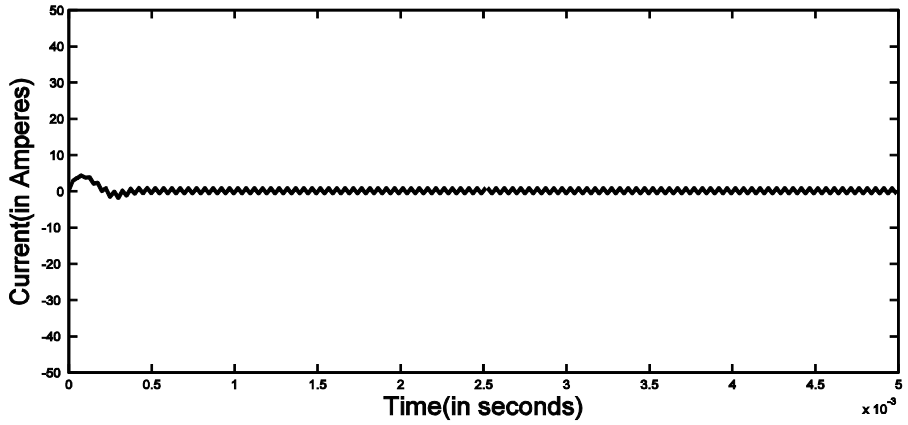

(a)

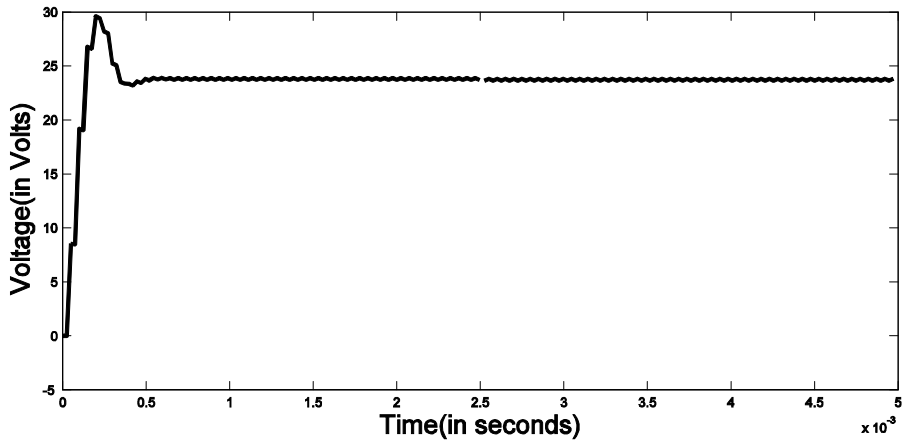

(b)

Fig. 3. 8: Closed loop response of boost converter when load resistance, R_L is 360 Ω

(a) Current through the inductor and (b) Voltage across capacitor

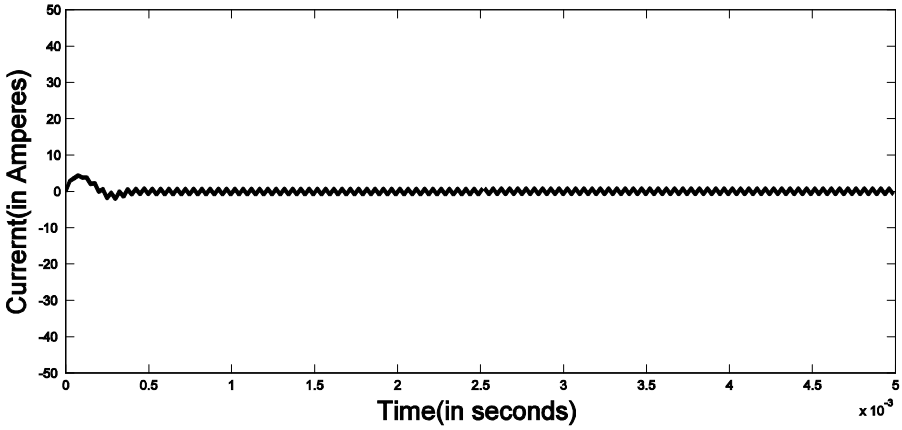

(a)

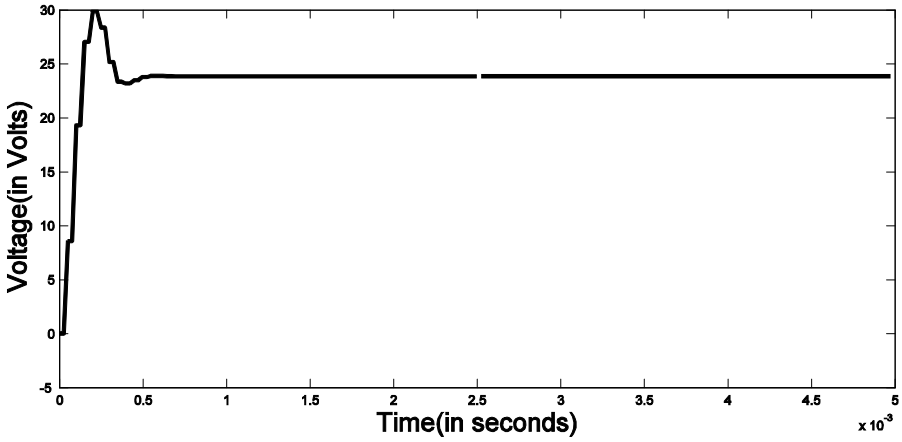

(b)

Fig. 3. 9: Closed loop response of boost converter when load resistance, R_L is 330 Ω
(a) Current through the inductor and (b) Voltage across capacitor

The open loop response of converter namely the inductor current and the output voltage for the corresponding load changes are shown in Figs. 3.4, 3.5 and 3.6 respectively. The output voltage of 24 V is achieved by maintaining the duty cycle at 0.5 for different load changes as shown in Figs. 3.4(a), 3.5(a) and 3.6(a). But the overshoot in the output response is very high and it increases with the increase in load resistance.

In addition to that, there is a presence of steady state error and delay in the settling time and rise time. To improve the performance of the boost converter there is a need for controller, a Fuzzy logic controller is chosen to meet the desired specifications. The

output response of the proposed system for different loads using FLC is shown in Figs. 3.7, 3.8 and 3.9 respectively.

The current through the inductor for different load changes are shown in Figs. 3.7(a), 3.8(a) and 3.9(a), it is observed that the current through the inductor increase with increase in the load. Figs. 3.7(b), 3.8(b) and 3.9(b) shows that the output voltage response of boost converter for different loads. From the voltage response of closed loop system it is observed that the response has is no overshoot, settling time, rise time, delay time, settling time and steady state error are reduced. Hence the overall performance of the system has improved using the fuzzy logic controller.

3.3. Transformer Less High Gain Boost Converter

The topology of Transformer less high gain Boost Converter (TFHBC) is shown in Fig.3.10. It mainly consists of three passive components, namely a resonant inductor, 'L_v'; resonant capacitor, 'C_v'; and the input inductor, 'L_{in}'. The gating signals given to the switches labeled S_1 and S_2 are identical and they are operated simultaneously as in [86]. The purpose of the switching module and resonant capacitor is to control the ON and OFF process of the rectifying diode.

3.3.1. Assumptions

The three assumptions considered in the analysis and operation of circuit are, all the components in the circuit are ideal, all sources over a switching period are constant and the ratio between the input inductor, 'L_{in}', and resonant inductor, 'L_v', should be much greater than '1' so that the input inductor can be assumed as a constant current source.

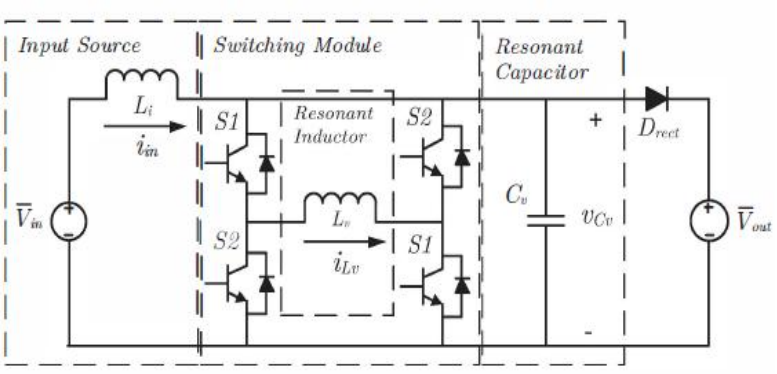

Fig. 3. 10 Transformerless High Boost DC-DC Converter, [86]

3.3.2. Operating Principle

Before the switching cycle begins, the current through the resonant inductor i.e. $i_{Lv}(t)$ is non zero and the voltage across the resonant capacitor i.e. $V_{cv}(t)$ is at 0 V when Switch S_2 is ON. The switching cycle of the converter consists of eight states as discussed below.

State 1: During state 1 S_1switch is turned ON and S_2 switch is turned "OFF"'. This causes the inductor to discharge its energy to the resonant capacitor nearby creating a rise in capacitor voltage $V_{Cv}(t)$ from 0 V to V_{out}.

State 2: When the capacitor voltage reaches to V_{out} state '1' ends which makes the rectifying diode D_{rect} to turn ON. Both the currents, namely I_{in} and $I_{Lv}(t)$ are fed to the load. During this period of the state, V_{out} is applied across the resonant inductor, L_v which causes inductor current to change at a constant rate. As $i_{Lv}(t)$ changes, it passes through zero current crossing and starts to divert I_{in} from the rectifying diode. Once when $i_{Lv}(t)$ equates to I_{in}, the rectifying diode turns OFF and there is no power transfer to the load, this ends State 2.

State 3: The rectifying diode is turned off at the beginning of State 3, but the resonant capacitor is still charged at V_{out} *volts*, which is discharged through the inductor L_v causing its current to increase. When C_v reaches 0 V, voltage is no longer applied to *Lv*, and $i_{Lv}(t)$ stays constant.

State 4: When $V_{cv}(t)$ reaches 0 V, state 4 begins. As there is no voltage applied across L_v, $i_{Lv}(t)$ remains constant during this state. Since there is no transfer of energy between these resonant components it is considered as a hold state.

State 5 to State 8: When switch S_1 is OFF and S_2 is turned ON State 5 begins, the capacitor C_v gets charged from the inductor. States 5 to 8 maintains the same order of events as State 1 to 4, the only difference is $i_{Lv}(t)$ is inverted, $i_{Lv}(t)$ conducts through the opposite half of the H-bridge.

3.4. Modeling of Multilevel Boost Converter

3.4.1. Power Circuit

The power circuit diagram of multilevel boost converter (MLBC) circuit consisting of three levels is shown in Fig. 3.11. It combines the circuit configuration of simple boost converter and switched capacitor technique to provide high voltage gain, as shown in Fig. 3.11. To generate an output which is N times the conventional boost converter the MLBC circuit includes only one MOSFET switch, one inductor, (2N-1) diodes and (2N-1) capacitors, [91]. Though the number of components namely capacitor and diodes are high these devices are of low voltage rating as each device blocks only one voltage level.

3.4.2. Modes of Operation

MLBC circuit operates in two modes, mode-1 when the switch is turned ON and mode-2 when the switch is turned OFF. The sequential operation of MLBC in two modes is given below:

In Mode-1, switch 'S_1' is turned ON, the inductor is connected to the voltage source. At this instant if the voltage across C_2 is less in comparison with voltage across C_1, C_1 charges C_2 through the diode D_2 and the switch. Simultaneously, if the voltage across C_2+C_4 is smaller than the voltage across C_1+C_3, C_1 and C_3 charges C_2 and C_4 through the diode D_4 as shown in Fig. 3.11, [91]. In the same interval the voltage across the capacitors C_1+C_3+C_5 discharges through the load.

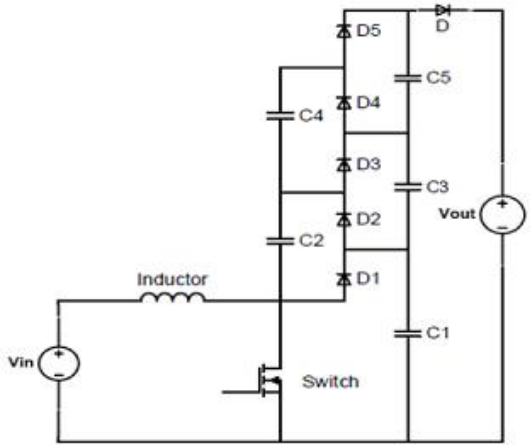

Fig. 3. 11 Multilevel Boost converter circuit, [91]

In Mode-2, switch 'S_1' is turned OFF, the diode D_1 is turned ON and the inductor charges the capacitor C_1 until the voltage across the capacitor $C_1$is equal to the sum of the voltages across the voltage source and the inductor. The voltage source, inductor and capacitor C_2 charges the capacitor C_1+C_3 through the diode D_3. The diode D_3 turns OFF when the voltage being charged is equal to being discharged and diode D5 turns ON. the

Through the diode D_5 the voltage source, inductor and capacitors C_2 and C_4 will charge capacitors C_5, C_3 and C_1 until the voltage until the voltage across discharging elements is equal to the voltage across charging elements, [87].

3.4.3. Design of multilevel boost converter

The design of the passive elements present in the power converter is very similar to that of conventional boost converter. For a conventional boost converter circuit, the relationship between input and output voltage is given by,

$$V_o = \frac{V_{in}}{(1-D)} \tag{3.27}$$

For an N level Multilevel Boost Converter, relationship between input and output voltage is given by,

$$V_o = \frac{NV_{in}}{(1-D)} \tag{3.28}$$

where N indicates the number of levels.

The design specifications are input voltage = 100V, output voltage = 1000V, switching frequency = 20 kHz and output power = 6.8 kW. The number of levels in MLBC that would give a voltage gain of 10, which can be found from equation (3.28). In addition, boost converters with lower levels (N=1, 2, 3) need to be operated at very high duty ratios; sometimes greater than 0.85 to achieve the required voltage gain. This is practically not possible. Hence, the number of levels is increased.

It is proposed to operate MLBC at a duty cycle of 0.75 with 4 levels in order to provide sufficient turn off time for the power device and avoid excessive voltage stress.

Based on the duty cycle and output power, the critical value of the inductance is found from the expression:

$$L_{crit} = \frac{D(1-D)R}{2f} \tag{3.29}$$

The capacitance offered can be found from the following expression, where R is resistance offered by the load, f is switching frequency.

$$C = \frac{D}{2fR} \tag{3.30}$$

3.5. Performance evaluation of TFHBC and MLBC for DC grid integration

A comparative analysis is made between two medium voltage boost converter circuits of same ratings namely TFHBC and MLBC circuits to evaluate the converter with high gain factor, high efficiency and low voltage stress. The specifications of TFHBC and MLBC are given in Table 3.3 and 3.4. Simulation of a four level multilevel boost converter is performed in MATLAB/Simulink environment to generate an output voltage of 1 kV. A DC input voltage of 100 V is applied to both the converters. The inductance, capacitance and duty cycle of MLBC are chosen as 1.2 mH, 35 μF and 0.6 to achieve a gain factor of 10. The output power delivered to the load is 8.35 KW. In MLBC the voltage across the individual capacitors is shown in Fig.3.12.

The input voltage of MLBC, voltage across the load is shown in Fig.3.13. The input current and the current delivered to the load are shown in Fig.3.14. From Fig. 3.12 it is observed that the voltage across capacitors C_1, C_3 C_5 and C_7 are 330 V, 250 V, 215 V and 205 V respectively. It is shown that voltage across the load is the algebraic sum of the voltages across the individual capacitors connected across it, i.e. $V_{C1}+V_{C2}+V_{C5}+V_{C7}$.

As shown in Table 3.5, the efficiency of MLBC is around 99.4%. The individual voltage across each capacitor is not exceeding 400 V. It is observed that though the output voltage is 1000V the voltage stress across the switch is only around 330 V.

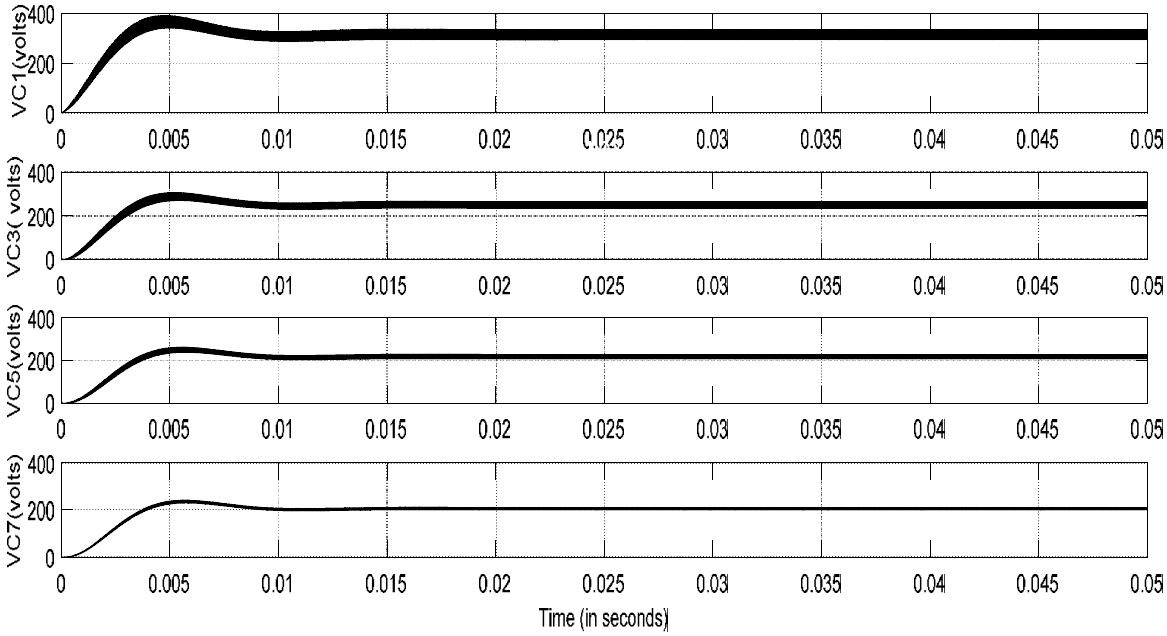

Fig. 3. 12: Voltage across capacitor C_1, C_3, C_5 and C_7 in MLBC.

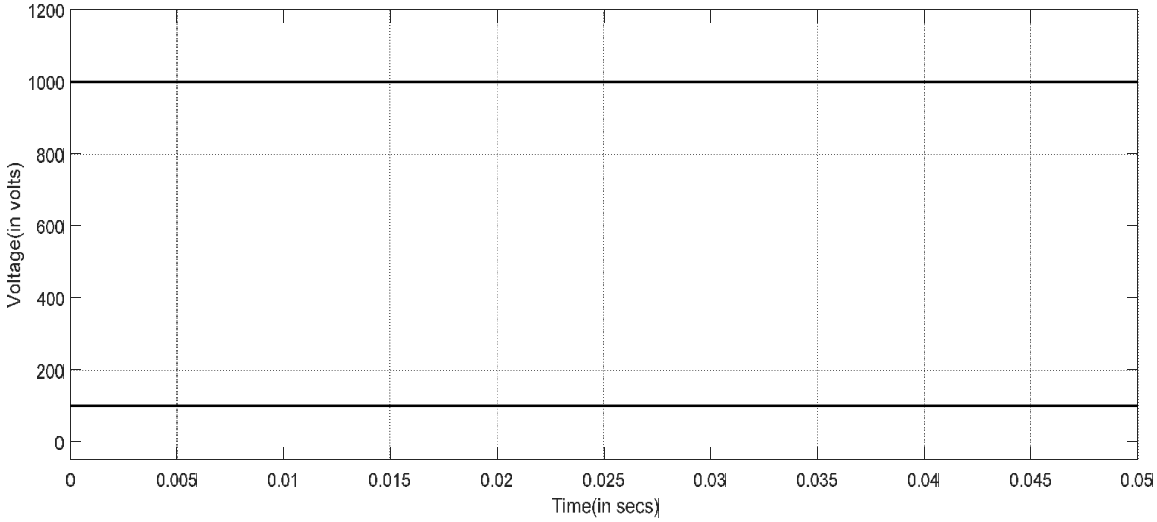

Fig. 3. 13: Input voltage, voltage across the load in MLBC.

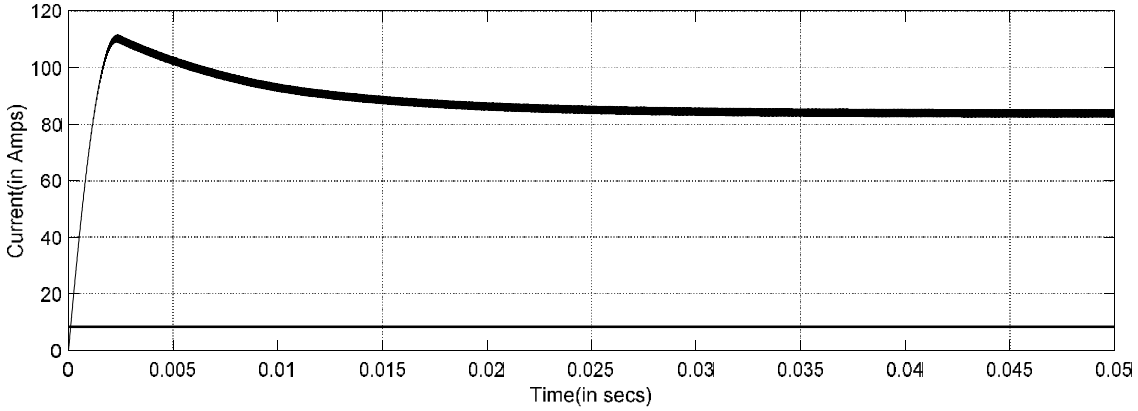

Fig. 3. 14: Input current, load current in MLBC.

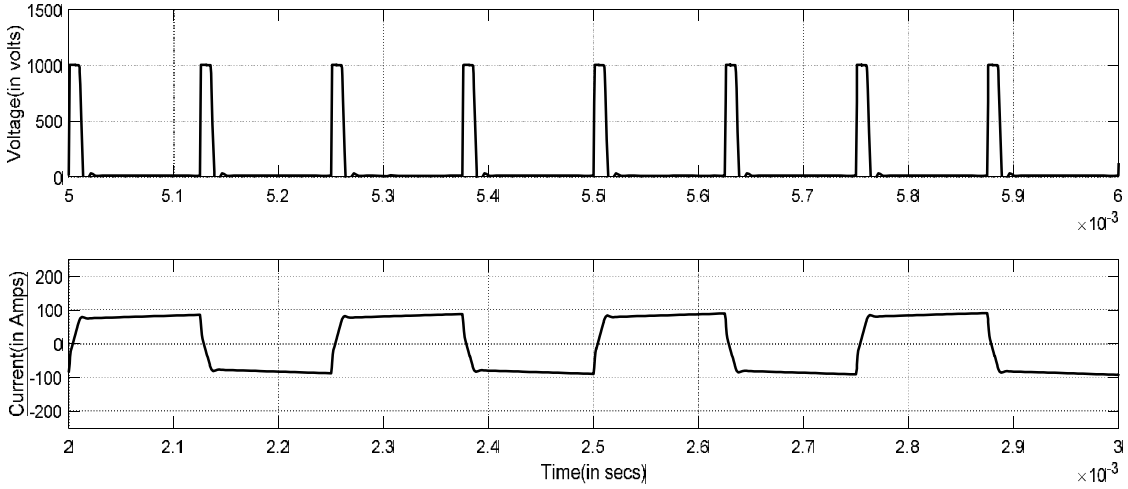

Fig. 3. 15: Voltage across capacitor C_1, current through the resonant inductor in TFHBC.

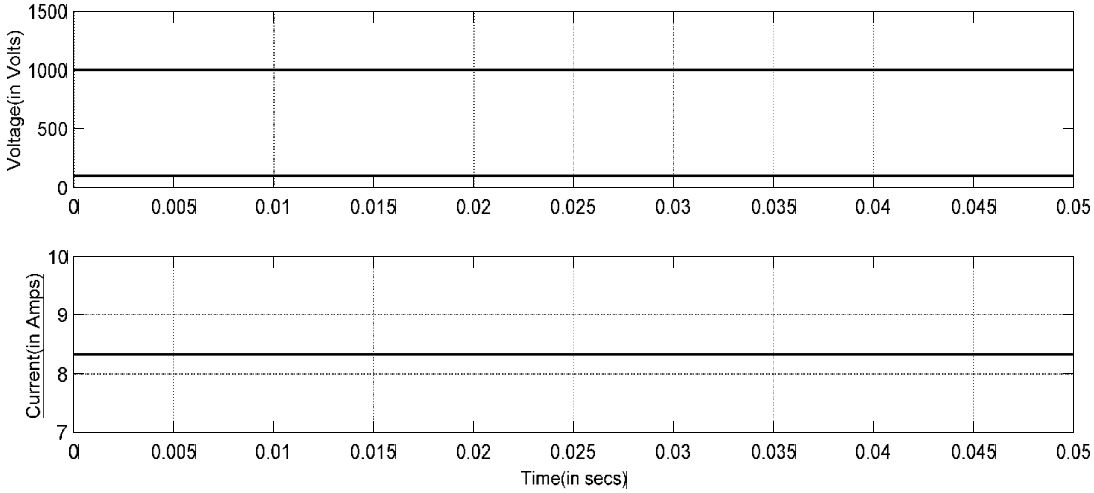

Fig. 3. 16: Voltage across the load, Input Voltage, Current through the load in TFHBC.

The performance of MLBC is compared with Transformer less high gain boost converter circuit. To generate an output voltage of 1 kV, 100 V DC input is given to the TFHBC circuit. The voltage across the capacitor, input current through the resonant and series inductor are shown in Fig.3.14 and 3.15. The voltage across the load and current drawn by the load is shown in Fig. 3.16. The Input current through series inductor of TFHBC is shown in Fig. 3.17.

From the results it is observed that the input and output currents of TFHBC circuit are 91.2 A and 8.35 A respectively. The output power delivered to the load is 8.35 KW maintaining an efficiency of 91.55%.

On comparing the results obtained by both the converters for the given specifications from Table 3.5, it is observed that the performance of MLBC is much better when compared to Transformerless high gain boost converter. For the given load, the efficiency of MLBC is 99.4%, whereas for TFHBC circuit it is 91.55%. The voltage gain of MLBC can be increased further by increasing the number of levels which includes addition of capacitor and diodes whereas in TFHBC difficulty will arise in choosing the capacitor of such high voltage rating and voltage stress across the switch will also be increased. The use of multilevel boost converter (MLBC) requires only low voltage devices as each device blocks only one voltage level, the voltage stress across the switch is also less for MLBC. The voltage stress across the switch is around 330 V in MLBC and it is nearly 1 kV in the latter case.

In addition to it, multiple sources can be connected to MLBC converter making this an attractive topology for renewable energy conversion. In addition to the above said advantages MLBC topology offers continuous input current, large conversion ratio

without maintaining extreme duty cycle. To achieve desired voltage level, either we can vary the number of levels or vary the duty cycle, but in TFHBC circuit duty cycle is fixed at 0.5, there is no control over duty cycle.

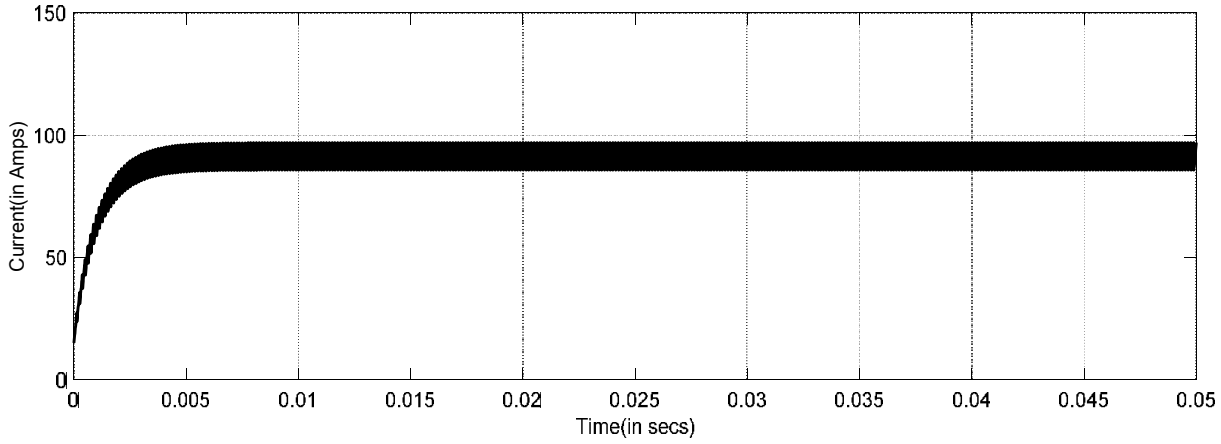

Fig. 3. 17: Input current through series inductor in Transformer less high boost DC-DC converter.

Table 3. 3: Transformerless High Gain Boost DC-DC Converter Specifications.

S.No	Converter Component	Value
1.	Lv	100 µH
2.	Lin	1 mH
3.	Cv	0.025 µF

Table 3. 4: Multilevel Boost Converter Specifications

S.No	Parameters	Rating
1	Inductor	500mH
2	Capacitor	105µF
3	Switching Frequency	20kHz
4	Input Voltage	1000V
5	Output Voltage	20000V
6	Duty Cycle ,D	0.6

Table 3. 5: Performance Specifications of MLBC and TFHBC

S.No	Parameter	Multilevel Boost Converter	Transformer less High Boost DC-DC Converter
1.	Vin	100 V	100 V
2.	Vo	1000 V	1000 V
3.	Iin	83.8 A	91.2 A
4.	Io	8.35 A	8.35 A
5.	Gain, G	10	10
6.	Efficiency, η	99.4	91.55

3.6. LCL DC-DC Boost Converter Topology

The circuit topology of DC-DC LCL Boost converter is shown in Fig. 3.18, [92]. It is built for two phases, can be extended to multiphase depending upon the application. The primary goal of the chosen LCL DC-DC converter is the controllable transfer of power from low voltage circuit to high voltage circuit; in addition to that, it maximizes the converter efficiency by eliminating the inner reactive current circulation which is achieved by matching voltage profiles. Issues associated with iron losses and manufacturing of medium and high frequency transformer are eliminated due to the absence of transformer. The converter circuit consists of DC-AC bridge with switches S_1, S_2, S_3, S_4, and the inner layer consisting of elements L_1, L_2 and C and DC-AC bridge of high voltage rating with switches S_5,S_6, S_7 and S_8.

The subscripts 1 and 2 in the Fig. 3.16 represents ports 1and 2. The transferred DC power is controlled in port1 whereas port-2 issued to align central AC voltage in line with the coordinate frame i.e. V_{cq}=0; which maintains power balance inside the converter. Under normal steady state $V_{cq}(pu)$ will be maintained at zero by port-2.In case if V_{cq}(pu)

exceeds zero then there is surplus injection of power will occur effecting the reference power. The performance of the converter in HVDC grid connected application will be discussed in chapter 6.

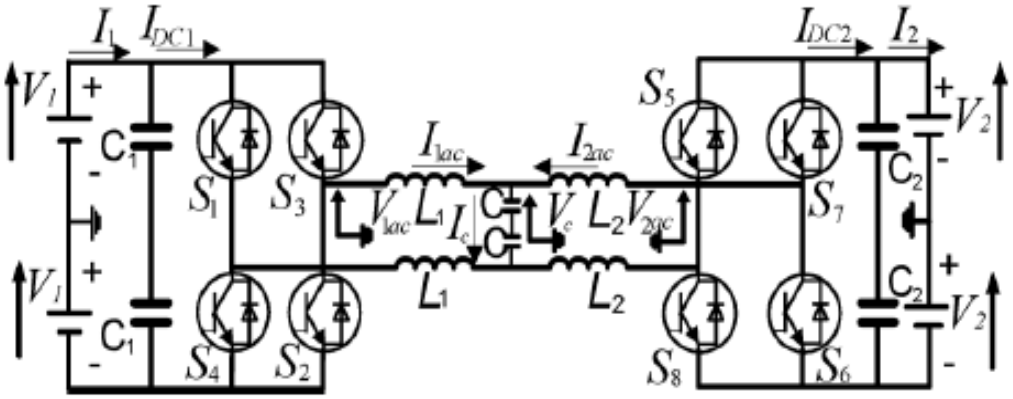

Fig. 3. 18: LCL DC-DC Boost Converter Topology for Two Phase, [92]

3.7. Summary

In this chapter a literature review is conducted on different DC-DC boost converters, in order to choose DC-DC boost converters for application in DC grid integration of solar PV and wind farms. The performance of the converters chosen is validated for low and medium voltage applications.

The open loop and closed loop operation of conventional DC-DC boost converter is analyzed using small signal mathematical modeling. From the simulation results it is observed that the corresponding change in the load resistance affects the output voltage and inductor current of the converter. The open loop response of boost converter offers large overshoot, large delay time, settling time and peak overshoot. Using fuzzy controller in closed loop operation, the performance of the system has improved the over shoot, steady state error, settling time, rise time, delay time are reduced.

A comparative study between two high voltage gain DC-DC boost converters for medium voltage applications is performed in this work. From the simulation results it is noticed that multilevel boost converter offers, a low voltage stress across the switch, continuous input current, higher efficiency than transformer less high gain boost DC-DC converter. It is easier to achieve high voltage gain in MLBC either by adjusting its duty cycle or by increasing the number of levels whereas in transformer less high gain boost DC-DC converter, the voltage stress across the switch and the rating of the capacitor will increase with its gain factor which increases the complexity in design and operation. LCL DC-DC converter is chosen for high voltage application, as it has the capability to achieve high stepping ratio at high power in high voltage DC grid connected applications..

Chapter-4

Performance Evaluation of Hybrid Controller

4.1. Introduction

In the previous chapter different DC-DC Boost converters needed for DC grid integration of RES are discussed. In the present chapter a novel topology to integrate solar and wind farms to high voltage DC grid is proposed. The proposed topology consists of a hybrid controller. The need for hybrid controller and its working are discussed. The Hybrid controller consists of Maximum Power Point Tracking (MPPT) controller along with voltage regulator, the MPPT controller helps in harnessing the maximum power at varying weather conditions whereas the voltage controller helps in reducing the distortion in output voltage. Different MPPT techniques namely Incremental Conductance, Perturb and Observe, Fuzzy logic and Random Search Method (RSM) based MPPT are discussed here. A comparative study is performed among these techniques to determine the efficient MPP tracker. In this chapter a voltage controller using RSM based two loop averaged current control (TLAC) technique is proposed. The performance of the proposed RSM based (TLAC) is compared with linear Proportional and Integral controller.

4.2. Need for Hybrid Controller

When renewable energy sources are connected to DC grid two major issues faced by the system are unreliable input and fluctuating grid voltage. As the input fed to the renewable energy sources namely solar and wind are unreliable it is necessary to operate

the system at a point where the maximum power can be extracted. To extract maximum power output from the PV panel MPPT control logic is commonly used. Likewise when RES are connected to DC grid, the output voltage fed to the grid should match with grid voltage, as the grid voltage fluctuates slightly due to the presence of disturbance, a regulated DC output according to grid requirement need to be fed. This is done by using a voltage controller.

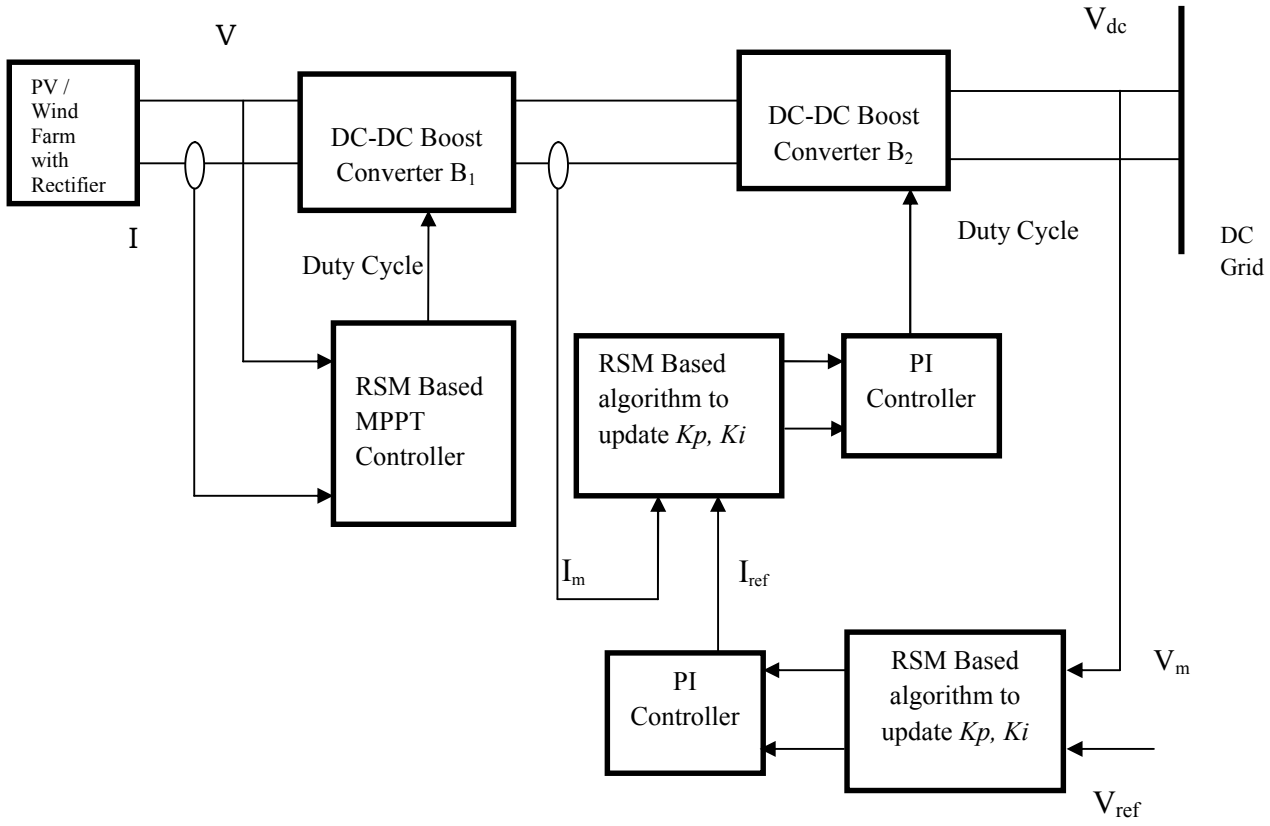

Fig 4. 1: Hybrid control architecture for PV and wind Farms in DC Grid Connected Applications.

The Hybrid controller proposed in the present system performs both MPPT tracking and voltage regulating action as shown in Fig. 4.1. The MPPT controller uses random search method (RSM) to track the global maximum power point and voltage regulating action is performed by using RSM based two loop average current (TLAC)

controller, which is used to maintain stable DC output irrespective of grid side disturbances.

When MPPT controller is used at converter B_1 the output voltage and current will have some perturbations due to change in the duty cycle of the converter, which will affect the performance of converter B_2 connected in cascade. The linear PI controller when used as a voltage controller will not consider the influence of input side perturbations due to which system performance will get detoriated.

The RSM based two loop average current controller proposed here will consider the influence of input side perturbations and grid side disturbances into account and maintains a stable DC output according to the grid demands. So, TLAC controller is chosen for the design of voltage regulator. Both these control actions i.e. MPPT control and voltage regulating action are achieved with the help of independent duty ratio control of DC-DC boost converters.

4.3. MPPT Controller

Conceptually, MPPT is a simple problem—it is basically an operating point matching between the source and power converter. The main objective of MPPT is to efficiently extract maximum power from the source to the load. According to maximum power transfer theorem, the output power delivered to the load is maximum when the impedance offered by the source matches with the load [93]. Hence the maximum power point tracking problem reduces to an impedance matching problem where the system should be operated at a point where the impedance offered by the source and the load seen by it are equal.

However, because of the non-linear input characteristics of the solar and wind farms and the consequence of the varying environmental conditions, tracking the correct maximum power point (MPP) can sometimes be a challenging task. Over the years, many MPPT techniques have been proposed by the researchers; which is evident from the increase in the number of research publications. The main objective of the MPPT algorithms is to achieve accurate and fast MPP tracking with reduced steady state oscillations at varying weather conditions. Among different MPPT techniques proposed in literature [94], more focus is on perturb and observe (P&O) [95], hill climbing [96], and incremental conductance (INC) methods [97]. It has been observed that the traditional methods of MPPT suffer from problems like oscillations around the operating point, complexity in operation, designer dependency and many computational difficulties.

Improved versions of perturb and observe are proposed in [98-100] but they have the drawback of being slow and generating perturbations under steady-state. To overcome the above-mentioned drawbacks, several methods have been proposed using artificial intelligence (AI)-based algorithms such as neural network (NN) [101] and fuzzy logic controller (FLC) [102]. But they face difficulties like large data storage requirement and extensive computation [103]. The calculation of error and change in error leads to increase in time response and decrease in accuracy of the MPPT to track the MPP, when FLC algorithm is implemented in digital controller addition of its noise factor would result in high oscillations in the output. So adaptive perturb and observe technique is proposed in [104] which combines advantages of P&O and FLC algorithms. Particle swarm optimization (PSO) technique [105], [106], and its improved versions like Firefly algorithm (FA) and Artificial Bee Colony (ABC) [107], [108], are developed to track the

Maximum Power Point (MPP) of a solar cell module, they have major advantage of being simple computational steps, guaranteed global convergence and easy to implement in hardware. But the viability of exploration of other optimization algorithms is not reported in the available literature. So, a derivative free optimization algorithm method namely random search method (RSM), based tracking algorithm is chosen for tracking Global Maximum Power Point [109]. It has simple computational structure, derivative free and it guarantees global convergence if the parameters are properly chosen in algorithm [110].

4.4.1. Incremental Conductance Technique

According to incremental conductance technique, when the incremental conductance, dI/dV is equal and opposite to the conductance offered, I/V then MPP is reached and there the algorithm ends and returns the corresponding value of operating voltage for maximum power point [97]. The major problem associated with this technique is that it requires many sensors to sense the operating voltage and current. The incremental conductance algorithm is shown in Fig. 4.2.

$$P = V \times I \tag{4.1}$$

Differentiating with respect to voltage

$$\frac{dP}{dV} = d(V \times I) \tag{4.2}$$

$$\frac{dP}{dV} = I + V \times \frac{dI}{dV} \tag{4.3}$$

When the maximum power point reaches zero then the condition will be:

$$\frac{dP}{dV} = 0 \tag{4.4}$$

Substitute equation (3) in (4)

$$I + V \times \frac{dI}{dV} = 0 \tag{4.5}$$

$$\frac{dI}{dV} = -\frac{I}{V} \tag{4.6}$$

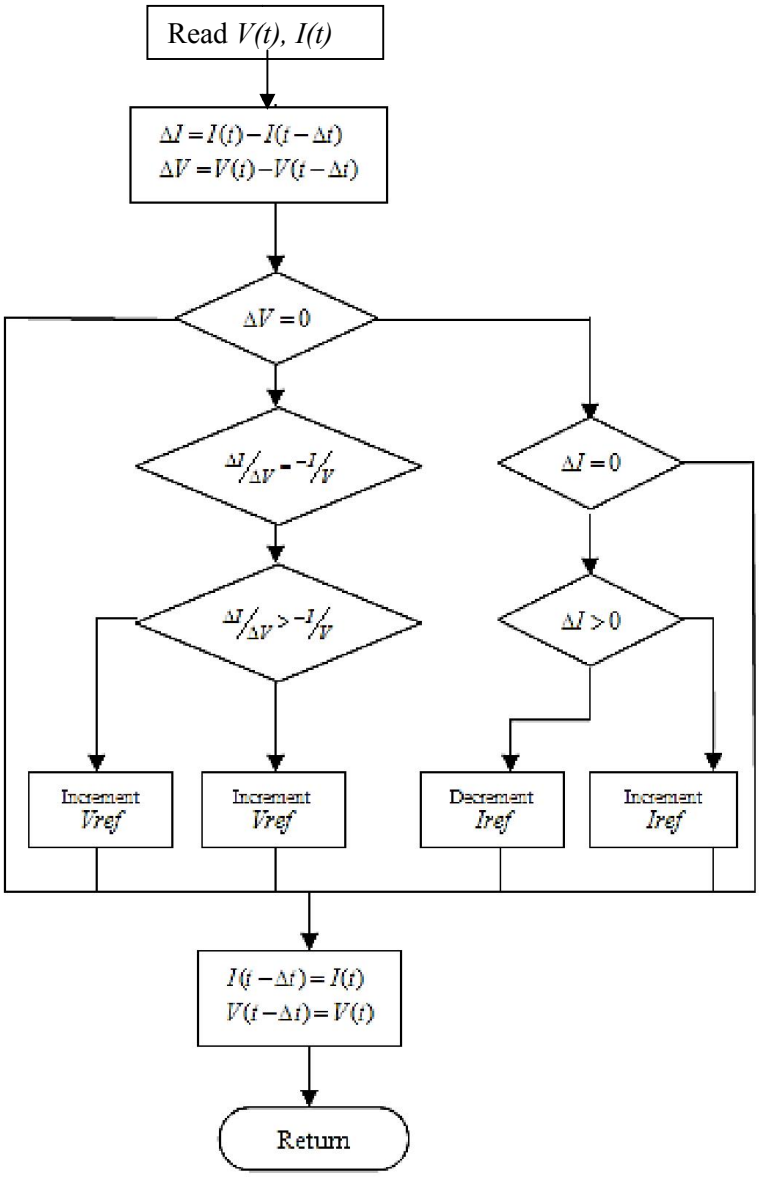

Fig 4. 2: Flow chart of MPPT control using Incremental conductance technique.

4.4.2. Perturb and Observe Technique

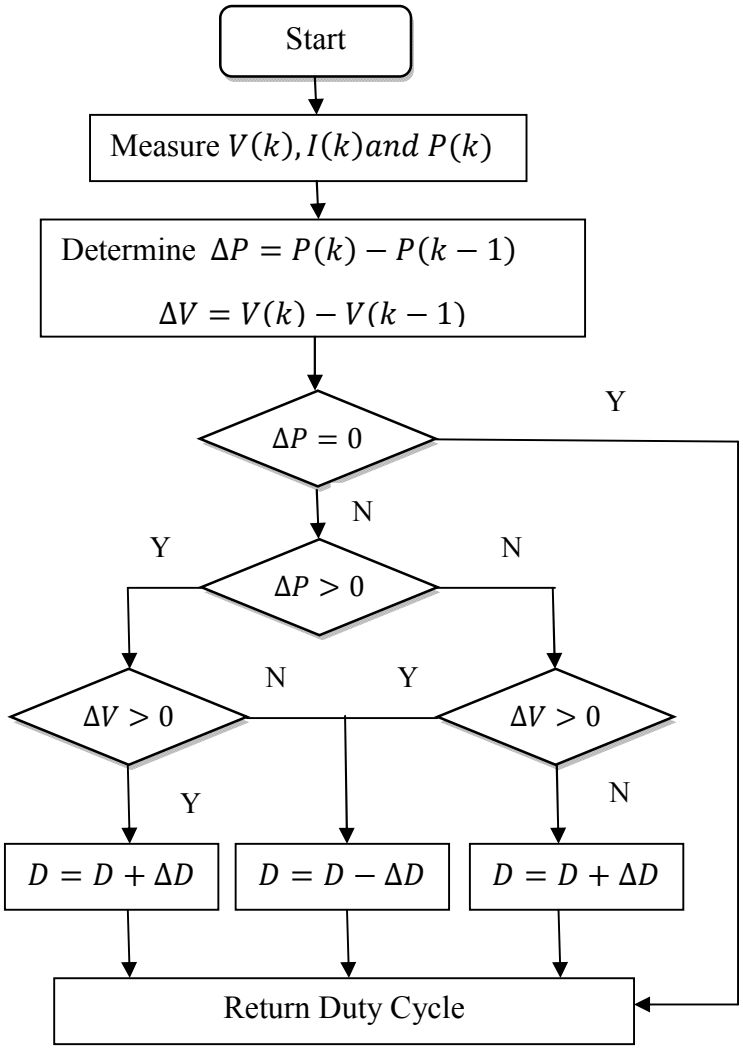

Fig 4. 3: Flowchart of Perturb and Observe Technique.

It is derived from hill climbing method. The flowchart for P&O algorithm is shown in Fig.4.3. In P&O technique the PV panel's output voltage and current are measured to calculate the corresponding power, [100]. A voltage perturbation is introduced by updating the duty cycle and the corresponding power is measured again. From those two steps the change is power is computed and if the change is positive, then the voltage is perturbed in the same direction as earlier, once if the change in power is negative then the direction of the voltage is changed as shown in Fig. 4.4. This process

continues until that maximum power point is attained. In this algorithm the change in duty cycle is maintained constant throughout the operation. But it has a drawback that the operating point keeps oscillating around the MPP.

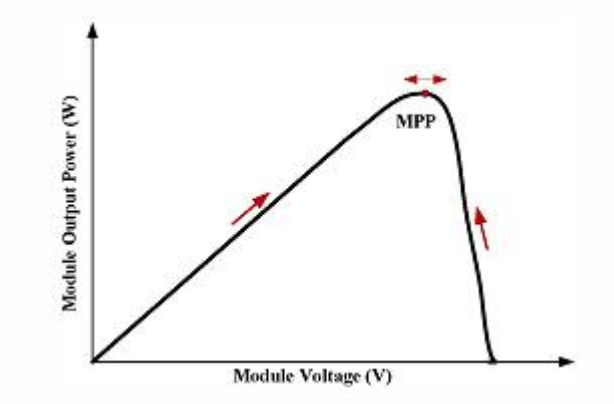

Fig 4. 4: P-V curve of a solar PV module, [100].

4.4.3. Fuzzy based MPPT technique

Unlike constant irradiation, where uniform shading conditions exists in PV system, under variable irradiations, global and local MPPs exist. Traditional algorithms like P&O algorithm or hill climbing techniques when used for tracking MPP the operating point oscillates around "global maxima". The FLC controller can be able to find the optimal point using the "expert knowledge". FLC implementation involves three basic steps namely "Fuzzification, Inference, and Defuzzification" as shown in Fig. 4.5. During "Fuzzification" input variable are changed to linguistic variables like NEB, NES etc. which represents negative extreme big, negative extreme small. The "inference mechanism" makes use of "fuzzy rule base" given in Table 4.1, for generating the output. "Mamdani fuzzy inference" is used for FLC, [102]. During "defuzzification" all the generated outputs of each rule are accumulated to produce a "crisp output" in numerical form, "common centroid method" is frequently used method for this step.

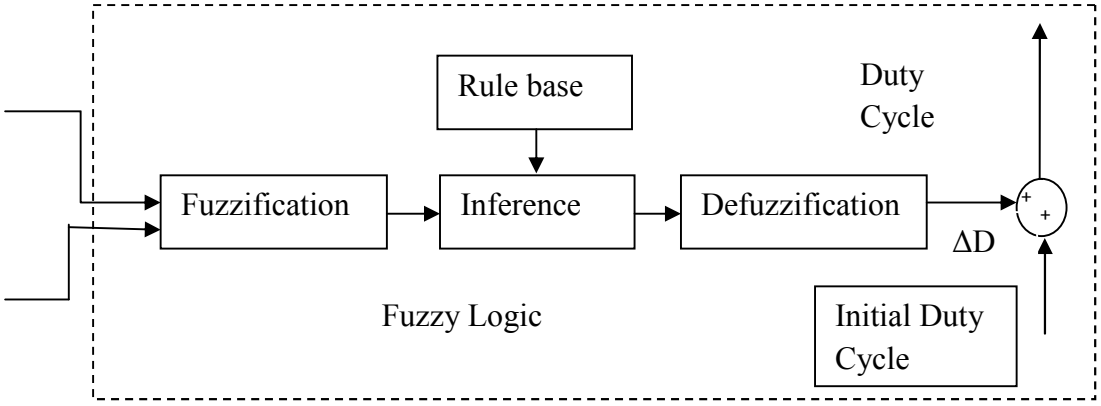

Fig 4. 5: Fuzzy MPPT Control logic.

Table 4. 1:Fuzzy rule base.

e / Δe	NB	NS	ZE	PS	PB
NB	ZE	ZE	PB	PB	PB
NM	ZE	ZE	PS	PS	PS
ZE	PS	ZE	ZE	ZE	NS
PM	NS	NS	NS	ZE	ZE
PB	NB	NB	NB	ZE	ZE

4.4.4. Random Search Method based MPPT Technique

Random Search Method is a direct search method that does not have any derivatives in its algorithm which makes computation very simple [110]. As many compilers that we work are associated with digital controllers and computer libraries have random generators, RSM method can be used either in maximization/minimization of optimization problems. Consider a function, $f(X_1, X_2, ...X_n)$ with n variables, which is to be maximized using RSM method. The step by step procedure is given below [109]:

1. Set iteration count, k as one. Set an arbitrary number to each variable x_i^k in between the limits $x_{i,\min}$ and $x_{i,\max}$. For a problem of dimension *'n'*, the function value is given by $f^k = f(X_1^k, X_2^k, \ldots . X_n^k) = f(X^k)$

2. Generate *'n'* random numbers $r_1, r_2, \ldots . r_n$, which are lying in the interval [−1, 1] and find the unit vector '*u'* given by,

$$u = \frac{1}{(r_1^2 + r_2^2 + \cdots + r_n^2)^{(1/2)}} \begin{Bmatrix} r_1 \\ r_2 \\ \vdots \\ r_n \end{Bmatrix} \tag{4.7}$$

3. Identify new vector X^{k+1} for the next iteration, and the function values using (4.8) and (4.9), where 'λ' is initial step length.

$$X^{k+1} = X^k + \lambda u \tag{4.8}$$

$$f^{k+1} = f(X^{k+1}) \tag{4.9}$$

4. Examine the values of f^{k+1} and f^k ›. If, $f^k > f^{k+1}$ updat the new values for *'x'* and '*f*' as in (4.10) and (4.11) and then go to step 2; else step 5.

$$X^{k+1} = X^k \tag{4.10}$$

$$f^{k+1} = f^k \tag{4.11}$$

5. If count of iteration, *k* is less than or equal to *N*, update '*k' as 'k* + 1' and find the new step length '$\lambda = \lambda \times q$'. Go to step 2 if new step length is greater than 'ε', the minimum allowable step length; else step 6. Here, '*q*' is a constant value within the interval [0, 1].

6. Stop the iteration and take the optimal solution $X^{opt} = X^{k+1}$.

4.4.5. Application of RSM for GMPP of PV systems

RSM technique is preferred in computing MPPT as it becomes competitive in cases where there is a limited memory available and the function to be optimized has multiple peaks. The step by step procedure of RSM towards MPPT is given below [109]:

1. Initialize step length 'λ', minimum allowable step length '$\in$'and a constant value '*m'* within the interval [0, 1].
2. In this step a random duty cycle 'd^k' is generated within the interval [$d_{\min}$, $d_{\max}$] which is given as input to the pulse generator of DC–DC boost converter and '*Vpv'* and '*Ipv'* of the solar array are sensed after allowing a reasonable settling time and then power output of PV system, 'P_{pv}^k' are computed.
3. Generate a random number 'r_1' within the interval [−1, 1] where $u = r_1$.
4. Compute new duty cycle; $d^{k+1} = d^k + \lambda \times u$ and find the corresponding power output of PV system, P_{pv}^{k+1}.
5. Compare the values of P_{pv}^{k+1} and P_{pv}^k. If $P_{pv}^{k+1} < P_{pv}^k$, set the new values as $d^{k+1} = d^k$ and $P_{pv}^{k+1} < P_{pv}^k$ and go to step 3; else go to step 6.
6. If $\lambda \leq \varepsilon$, stop the program and go to step 7; else set $\lambda = \lambda \times q$ and go to step 3.
7. Take the optimal duty ratio $d^{opt} = d^{k+1}$ at GMPP.

4.4.6. Comparison of MPPT Techniques

To evaluate the performance of different MPPT Techniques PV array fed DC-DC Boost Converter is chosen here. The specifications of each PV module are given in Table 4.2; five such modules are connected in series and sixty six of them in parallel to form an

array. At constant irradiation it generates a power output of 100 kW. The I-V and P-V characteristics of PV array at 25 ^{o}C under different irradiations are shown in Fig. 4.6.

DC-DC Boost converter is designed to handle a power of 100 kW. The specifications of the boost converter are given in Table 4.3. For a constant irradiation of 1000 W/m^2, PV array generates an output voltage of nearly 260 V which is stepped up to a voltage of nearly 525 V using conventional boost converter circuit. If the input irradiation varies as shown in Fig. 4.7, then the voltage and current response of converter are shown in Fig.4.8 and 4.9. From the results it is observed that at an irradiation of 1000 W/m^2 an output voltage of 525 V is generated as the irradiation varies the output voltage varies in proportion to that.

Different MPPT techniques like incremental conductance, perturb and observe, fuzzy logic control and random search method are used to track the maximum power from the PV array as shown in Fig. 4.10. It is observed that there are some oscillations in the output response when P&O technique is used because of the perturbations in duty cycle. The incremental conductance based MPPT creates huge transient response during starting and tracks the maximum power thereafter. Fuzzy logic control based MPPT is able to track the maximum power but its performance is not satisfactory at higher irradiance level. RSM based MPPT controller is able to track the maximum power at different irradiations with good tracking efficiency when compared to other MPPT controllers.

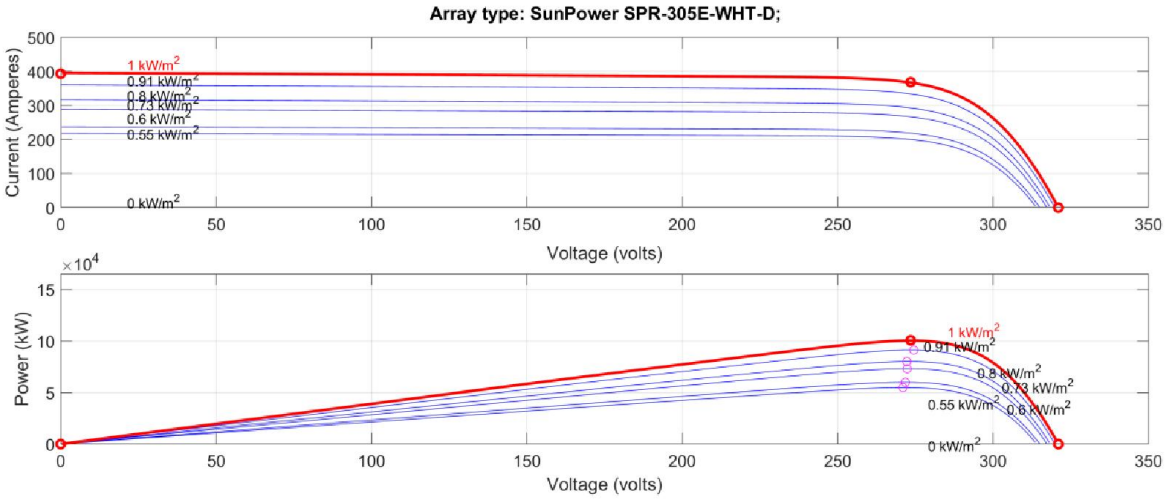

Fig 4. 6: I-V and P-V curves of solar PV array.

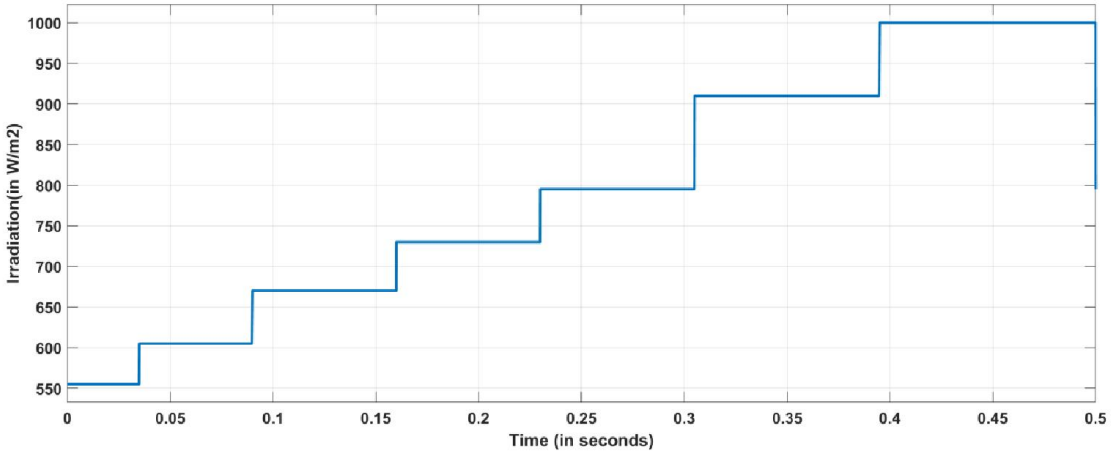

Fig 4. 7: Variable input irradiation.

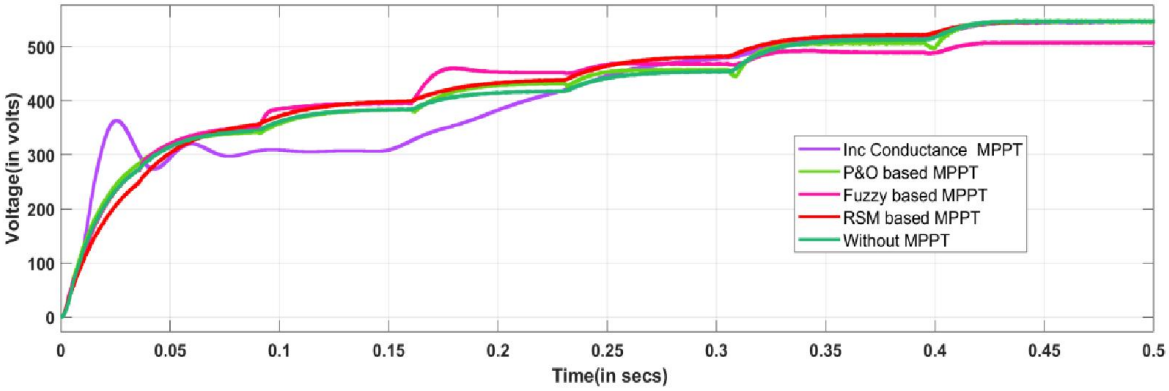

Fig 4. 8: Voltage response of boost converter for variable irradiation using different MPPT techniques.

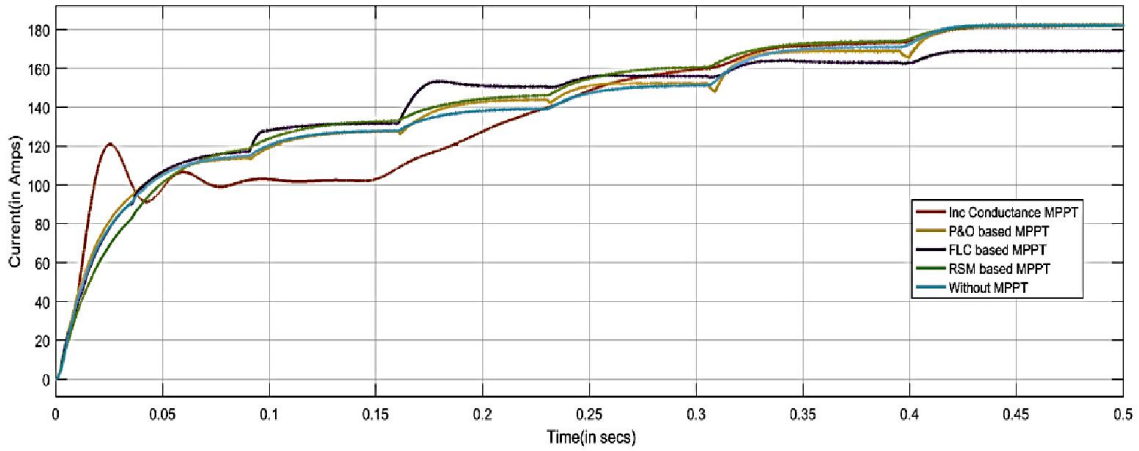

Fig 4. 9: Current response of boost converter for variable irradiation using different MPPT techniques.

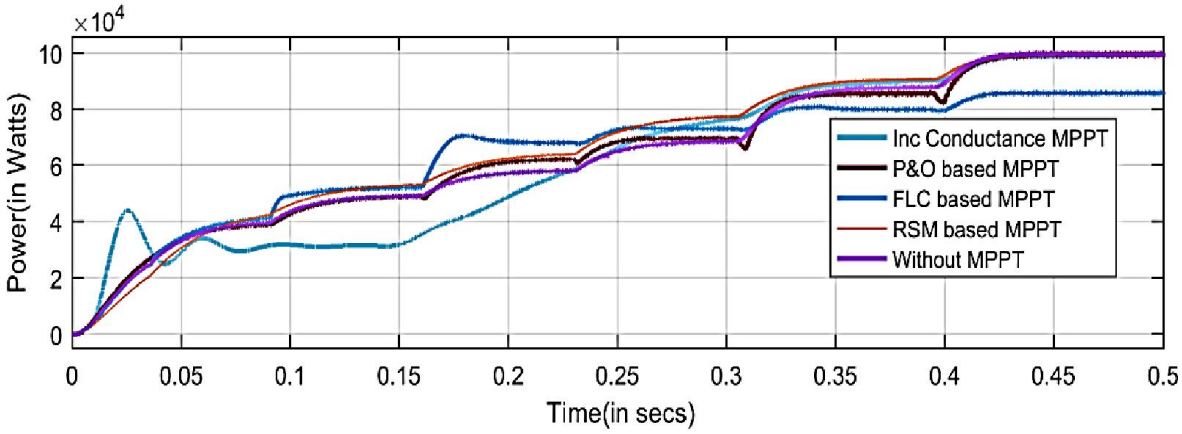

Fig 4. 10: Output power of boost converter for variable irradiation using different MPPT techniques.

Table 4. 2: Parameters of solar PV module.

S.No	Parameters	Rating
1	Maximum power	305.3 W
2	Open circuit voltage	64.2 V
3	Maximum power voltage	54.7 V
4	Short circuit current	5.96 A
5	Maximum power current	5.58 A
6	Number of PV cells per module	66

Table 4. 3: Boost converter-1 Specifications.

S.No	Parameters	Rating
1	Inductor	3mH
2	Capacitor	0.009 F
3	Switching Frequency	5000 Hz
4	Input Voltage	256.8
5	Output Voltage	500 V
6.	Output Current	5.58 A
7	Duty Cycle, D	0.4864

4.4. Voltage Droop Control Techniques

DC-DC boost converters are used in grid connected applications of RES system, for proper utilization of renewable energy since the output voltage generated from solar PV array and wind farms are very low. They are also used in regulating DC output voltage and current delivered to the load and also to track the maximum power point (MPP) of the PV module. If the load or grid voltage fluctuates due to any disturbance, then boost converter can act as a voltage regulator and generates a stable DC output by adjusting its duty cycle. In this section different controllers used in regulating DC voltage are discussed in brief.

4.5.1. PI based droop controller

In many industrial applications proportional, integral plus differential controller arrangement is commonly used to optimize the chosen control system. It offers many advantages like provides faster response to change in the controller input, reduces steady state error and eliminates oscillations.

The PI controller output is given by

$$u(t) = K_p e(t) + K_i \int e(t)dt \quad (4.12)$$

The control signal generated by proportional controller is proportional to the product of error signal and the proportional gain constant 'K_p'. The rise time of the resultant response is effected by proportional controller. If an integrator is added to the proportional system, the control signal is proportional to the integral gain 'K_i'. The steady state error 'e_{ss}' will be affected with it. The combined action of them has the advantage of each of the two individual control actions, [112].

In the proposed system PI controller is used to regulate the DC output voltage fed to the grid. Using Zeigler-Nichols technique proportional and integral constants are calculated. The PI controller will generate the duty cycle as output as shown in Fig. 4.11. By controlling the duty cycle of conventional boost converter the desired output voltage i.e. the grid voltage is generated.

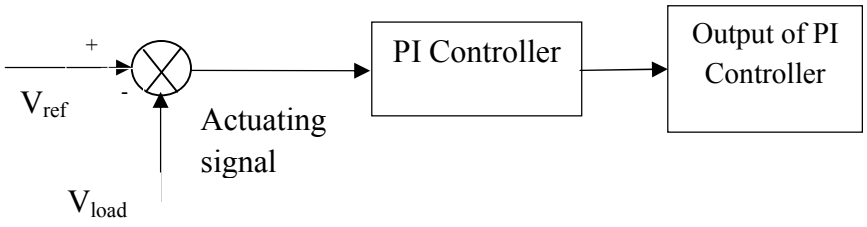

Fig 4. 11: Block diagram of PI controller

4.5.2. RSM based two loop average current controllers

RSM based two loop average current controller is proposed here to produce stable DC output. The objective function for inner current controller and outer voltage controller are given here along with the constraints. Using RSM method optimal values of 'K_p' and 'K_i' are found for both the cases.

The objective function for outer voltage controller

$$F(\theta)=\sum_{0}^{t_s}(Vo-V_r)^2 \tag{4.15}$$

Subject to constraints $\theta(lower)\le\theta\le\theta(upper)$

Here $\theta=\{K_p,K_i\}$

The objective function for inner current controller is

$$F(\theta)=\sum_{0}^{t_s}(I_L-I_r)^2 \tag{4.16}$$

Subject to constraints $\theta(lower)\le\theta\le\theta(upper)$

Here $\theta=\{K_p,K_i\}$

where,

Vo = measured output voltage of boost converter B_2

Vr = desired grid voltage to be maintained

I_L= input current to boost converter B_2

Ir = reference current to inner current controller

Step wise procedure for designing voltage controller using RSM technique is given below:

1. Set the initial start value for 'K_{p1}', 'K_{i1}' as '1' and initial step length 'λ=1', and iteration count N=20 and the minimum allowable step length ε = 0.1.
2. Find the objective function F_1 = F (K_{p1}, K_{i1}), which is a function of 'K_{p1}', 'K_{i1}' as given in equation (4.15) and (4.16)
3. Start the iteration count with initial value for 'i = 1'.

4. Generate 'r_1', 'r_2' randomly between the limits [−1, 1] and find the unit vector 'u'.
5. Update the new values for 'K_p', 'K_i' using

   $K_p = K_{p1}+\lambda u,\ K_i = K_{i1}+\lambda u$

   and find the corresponding objective function value from $F= F(X)$.
6. Compare the objective functions F and F_1. If $F < F_1$, update $K_{p1} = K_p$, $K_{i1} = K_i$ and $F_1= F$ and go to step 3. Else the new step length $\lambda = \lambda/2$. If $\lambda \leq \varepsilon$, go to step 7. Otherwise go to step 4.
7. Stop the procedure and take the optimal values for $K_{p\text{opt}} \approx K_{p1}$, $K_{iopt} \approx K_{i1}$ and $F_{opt} \approx F_1$.

It can be noticed that RSM converges the objective function rapidly, to one of the lowest values.

4.5.3. Results and Discussion

A comparative analysis is performed between PI controller and two loop average current controller based voltage regulators in this section. To evaluate the performance of voltage regulators a 500/1000 V DC-DC boost converter is chosen. The specifications of the converter are given in Table 4.5. For a constant DC input voltage of 500 V the boost converter generates an output voltage of 1000 V at 0.5 duty cycle without droop controller as shown in Fig. 4.12.

If the load on the converter varies with a voltage requirement as shown in Fig. 4.12(d) then the performance of the converter with PI based voltage controller and two loop average current controller are shown in Fig. 4.12(b) and 4.12(c). The open loop response of the converter without a voltage controller is shown in Fig. 4.12(a). From the

graphs it is observed that two loop average current controller is able to regulate the DC output voltage of the converter according to the requirement.

Whereas the PI controller can regulate the voltage between 0 to 0.28 s as the '*Kp'* and '*Ki'* constants are set to achieve the desired voltage of 1040 V in that range. As the desired voltage changes then '*Kp'* and '*Ki'* constants are to be updated with the corresponding change due to which the voltage curve doesn't follows the desired response after 0.28s. The two loop average current controller that uses random search method is able to achieve the desired response without any delay or oscillations as shown in Fig. 4.12.

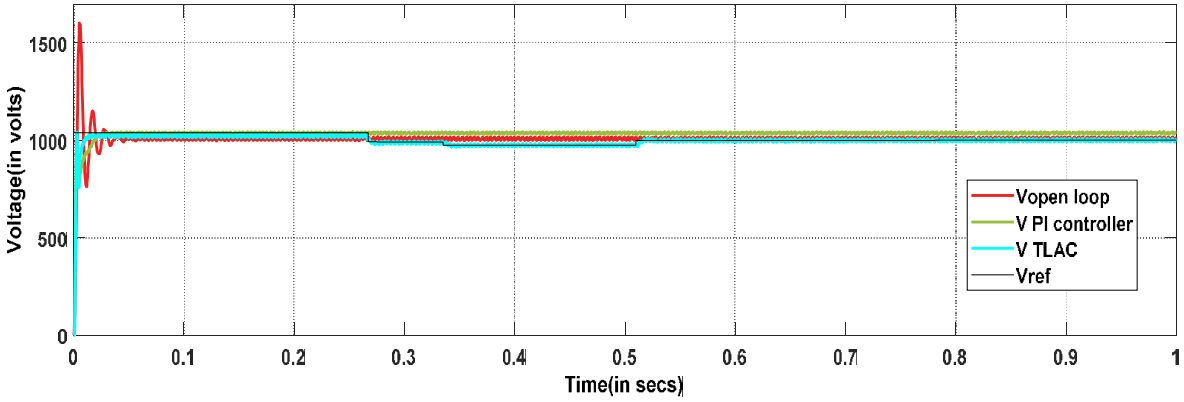

Fig 4.12: Desired response and actual voltage response of Boost converter with and without voltage regulator.

Table 4.4: Boost converter-2 specifications.

S.No	**Parameters**	**Rating**
1	Inductor	50 mH
2	Capacitor	15 µF
3	Switching Frequency	5000 Hz
4	Input Voltage	500 V
5	Output Voltage	1000 V

4.5. Summary

The major contribution of this chapter is, a hybrid controller proposed to address two challenges faced during DC grid integration i.e. extracting the maximum power from the variable input and regulating DC voltage according to the grid requirement. For efficient MPPT tracking a comparative study is performed among different MPPT control techniques like incremental conductance, perturb and observe, fuzzy logic and random search method. From the results it is observed that RSM based MPPT controller performs well under varying weather conditions and is able to track the maximum power from the source with good tracking efficiency and less oscillations.

Second major contribution of this chapter is a random search method two loop average current controller is proposed to provide stable DC output at low voltage DC grid under grid side disturbances. To validate the effectiveness of the proposed controller its performance is compared with linear PI controller. From the results it is observed that the proposed controller performs well at varying load conditions, producing a stable DC output with less delay time and oscillations. In addition to load side disturbances, it performs well under input side perturbations that can occur in the system.

Chapter 5

Performance Evaluation of DC Grid Connected Solar PV System Using Hybrid Controller

5.1. Introduction

In the previous chapter the performance of proposed hybrid controller is evaluated by comparing with other MPPT and voltage regulating techniques. In the present chapter three different configurations are proposed to integrate solar photo voltaic installations to DC grid, which at a later stage aided to build a novel topology for integrating solar PV and wind farms to high voltage DC grid as discussed in chapter 6. The main objective of these configurations is to address two major challenges faced during DC grid integration of PV system namely maximum power extraction from time varying input and to provide stable DC grid voltage. The hybrid controller proposed in the previous chapter is used in one of these configurations. The performance of the proposed configurations is evaluated under different combinations of input and output variations. The stability analysis of TLAC controlled DC-DC boost converter is also discussed in this chapter.

5.2. Modeling of Solar PV Module

Single diode mathematical model of silicon PV module is shown in Fig. 5.1, which consists of a photocurrent source generator $I_{ph\text{-}m,}$ a nonlinear PN junction diode, internal series resistance *Rs* and shunt resistance R_p. The shunt resistance, R_p will control the leakage current from the module to ground, [116].

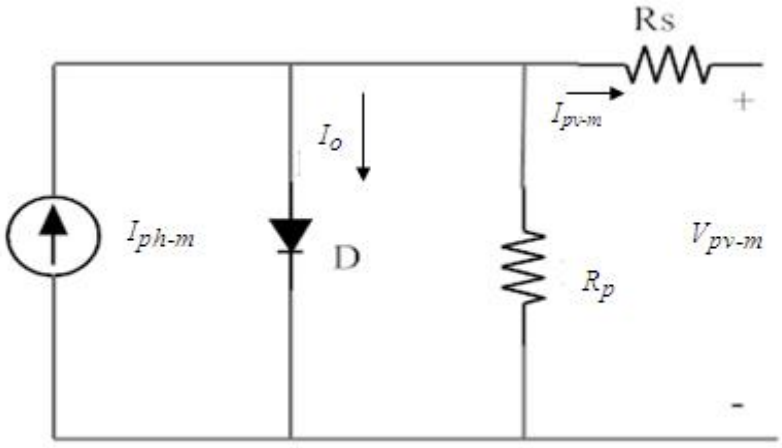

Fig.5.1: PV module representation using single diode.

From the single diode mathematical model, the output current in terms of photocurrent and output voltage is given by as in [117],

$$I_{pv-m} = I_{ph-m} - I_s\left(\exp\frac{(V_{pv-m}+R_sI_{pv-m})}{\eta V_t} - 1\right) - \frac{V_{pv-m}+R_sI_{pv-m}}{R_p} \tag{5.1}$$

When R_p tend to infinity,

$$\frac{dI_{pv-m}}{dV_{pv-m}} = -\frac{I_o}{\eta V_t}\left(\exp\left(\frac{V_{pv-m}+R_sI_{pv-m}}{\eta V_t}\right) - \left(1+R_s\frac{dI_{pv-m}}{dV_{pv-m}}\right)\right) \tag{5.2}$$

From the above equation, series resistance offered by PV module under open circuit is

$$R_s = -\frac{dI_{pv-m}}{dV_{pv-m}} = -\frac{1}{X_V} \tag{5.3}$$

Where

$$X_V = \frac{I_o \exp(V_{oc-m}/\eta V_t)}{\eta V_t}$$

The photocurrent, $I_{ph\text{-}m}$ of PV module is given by,

$$I_{ph-m} = (I_{sc-N} + k_i\Delta T)G \tag{5.4}$$

The voltage across PV module under open circuit, $V_{oc\text{-}m}$, in terms of irradiation, change in temperature, thermal voltage and open circuit voltage is given by,

$$V_{oc-m} = V_{oc-N} + V_{t-N} \ln(G) + k_v \Delta T \quad (5.5)$$

Where,

$I_{pv\text{-}m}$ = PV module output current (A)

$V_{pv\text{-}m}$ = Output voltage of PV module (V)

$I_{ph\text{-}m}$= Photon Current (A)

$V_{oc\text{-}m}$= voltage across open circuit (V)

V_t= Thermal voltage at panel surface Temperature, T_1 (V)

$V_{t\text{-}N}$= Thermal voltage at panel surface Temperature, T_N (V)

$I_{sc\text{-}N}$= Current under short circuit (A)

$V_{oc\text{-}N}$= Voltage under open circuit (V)

I_o= Current through diode in saturation mode (A)

q = Electron Charge (C)

η = Diode Ideality factor

R_S, R_P = Series and shunt resistance of PV module (Ω)

N_s= No. of Cells in Series

G= Solar irradiation (kW/m^2)

k_i ,kv= Current, voltage temperature coefficient

5.3. Proposed Configuration-1 for DC grid Integration of Solar PV System

In the proposed system, as shown in Fig. 5.2, the DC-DC Boost converter is connected to each of the solar PV unit. The outputs of these converters are series connected and fed to the DC grid. Some of these converters will take care of MPPT,

while the others will function as voltage regulators. To perform simulation study the outputs of two PV fed DC-DC Boost converters are connected in series and finally the series connected output is tied up to the DC grid. While one of these DC-DC Boost converters will take care of MPPT, the other will function as voltage regulating agents thus achieving the dual functionality of MPPT as well as voltage regulation of the DC bus.

In a solar PV generator the generated output varies with the change in atmospheric temperature and solar input irradiation. Since the dynamics of temperature being slow compared to input irradiation it will not affect the performance of PV system. The output current and voltage of PV array and hence the output power gets influenced by change in the input irradiation [64]. Due to simplicity in approach incremental conductance technique is chosen for MPPT and fuzzy logic control technique for voltage regulation.

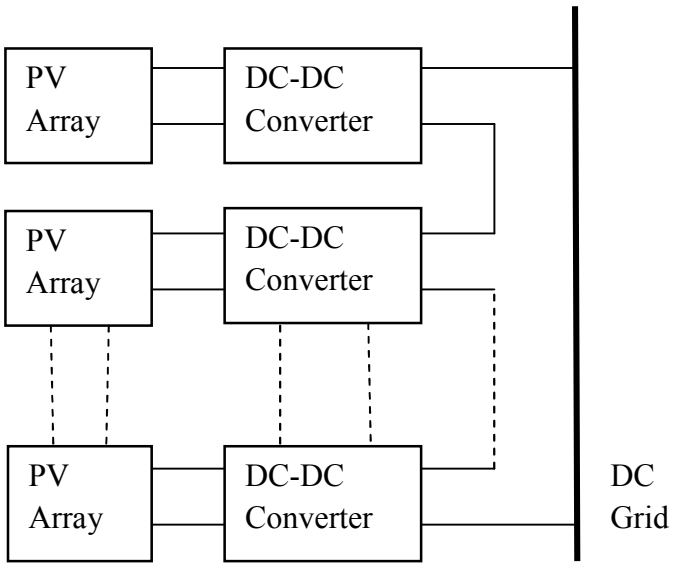

Fig.5. 2: DC grid connected solar PV system.

The specifications of PV module and converter are given in Table 5.1 and 5.2. Many such modules are connected in series and parallel to form PV array of desired rating. The input and output voltage response of converter connected to PV array of subsystem-1, are shown in Fig. 5.3. The output voltage across the grid and current fed to the grid are shown in Fig. 5.4 and Fig. 5.5.

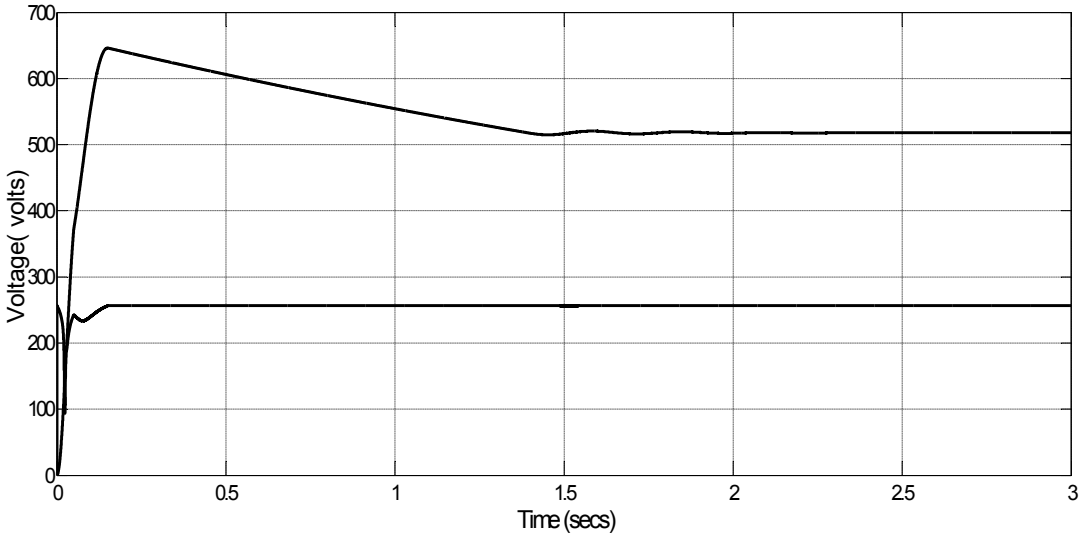

Fig.5. 3: Input and output voltage of boost converter.

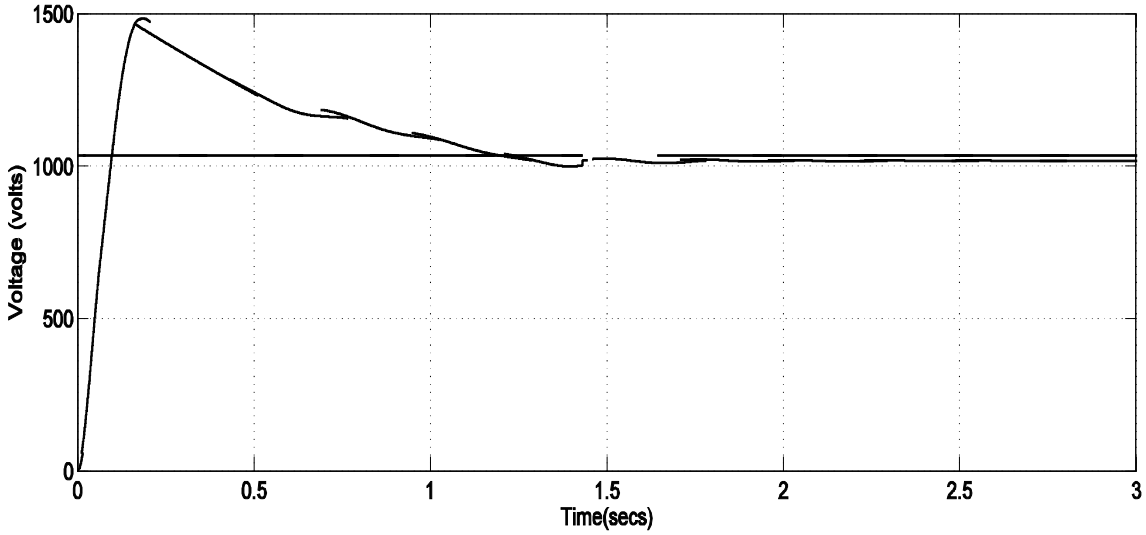

Fig.5. 4: Open loop voltage response of proposed system.

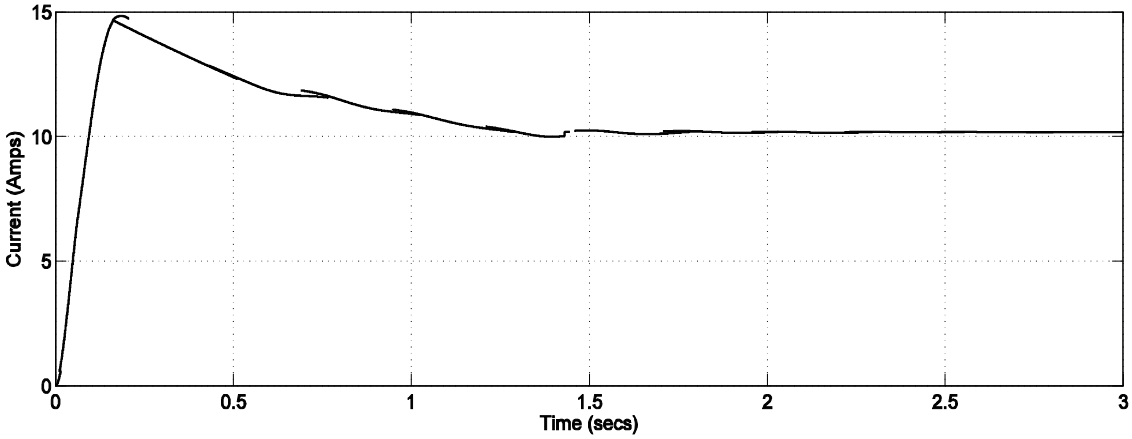

Fig.5. 5:Open loop current response of proposed system.

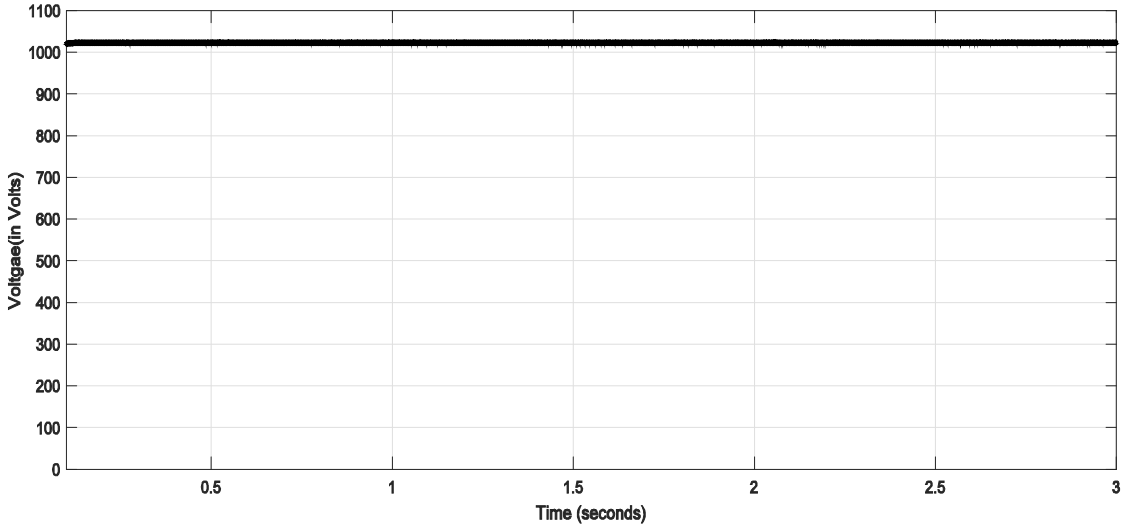

Fig.5. 6: Output voltage of closed loop boost converter.

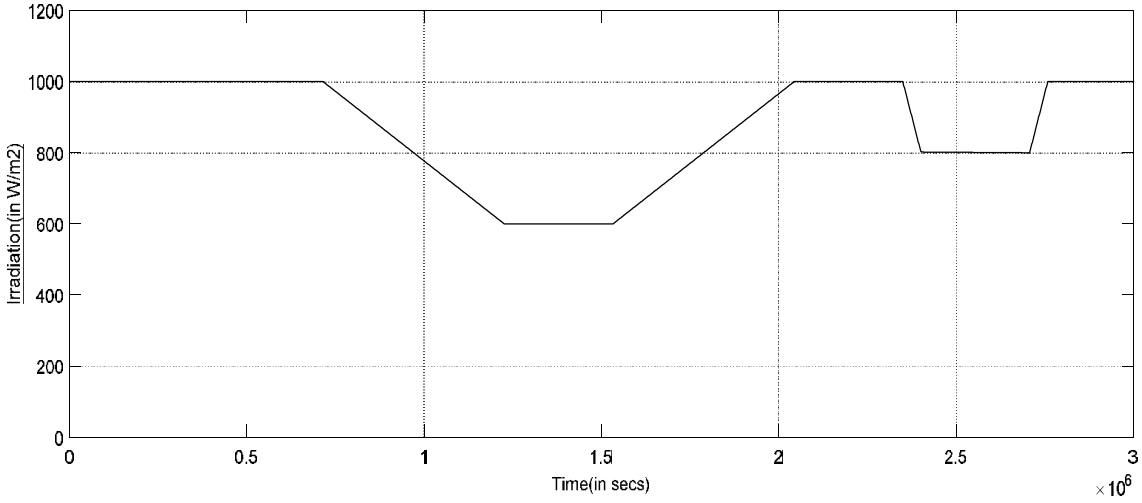

Fig.5. 7: Fluctuating input(irradiation)

Each PV array can generate an output voltage of 255V which is given as input to the boost converter as shown in Fig. 5. 3. The output of the boost converter is around 510 V at 0.5 duty cycle under constant irradiation. Two such boost converters are connected in series to generate an output voltage of 1020 V. The output voltage and current response of the proposed system without fuzzy based voltage regulator is shown in Fig. 5.4 and Fig. 5.5. From the voltage response it is clear that though the desired grid voltage is 1035 V where as the proposed system (without fuzzy logic controller) could generate an output voltage 1020 V. When the voltage regulating unit is present in the system, with the change in the grid voltage the voltage fed by the proposed system changes accordingly as shown in Fig. 5.6.

When the irradiation to the PV array (subsystem-1) varies as shown in Fig. 5.7, the output voltage and current response of the proposed system for the fluctuating input are shown in Fig. 5.8 and Fig. 5.9. Irrespective of change in input the output voltage of the system is stable using MPPT controller and voltage regulator as shown in Fig. 5.9.

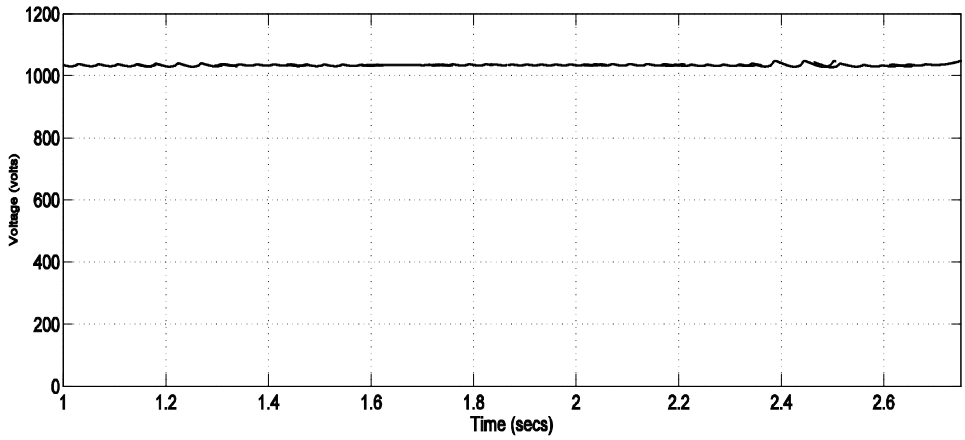

Fig.5. 8: Output voltage response for the fluctuating input.

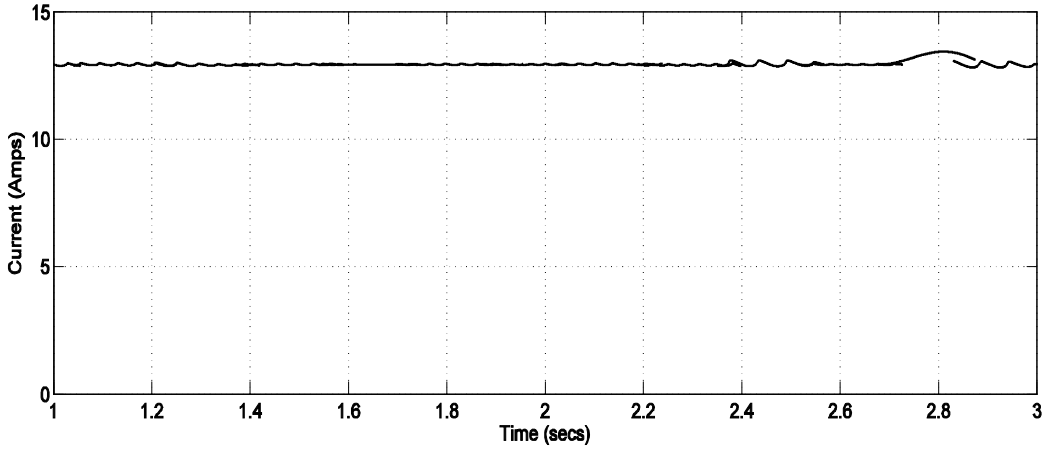

Fig.5. 9: Output current response for the fluctuating input

By increasing the number of subsystems the proposed configuration can be used for high voltage DC grid connected applications. But the hybrid control action would become complex with increase in the number of subsystems. The proposed system has a drawback that, if the irradiation is low in few subsystems then the desired grid voltage can be maintained by adjusting duty cycle of other converters using droop controller but when partial shading prevails in those subsystems which acts as voltage regulators, then the desired grid voltage is difficult to maintain by adjusting the duty cycle at the rest of the subsystems.

Table 5. 1: Parameters of solar PV Module

S.No	Parameters	Rating
1	Maximum power	305.3 W
2	Voltage under open circuit	64.2 V
3	Voltage at maximum power	54.7 V
4	Current under short circuit	5.96 A
5	Current at maximum power	5.58 A
6	Number of PV cells per module	66

Table 5. 2: Boost converter specifications for configuration-1

S.No	Parameters	Rating
1	Inductor	3mH
2	Capacitor	0.009 F
3	Switching Frequency	5000 Hz
4	Input Voltage	256.8
5	Output Voltage	510 V
6.	Output Current	5.58 A

5.4. Proposed Configuration-2 for DC grid Integration of Solar PV System

To provide MPPT and voltage regulation action at the same time the configuration of each subsystem is changed as shown in Fig. 5.10. Each subsystem consists of PV array, two boost converters and hybrid controller. PV array fed DC-DC boost converter B_1 is connected to boost converter B_2 whose outputs is fed to DC grid.

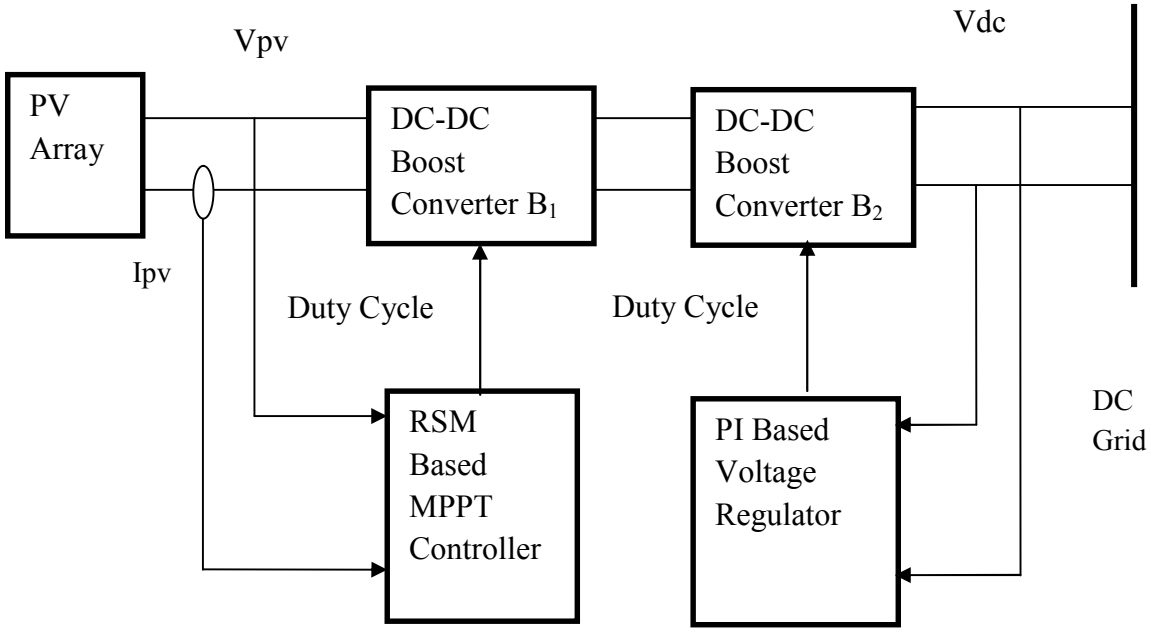

Fig.5. 10: Hybrid control scheme-2 for DC grid connected PV system.

The hybrid controller proposed here includes MPPT controller and voltage regulator. The MPPT controller uses random search method to track the global maximum power point and voltage regulating action is performed by using PI controller, which is used to maintain stable DC output irrespective of grid disturbances. Both these control actions are achieved with the help of independent duty ratio control of DC-DC boost converters.

The I-V and P-V characteristics of PV Cell are shown in Fig. 5.11 and 5.12. From which the open circuit voltage and short circuit current of PV cell can be calculated. For a constant input irradiation of 1000 W/m^2 PV array generates a constant DC output voltage of 320 V which when given as input to boost converter B_1 generates an output voltage of 640 V. A constant DC output of 1280 V is fed to DC grid from converter B_2 taking an input of 640V from converter B_1. The specifications of PV array, boost converter B_1 and B_2 are given in Table 5.3, 5. 4 and 5.5.

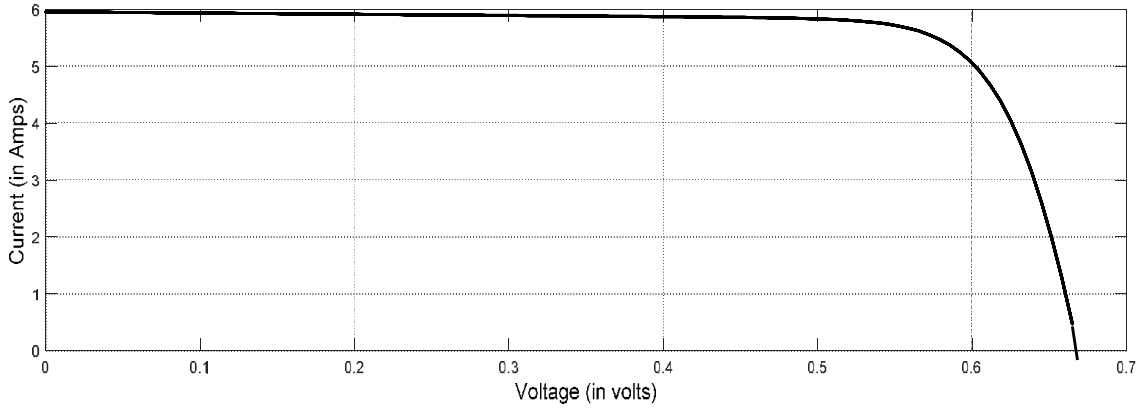

Fig.5. 11: I-V Characteristics of PV cell.

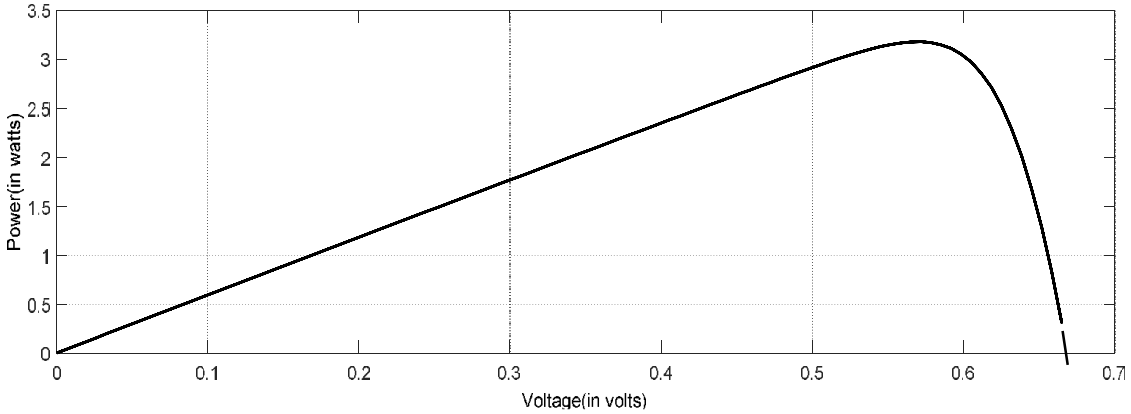

Fig.5. 12: P-V Characteristics of PV cell.

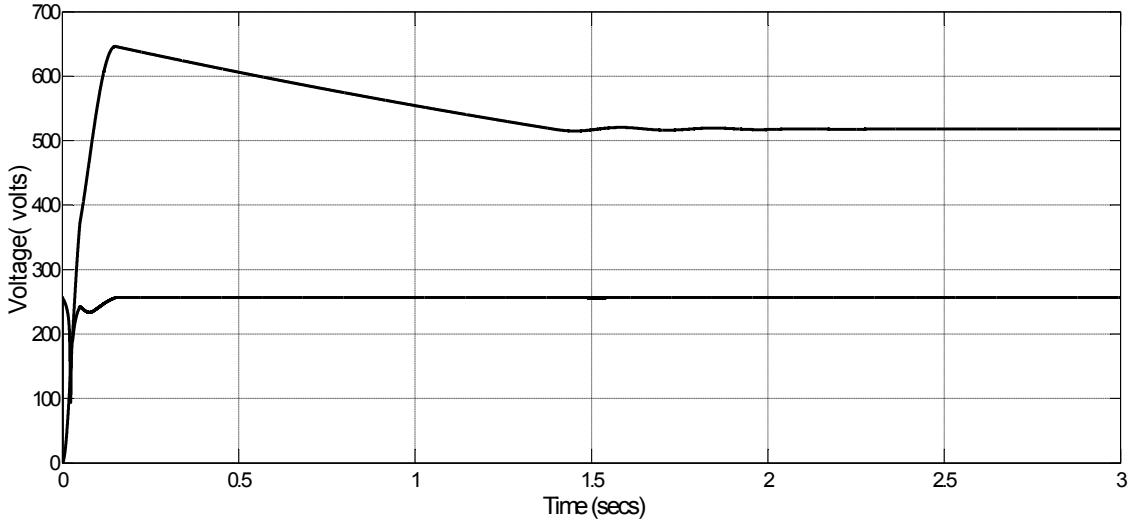

Fig.5. 13: Input and output voltage of boost converter1, $B_1$with MPPT control.

The input and output voltage response of converter, B_1 is shown in Fig. 5.13. For time varying input solar irradiation as shown in Fig. 5.14, the MPPT controlled output voltage response of boost converter B_1 is shown in Fig. 5.15. The output voltage response of converter B_2, without voltage regulating unit is shown in Fig. 5.16. Due to disturbances if the grid voltage is changed to 1260 V then there is difference in voltage between the actual voltage fed i.e. 1280 V and grid voltage as shown in Fig. 5.16. Using a PI based

voltage controller in feedback the desired grid voltage of 1260 V is achieved by adjusting the duty cycle as shown in Fig. 5.17.

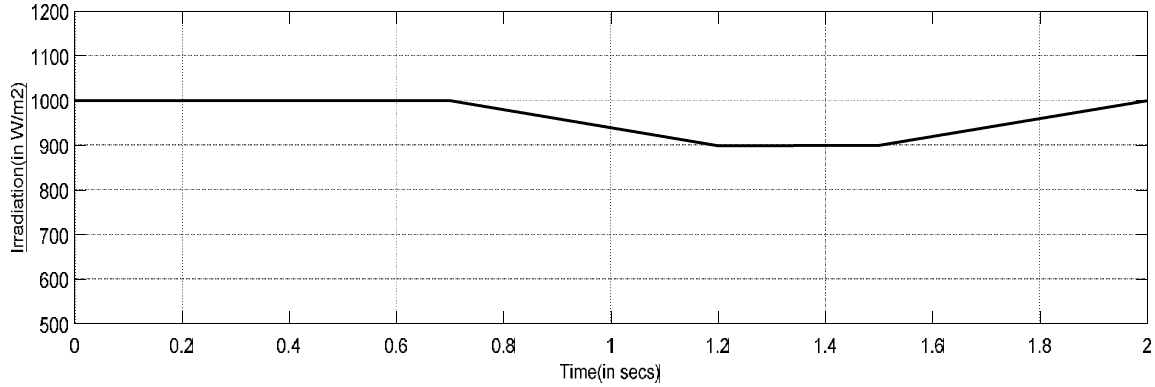

Fig.5. 14: Fluctuating input(irradiation).

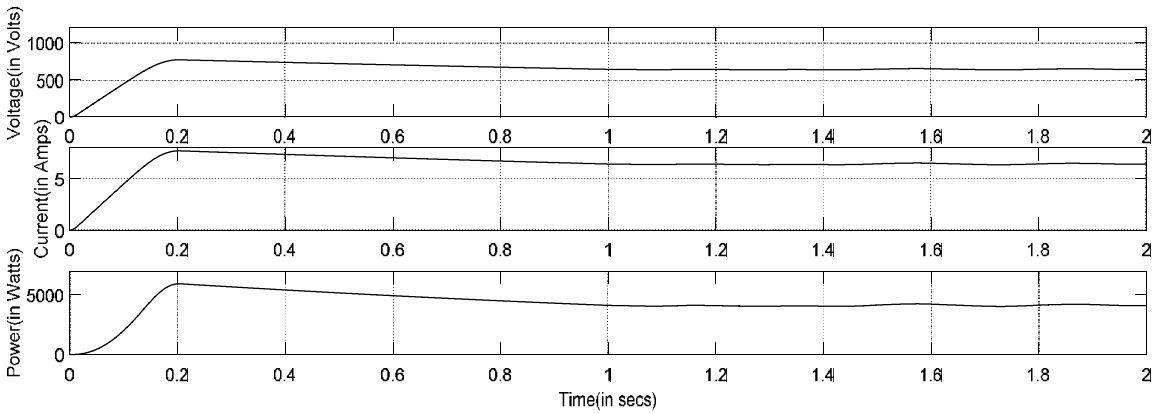

Fig.5. 15: MPPT controlled output voltage, current and power response of boost converter 1.

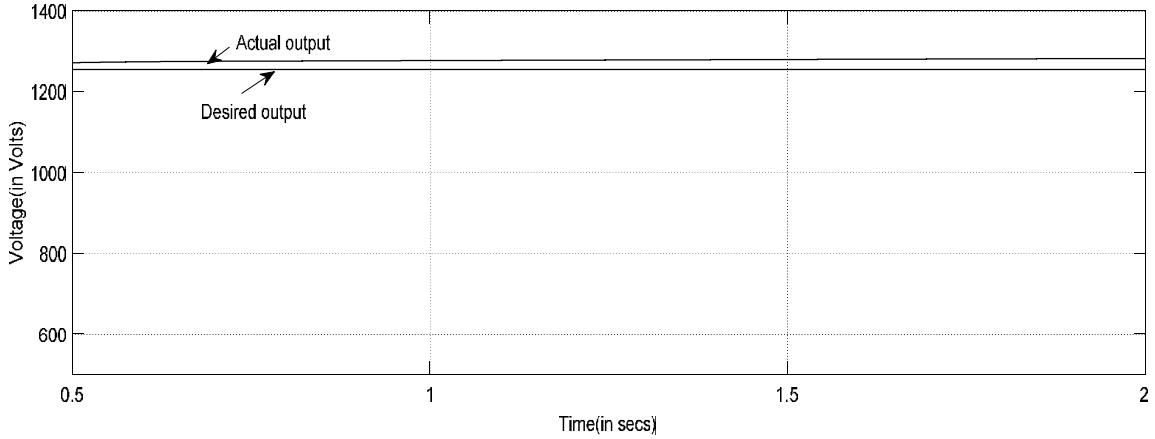

Fig.5. 16: Open loop voltage response, desired response of proposed system.

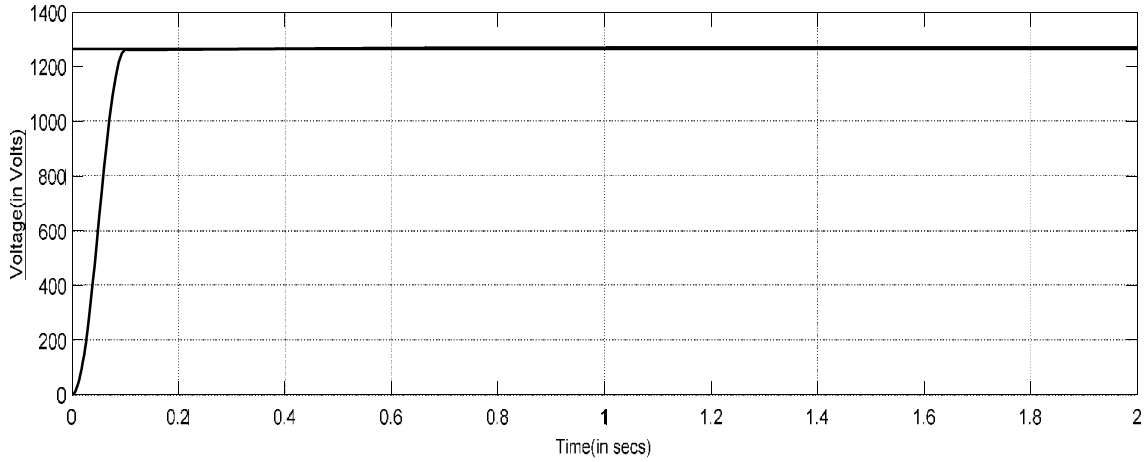

Fig.5. 17: The output voltage response with voltage regulator and MPPT for the fluctuating input.

Table 5. 3: Parameters of solar PV Module

S.No	Parameters	Rating
1	Voltage under open circuit	64.2 V
2	Voltage at maximum power	54.7 V
3	Current under short circuit	5.96 A
4	Current at maximum power	5.58 A
5	Number of PV cells per module	96

Table 5. 4: Boost converter-1 specifications for Configuration-2

S.No	Parameters	Rating
1	Inductor	10.26 mH
2	Capacitor	40 nF
3	Switching Frequency	5000 Hz
4	Input Voltage	320 V
5	Output Voltage	640 V
6	Duty Cycle, D	0.5

In the proposed system DC-DC boost converter, B_1 along with MPPT controller is used to generate stable DC output of 640 V irrespective of change in input irradiation

whereas the other converter along with PI controller will control its output voltage according to the grid requirement by adjusting the duty cycle, thus achieving the dual functionality of MPPT as well as voltage regulation of DC bus.

The PI based voltage controller considers only grid side perturbations neglecting the input side perturbations which will occur due to MPPT control action at converter B_1, for wide variation in input irradiation. In addition to that, the PI based voltage controller cannot generate a stable DC output according to the grid requirement if the grid voltage is changing dynamically. To overcome this issue RSM based two loop average current controller is proposed to generate steady DC output under grid side and input side fluctuations.

Table 5. 5: Boost converter-2 specifications for configuration-2

S.No	Parameters	Rating
1	Inductor	45 mH
2	Capacitor	10 μF
3	Switching Frequency	5000 Hz
4	Input Voltage	640 V
5	Output Voltage	1280 V
6	Duty Cycle, D	0.5

5.5. Proposed Configuration-3 for DC Grid Integration of Solar PV system

The proposed configuration overcomes the drawbacks of the previous topologies and also provides efficient MPPT tracking and voltage regulating actions under varying load and weather conditions. It consists of several subsystems; each subsystem consists of a PV array fed DC-DC converter B_1, grid connected DC-DC converter B_2 and a hybrid controller to perform MPPT and voltage regulating action. The outputs of these DC-DC converters B_2 present in each subsystem configuration are series connected and fed to

high voltage DC grid as shown in Fig. 5.18. The hybrid controller designed here combines RSM based MPPT controller and a voltage droop regulator, that uses RSM based two loop average current control technique as shown in Fig.5.19.

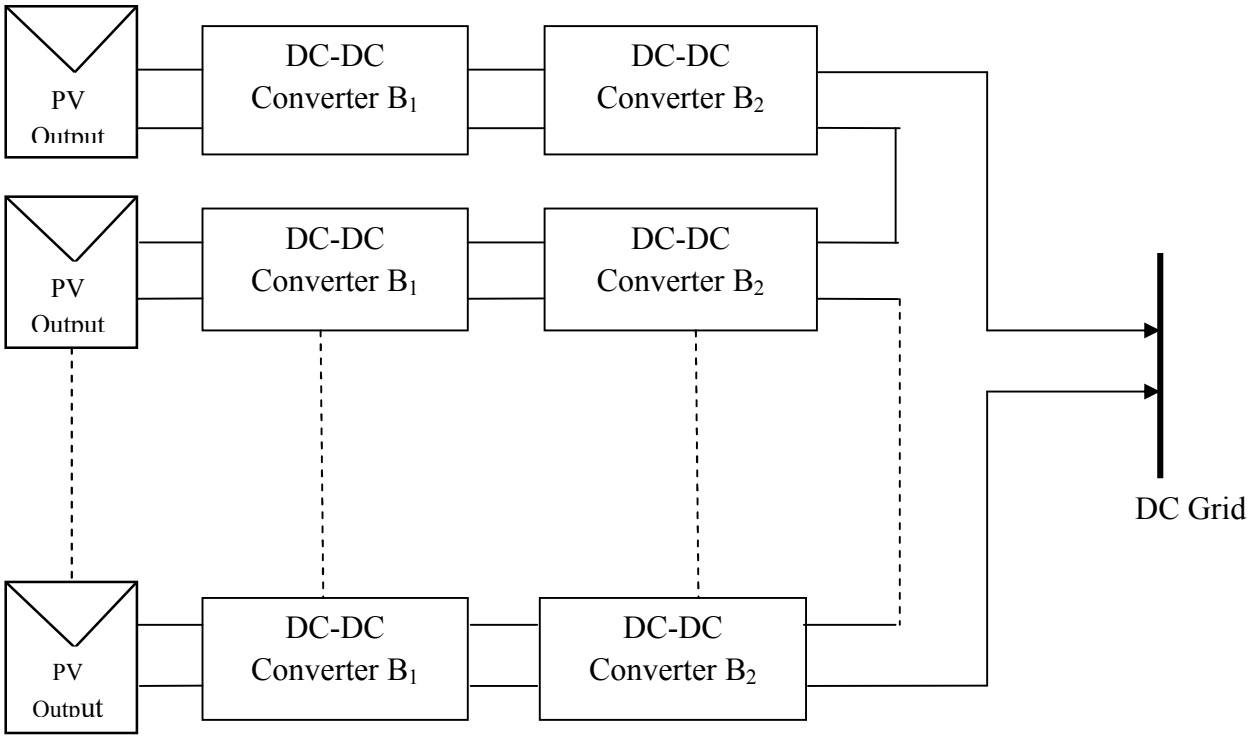

Fig.5. 18: Proposed configuration for DC Grid Integration of large solar PV system.

Two stage converters configuration is chosen over single stage converter as it is difficult to implement MPPT and voltage droop controller action at one converter. The RSM based MPPT controller along with Boost converter B_1 will track the MPP by controlling the duty cycle of Converter B_1, whereas the voltage droop controller will regulate the DC output by adjusting the duty cycle of DC-DC Converter B_2 considering both input and grid side perturbations using two loop average current controller. The specifications of each PV module are given in Table 5.5; four such modules are

connected in series to form an array. The specification of converter B_1 and B_2 are given in Table 5.6 and 5.7.

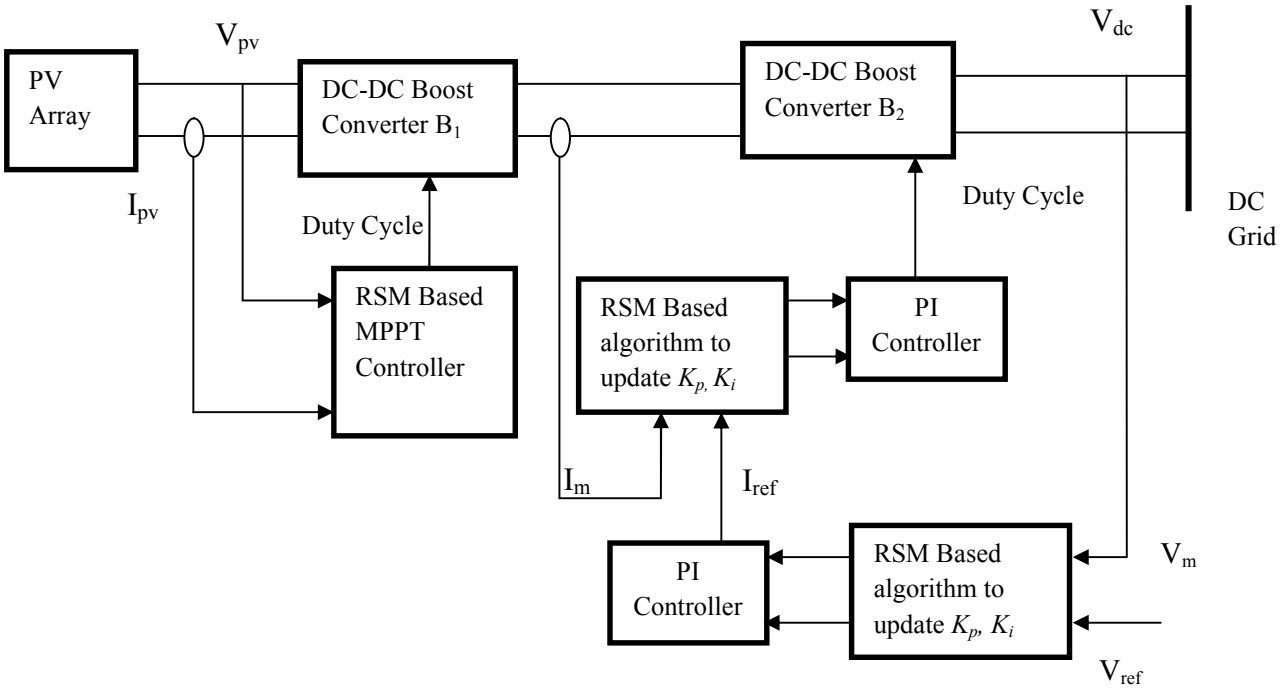

Fig.5. 19: Subsystem layout with hybrid control architecture in proposed DC Grid connected solar PV system.

Each subsystem consists of PV array fed two stage DC-DC converter setup with hybrid controller whose specifications are 2.8 kW, 1000 V and 2.8 A. Eleven such subsystems are connected in series to generate a DC grid voltage and current of 11 kV, 2.8 A and power output of 30.8 kW.

At 1000 W/m^2 irradiation PV array in each subsystem generates an output voltage of 256.8 V which is stepped up to a voltage of nearly 500 V using conventional boost converter circuit B_1. The output of converter B_1 when given as input to DC-DC converter B_2 generates an output of 1000 V at 0.5 duty cycle. Eleven such subsystems are series connected to produce an output voltage of 11 kV which is fed to 11 kV DC grid. The

performance of proposed grid connected system is studied under different input and output disturbances.

5.5.1. Case A: At constant input irradiation and fixed load

For a constant input irradiation of 1000W/m^2 as shown in Fig. 5.20, the voltage and current response of converter B_1 within subsystem-1 are shown in Fig. 5.21. It is observed that a stable DC output voltage of 500 V and current of 5.58 A are generated.

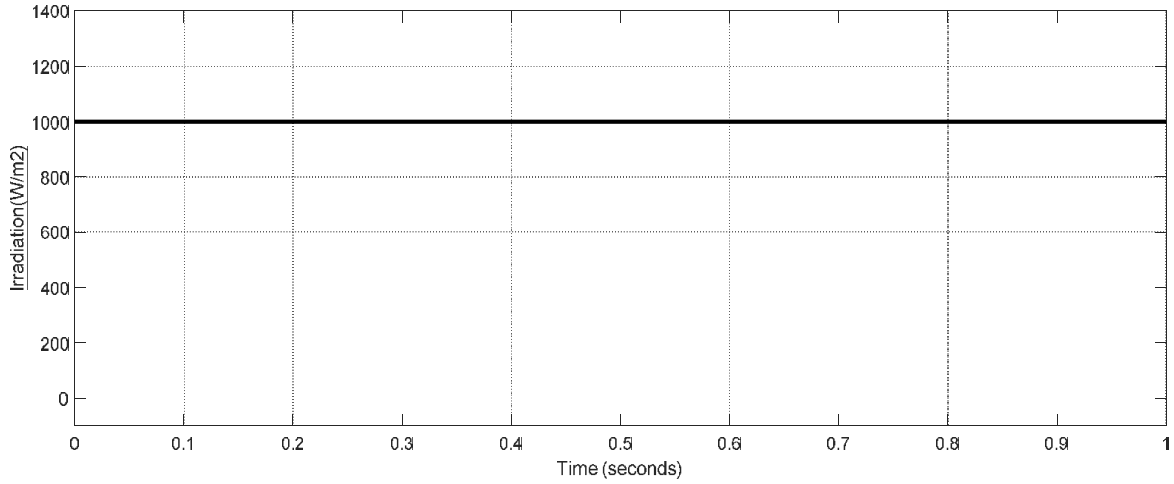

Fig.5. 20: Constant irradiation of 1000 W/m^2

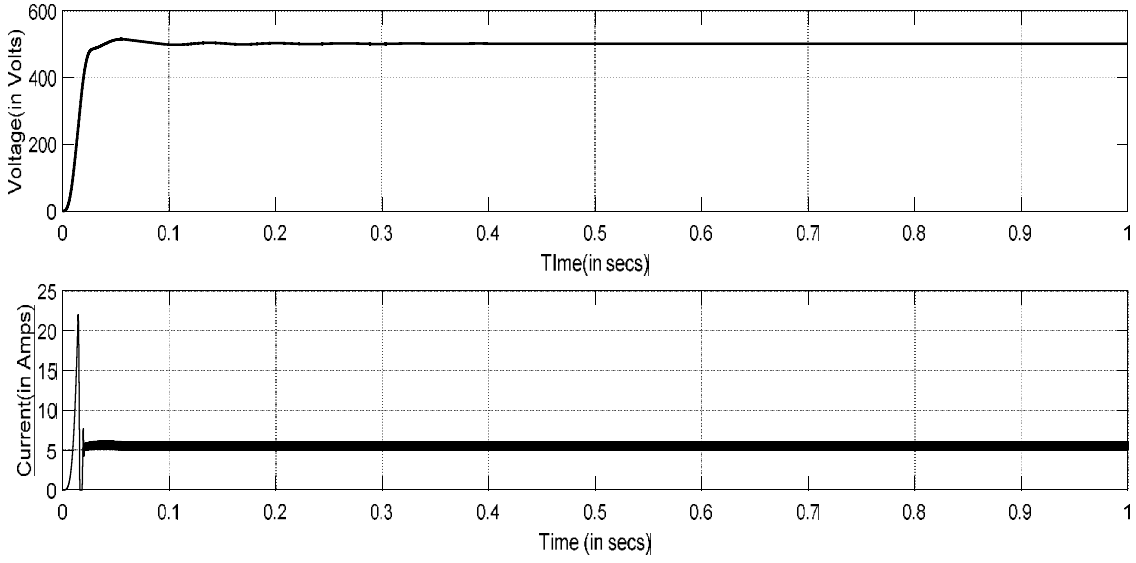

Fig.5. 21: Voltage and current responses of converter B_1.

The output voltage and current response of converter B_2 are shown in Fig.5.22, from which it is observed that an output voltage of 1000 V and current of 2.79 A are generated by each subsystem at constant input irradiation and the overall system response is 11000V as shown in Fig. 5.23. It is observed that output voltage response of converter B_2 and overall response of proposed system has a transient in the beginning for fraction of seconds, because of the delay in the operation of voltage controller.

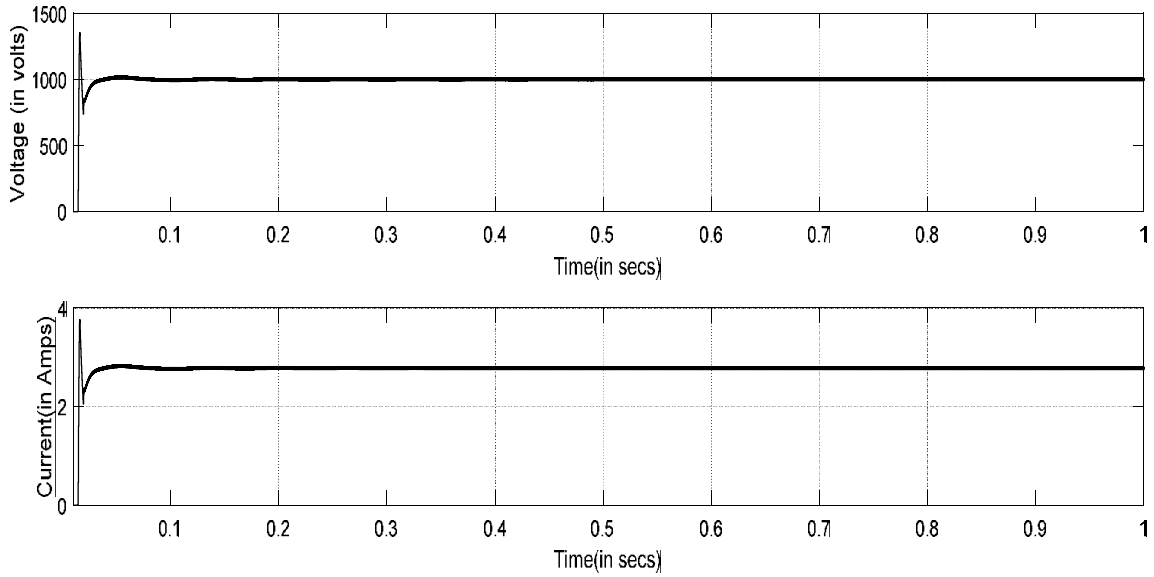

Fig.5. 22: Voltage and current responses of converter B_2.

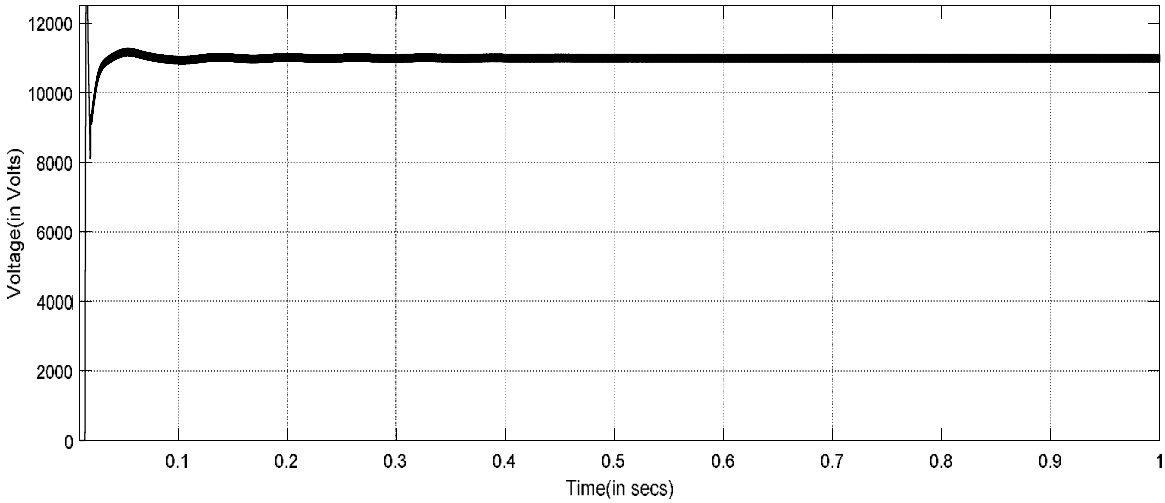

Fig.5. 23: Output voltage fed to DC grid.

5.5.2. Case B: At variable irradiation and fixed load

For a variable solar input as shown in Fig.5.24, the voltage and current response of converters B_1 and B_2 are shown in Fig.5.25 and 5.26.

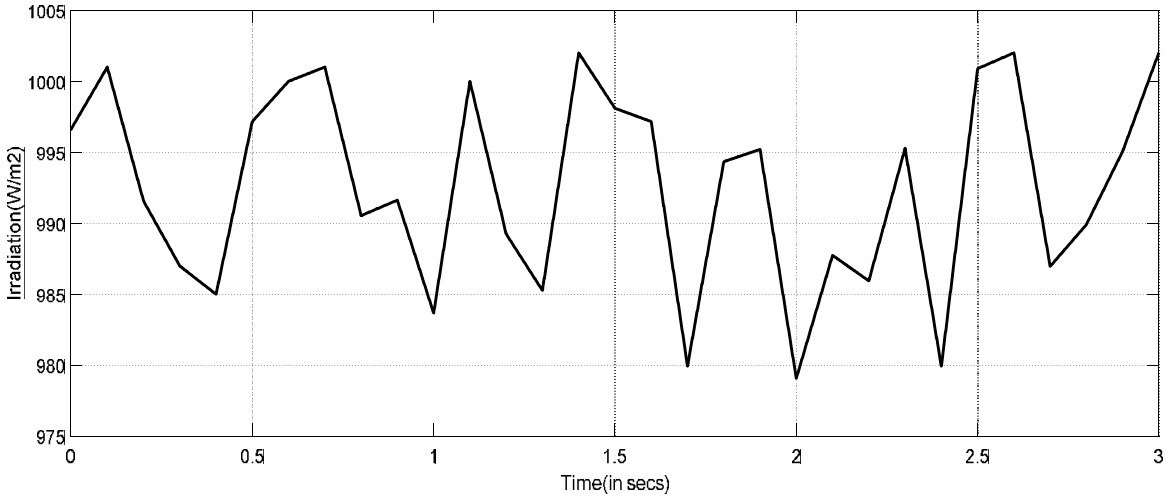

Fig.5. 24: Variable input irradiation.

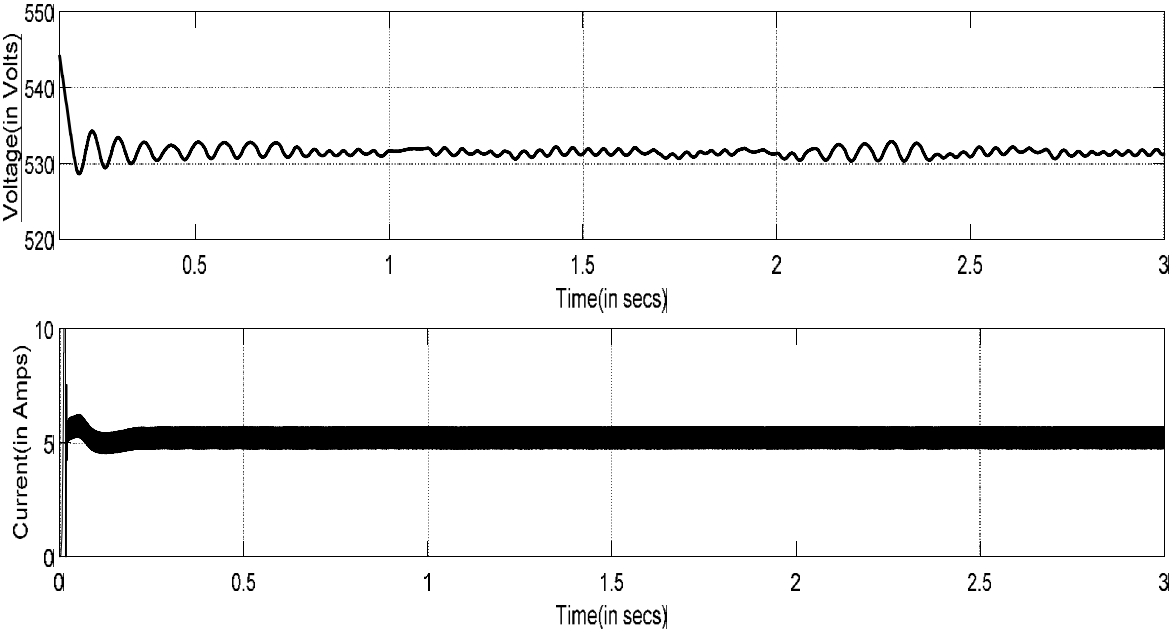

Fig.5. 25: Output voltage and current response of converter-1 at variable irradiation.

It is observed that MPPT controller can track the maximum power but cannot maintain stable DC output. Due to which there are some perturbations in the output response as shown in Fig. 5.25, which would impact the performance of converter B_2 in the absence of RSM based TLAC controller. The output response of converter 2 is shown in Fig.5.26 and the output voltage is stable due to presence of voltage controller. The overall performance of proposed system with hybrid controller is shown in Fig. 5.27.

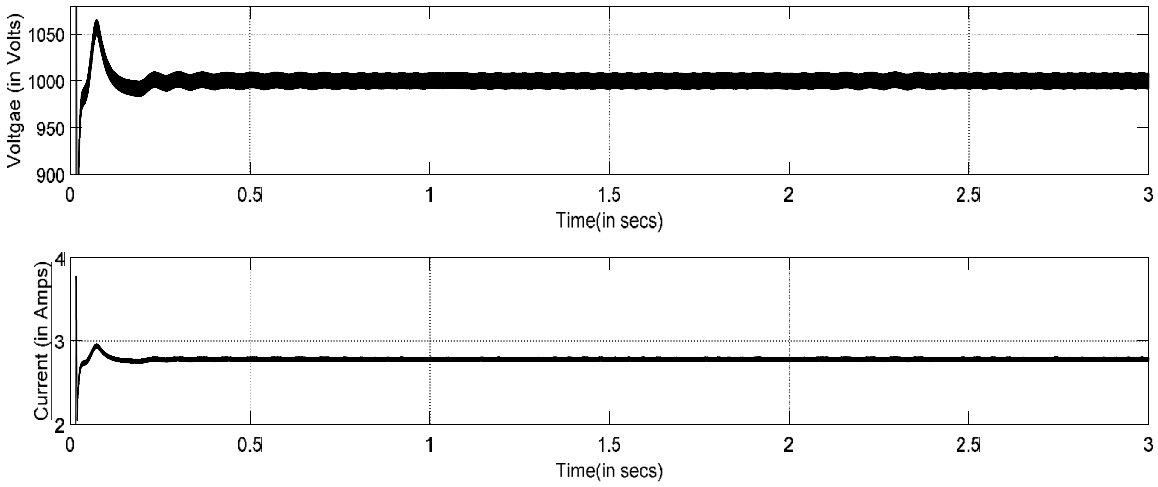

Fig.5. 26: Output voltage and current response of converter-2 at variable irradiation.

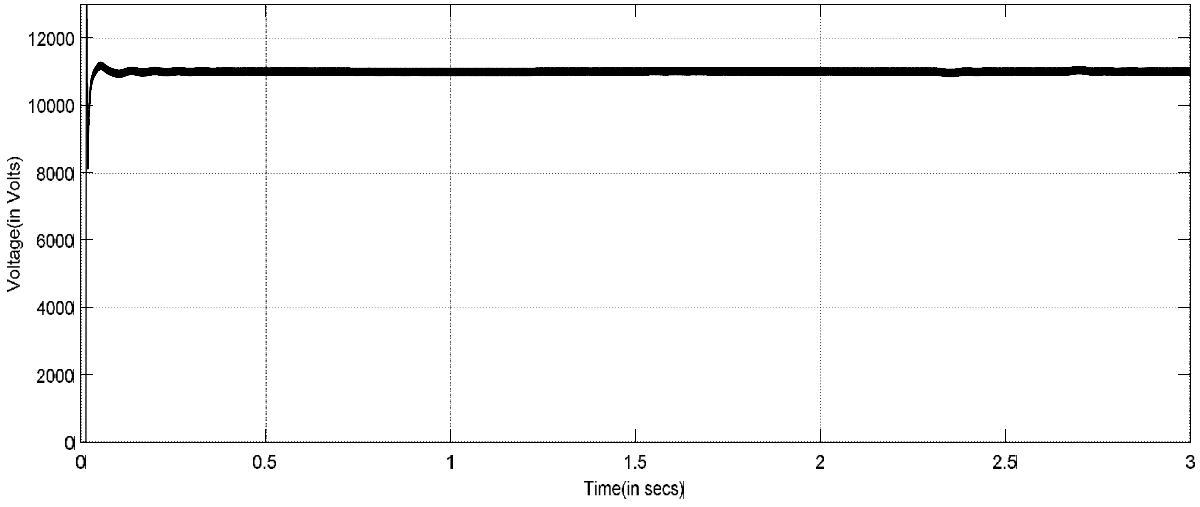

Fig.5. 27: Overall DC voltage and fed to the DC grid.

5.5.3. Case C: Variable input and fluctuating output

The performance of the proposed system for varying input irradiation and for grid side disturbances caused due to sudden change in the load are analyzed here. Due to disturbances in load, if the grid voltage is changed to 10.8 kV then the proposed system is able to generate the desired grid voltage by using RSM based two loop average current control based voltage regulator. For the variable input irradiation as shown in Fig. 5.28, the response of converter B_1 and B_2 are shown in Fig. 5.29 and Fig. 5.30.

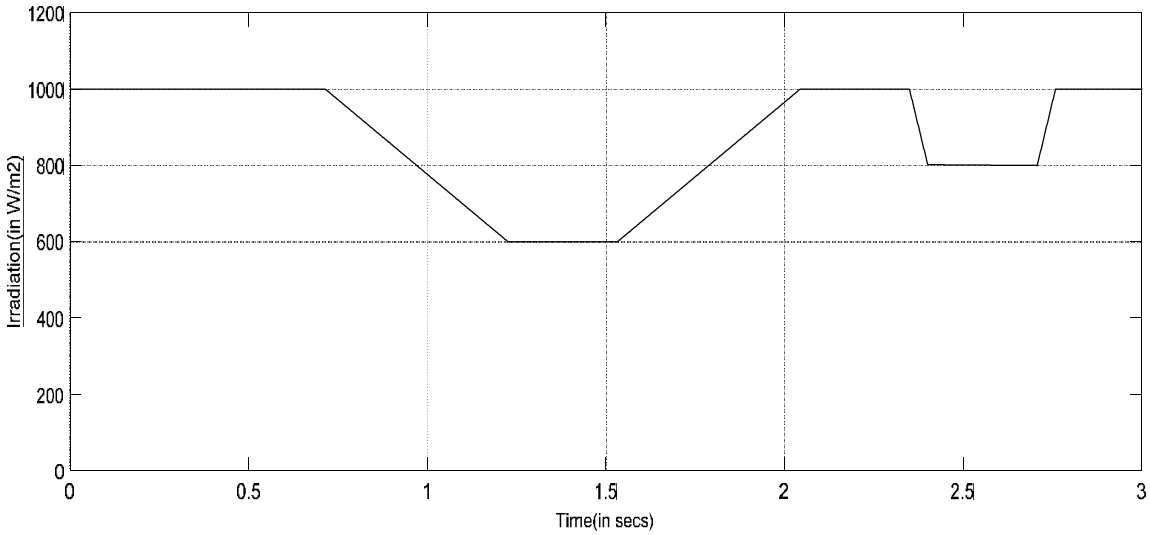

Fig.5. 28: Variable irradiation to PV array in one of the subsystems.

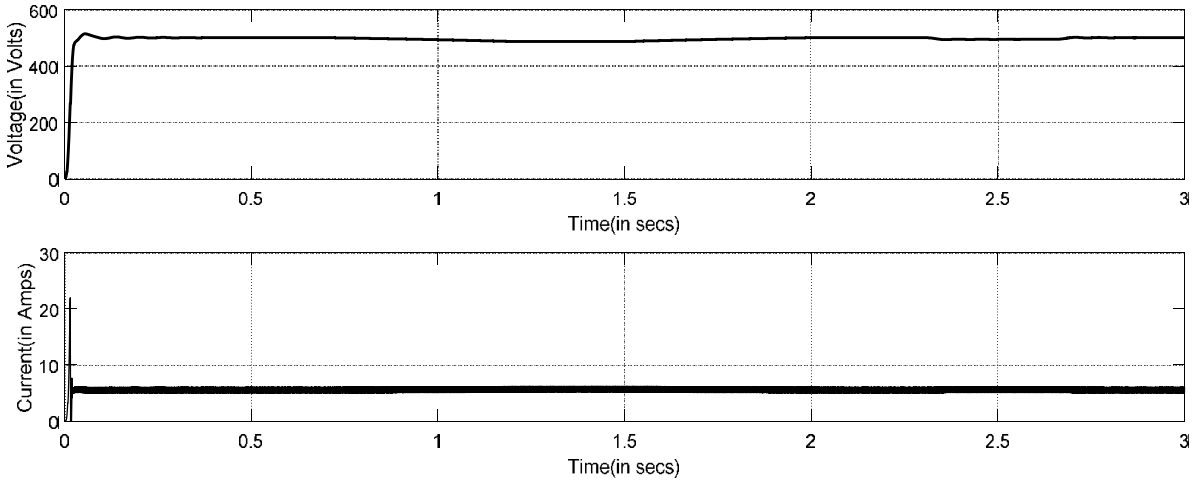

Fig.5. 29: Voltage and current responses of converter B_1.

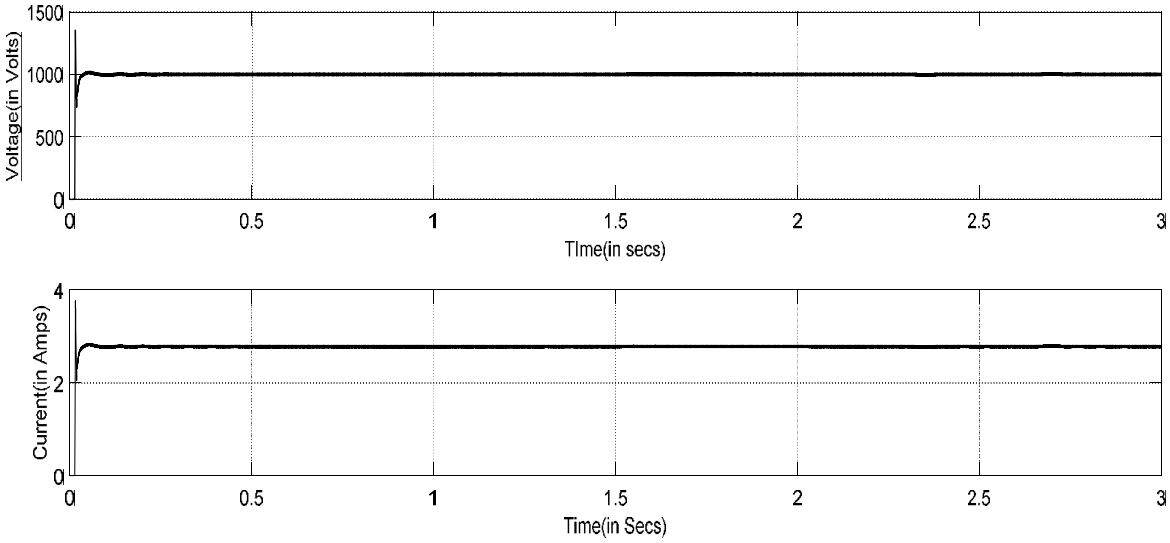

Fig.5. 30: Voltage and current responses of converter B_2.

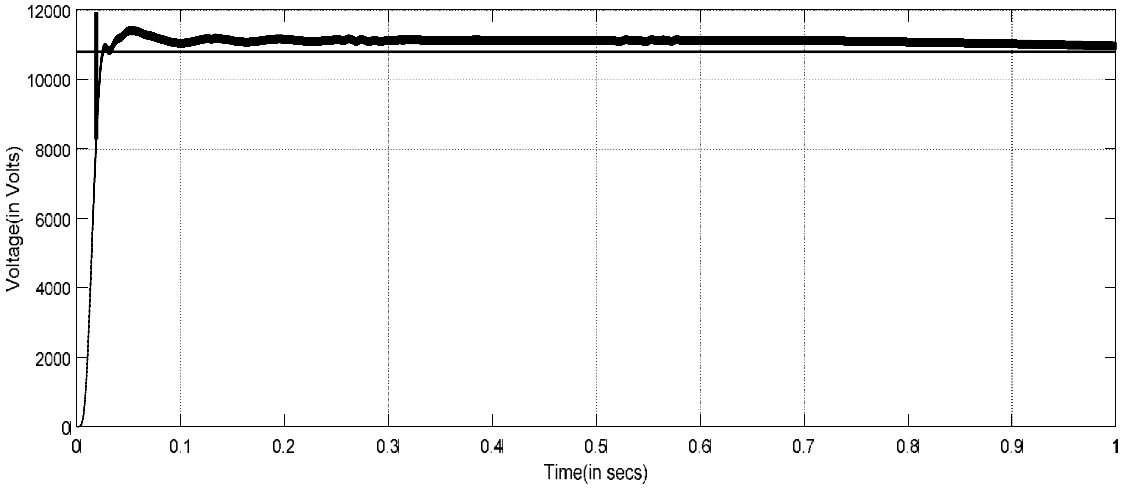

Fig.5. 31: Voltage fed to the DC grid without voltage droop controller, Desired DC grid voltage.

From the response it is observed that there are some perturbations in input fed to boost converter-2 because of MPPT control action and there are grid side fluctuations due to load disturbance, irrespective of that the desired grid voltage is achieved by controlling the duty cycle using RSM based two loop average current controller. The overall

response of the proposed system with MPPT control and without voltage regulating action is shown in Fig. 5.31; it is noticed the output voltage fed to the grid is different from desired grid voltage of 10.8 kV. From Fig. 5.32, it can be observed that due to the presence of hybrid control action the proposed system is able to generate the same output voltage as the grid demands.

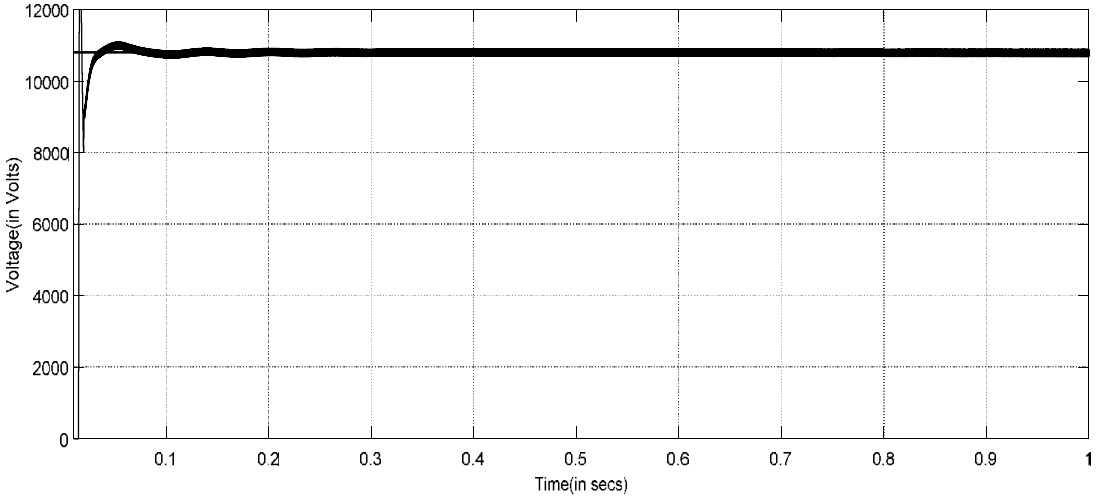

Fig.5. 32: Voltage fed to the DC grid with voltage droop controller, Desired DC grid voltage

Table 5. 6: Boost converter-1 specifications for Configuration-3

S.No	Parameters	Rating
1	Inductor	3mH
2	Capacitor	0.009 F
3	Switching Frequency	5000 Hz
4	Input Voltage	256.8
5	Output Voltage	500 V
6.	Output Current	5.58 A
7	Initial Duty Cycle, D	0.4864

Table 5. 7: Boost converter-2 specifications for Configuration-3

S.No	Parameters	Rating
1	Inductor	50 mH
2	Capacitor	15 μF
3	Switching Frequency	5000 Hz
4	Input Voltage	500 V
5	Output Voltage	1000 V

5.5.4. Partial Shading Condition

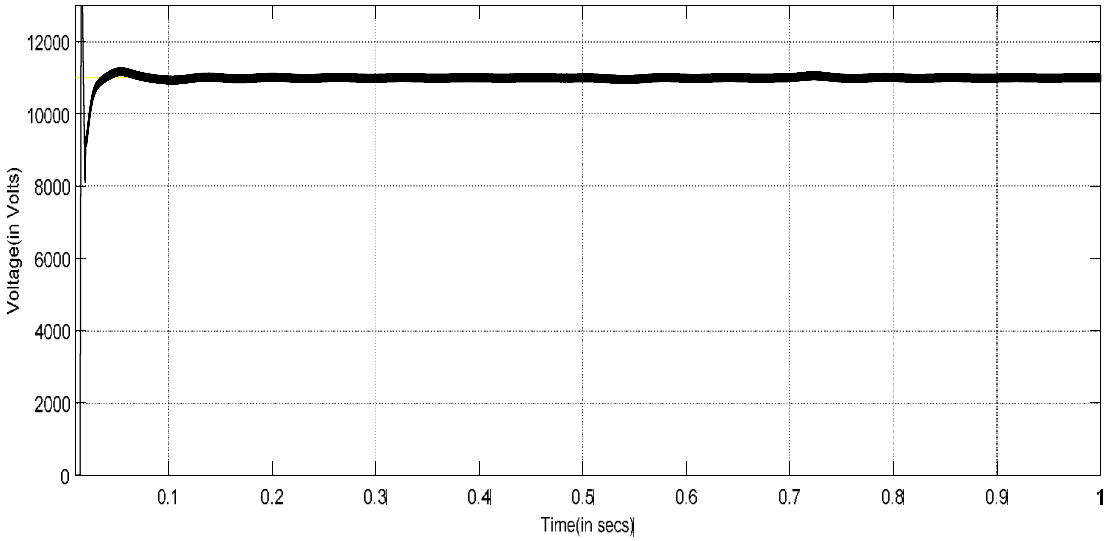

Fig.5. 33: Output voltage fed to DC grid under partial shading conditions in few subsystems.

In the system proposed, if one of the subsystems faces partial shading condition where as the others are fully exposed to sunlight then MPPT controller will try to extract the maximum power from the available P-V characteristics by controlling the duty cycle to new maximum power operating voltage. The rest of the converters along with voltage regulating unit will try to maintain desired grid voltage as shown in Fig. 5.33.

Compared to AC grid connected model of PV system the proposed DC grid connected model have no reactive power flow, reduced size and weight of conductor,

saving in copper and simple paralleling procedures. In addition to that, there are no reactive power compensators, frequency regulating devices and power factor correcting devices which saves the cost of investment.

From the results and analyses, it is observed that the proposed system performs well under different climatic conditions and varying load conditions the hybrid controller used here performs dual tasks of harnessing maximum power and regulating DC output. But the proposed system has drawback that if one of the subsystem fails to operate then the desired DC grid voltage is maintained by improving the voltage feeding capability of the rest of the subsystems which might exceed the converter capability. To overcome this drawback a novel topology is proposed in chapter 6 to integrate PV and wind farms to high voltage DC grid.

5.6. Stability Analyses of Boost Converter for Voltage Regulation

As a closed-loop control system, the on-off time of the switches need to be regulated to maintain the stable output and to achieve good static and dynamic characteristics by using the closed loop feedback.

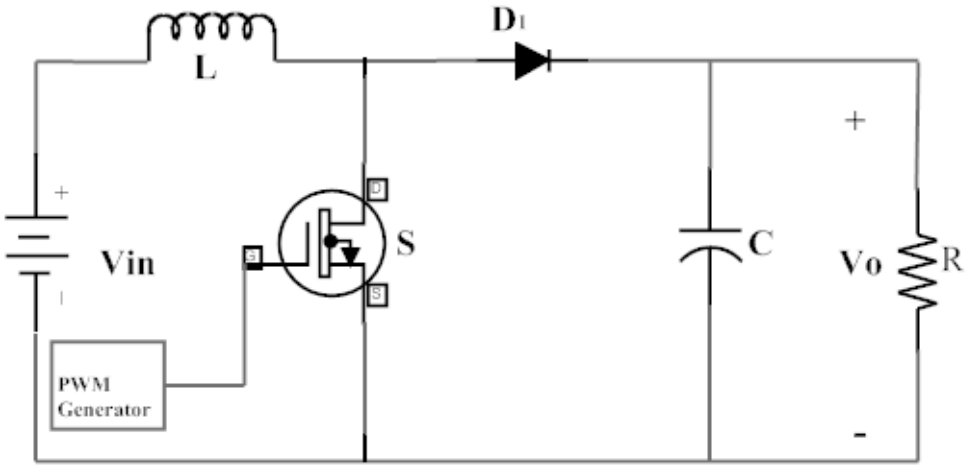

Fig.5. 34: Boost Converter Circuit.

5.6.1. Small Signal Modeling of DC-DC Boost Converter

The transfer function relating input and output parameters are derived using small signal modeling of DC-DC boost converter shown in Fig. 5.34, as discussed in section 3.3. The presence of nonlinear elements like IGBT switch and diode makes the converter a nonlinear time-varying system [118]. To linearize the non linear system, small-signal analysis method is used, which is commonly used in the dynamic modeling and analysis of switched converter topologies.

Small-signal linear dynamic model of the switching converter can be obtained with an assumption that the boost converter works at a stable operating point, [119]. If the disturbance signal was very small, it can be considered as the linear system under steady state. From this analysis, the transfer function for output voltage to duty ratio, output current to duty ratio and output voltage to output current are obtained. Small Signal modeling of DC-DC converter considering the ON state and OFF state equations are given below [119].

$$\begin{bmatrix} sL & 1-D_1 \\ 1-D_1 & -\left(sC+\frac{1}{R}\right) \end{bmatrix} \cdot \begin{bmatrix} \hat{i}_L(s) \\ \hat{v}_o(s) \end{bmatrix} = \begin{bmatrix} V_o(s) \\ I_L(s) \end{bmatrix} \hat{d}(s) + \begin{bmatrix} 1 \\ 0 \end{bmatrix} \hat{v}_{in}(s) \tag{5.6}$$

$$\begin{bmatrix} \hat{i}_L(s) \\ \hat{v}_o(s) \end{bmatrix} = \begin{bmatrix} sL & 1-D_1 \\ 1-D_1 & -\left(sC+\frac{1}{R}\right) \end{bmatrix}^{-1} \begin{bmatrix} V_o(s) \\ I_L(s) \end{bmatrix} \hat{d}(s) + \begin{bmatrix} sL & 1-D_1 \\ 1-D_1 & -\left(sC+\frac{1}{R}\right) \end{bmatrix}^{-1} \begin{bmatrix} 1 \\ 0 \end{bmatrix} \hat{v}_{in}(s) \tag{5.7}$$

Solving the above matrix, the relation between the output voltage and duty ratio control in transfer function form is given by,

$$\frac{\hat{v}_o(s)}{\hat{d}_0(s)} = \frac{(1-D_1)V_o - (L_1 I_L)s}{(L_1 C_1)s^2 + \frac{L_1}{R}s + (1-D_1)^2} \tag{5.8}$$

Similarly the transfer function of load current and duty ratio control is given by,

$$\frac{\hat{i}_L(s)}{\hat{d}_0(s)} = \frac{(C_1V_o)s + 2(1-D_1)I_L}{(L_1C_1)s^2 + \frac{L_1}{R}s + (1-D_1)^2} \tag{5.9}$$

The transfer function relating input current and output voltage is given by,

$$\frac{\hat{v}_o(s)}{\hat{i}_L(s)} = \frac{(1-D_1)V_o - (L_1I_L)s}{(C_1V_o)s + 2(1-D_1)I_L} \tag{5.10}$$

Where

V_o is the output voltage

I_L is current through the inductor

d_o is duty cycle of boost converter

V_c is voltage across the capacitor

The DC-DC converter B_2 consists of a series inductance of 50mH, shunt capacitance of 15 μF, diode and MOSFET switch with duty cycle of 0.5 and switching frequency 5 kHz. The input voltage is nearly 500 V at uniform irradiation and the output voltage is 1000 V, substituting the converter specifications in equation (5.9) and (5.10) gives the following transfer functions:

$$Tpv = \frac{\hat{v}_o(s)}{\hat{d}(s)} = \frac{500 - 0.279s}{75\times10^{-8}s^2 + 13.9\times10^{-5}s + 0.25} \tag{5.11}$$

$$Tpc = \frac{\hat{i}_L(s)}{\hat{d}(s)} = \frac{15\times10^{-3}s + 5.58}{75\times10^{-8}s^2 + 13.9\times10^{-5}s + 0.25} \tag{5.12}$$

Bode plot for the above open loop transfer functions are shown in Figure 5.35 and 5.36. It is observed that the "phase margin" is -90^o and "gain crossover frequency" is 2×10^4 rad/s for transfer function relating voltage and duty ratio. From the bode plot of

current to duty ratio control shown in Fig. 5.36, it is observed that "phase margin" is -90^{o} and "gain crossover frequency" is 3×10^{5} rad/s.

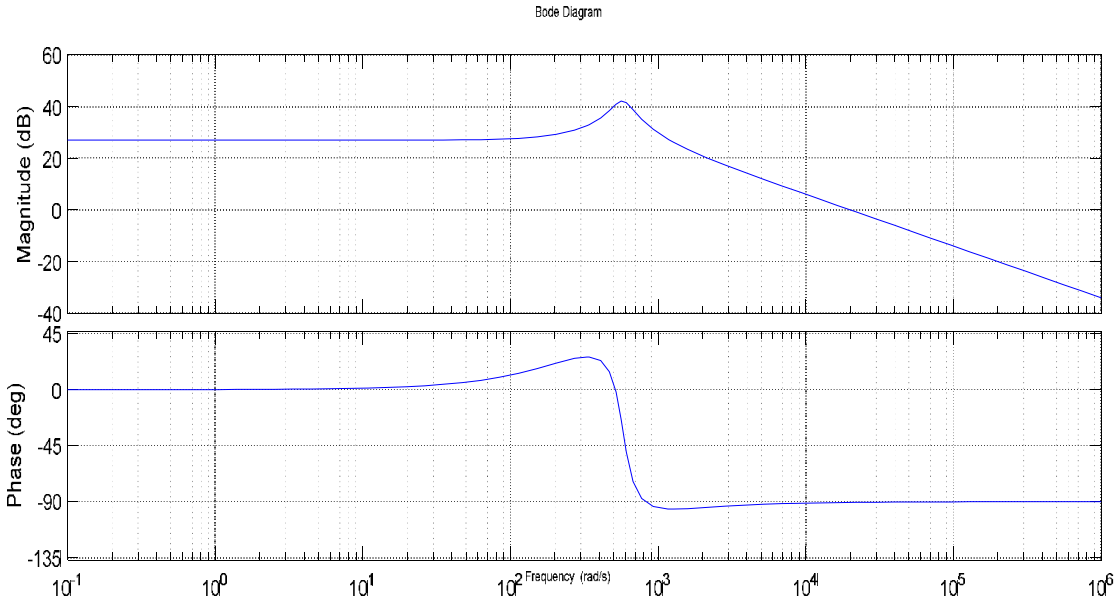

Fig.5. 35: Bode plot of transfer function in (5.11)

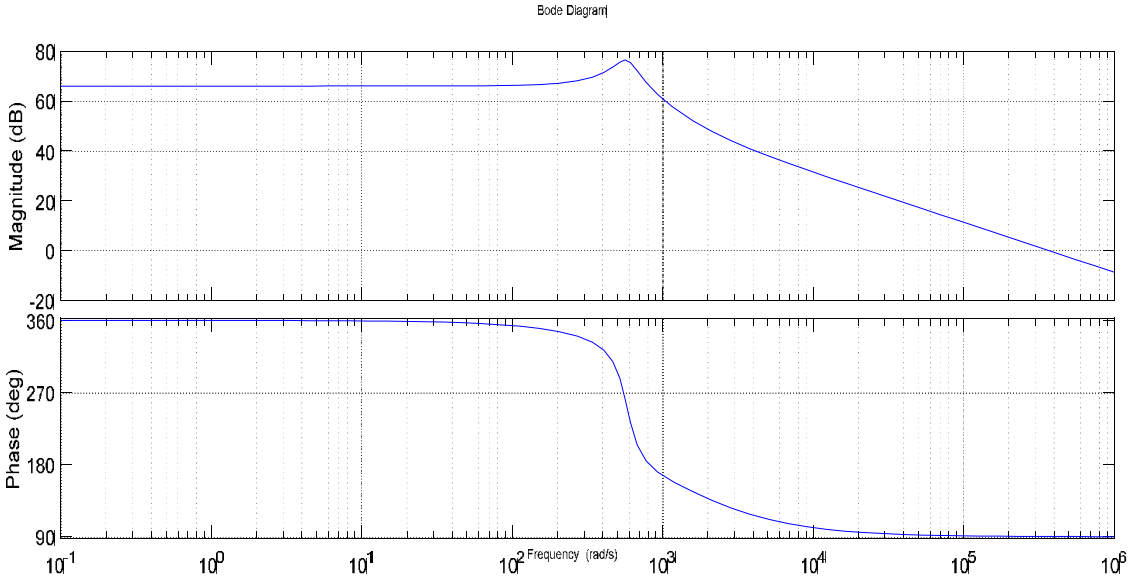

Fig.5. 36: Bode plot of transfer function in (5.12).

For proper design of closed-loop control system, the open loop transfer function of the final circuit should meet certain conditions for stability i.e. the "cross over

frequency" of open loop transfer function should have lesser phase margin (positive).To prevent quick changes in circuit, system should maintain higher bandwidth for quick response and improved system dynamic performance.

To enhance the frequency domain characteristics of the original system, "two loop average current control technique" is chosen here. For stable operation of PV and converter circuits, the bandwidths (BW) of two loops are separated with a slow moving voltage loop and a fast acting current loop.

5.6.2. Inner Current Control loop

The dynamics of inner loop (higher BW) are faster when compared to outer voltage loop (low BW) due to which the current in inductor changes faster than the voltage [120]. The block diagram of "inner current control loop" is shown in Fig. 5.37.

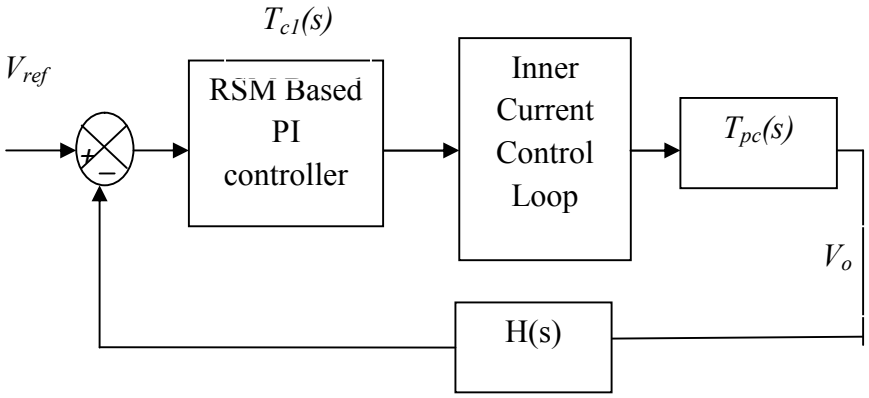

Fig.5. 37: Inner current control loop.

A triangular waveform is chosen as a reference modulating signal, whose frequency is same as switching frequency of the switch.

$$Vmp = K\frac{V_o - V_{in}}{L}.\frac{T_s}{2} = 500 \tag{5.13}$$

where K is a sensor multiplying factor, if it is a Hall effect sensor it is 1 V/A.

$Tm(s) = 1/Vmp = 0.002$

The PI controller transfer function is given by

$$T_{c1}(s) = K_p + \frac{K_i}{s} = \frac{K_p\left(s + \frac{K_i}{K_p}\right)}{s} \tag{5.14}$$

From random search method optimal values of K_p and K_i are found to be 0.436 and 2411.43. The "open loop transfer function of current control loop" is given by

$$T_{OL1}(s) = T_{c1}(s)T_m(s)T_{pc}(s)\,H_1(s) \tag{5.15}$$

On substituting the above equations in (5.23),

$$T_{OL}(s) = \frac{6.54\times10^{-3}s^2 + 38.6s + 1.35\times10^4}{75\times10^{-8}s^3 + 13.9\times10^{-5}s^2 + 0.25s} \tag{5.16}$$

From the bode plot shown in Fig. 5.38 it is observed that the phase margin is reduced and low frequency gain is improved indicating K_p and K_i values are optimal.

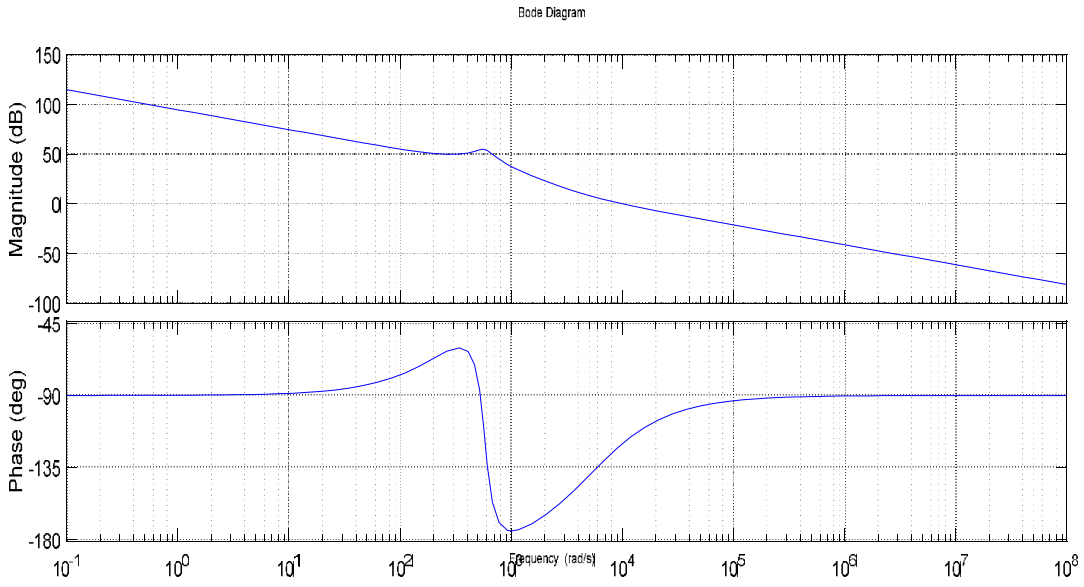

Fig.5. 38: Bode plot of transfer function in (5.16).

5.6.3. Outer Voltage Control Loop

It generates the reference parameter for inner current loop sensing the voltage as shown in Fig. 5.39. While designing voltage loop, the dynamics of inner loop are neglected since the fast acting current loop corrects the current errors quickly [120]. Hence, the sudden changes in duty cycle can be neglected in (5, 17), i.e., $\hat{d}(s) = 0$, Replacing d with D.

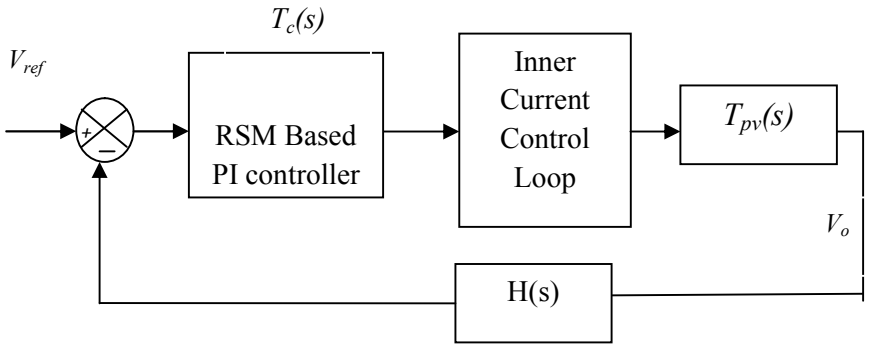

Fig.5. 39: Outer voltage control loop.

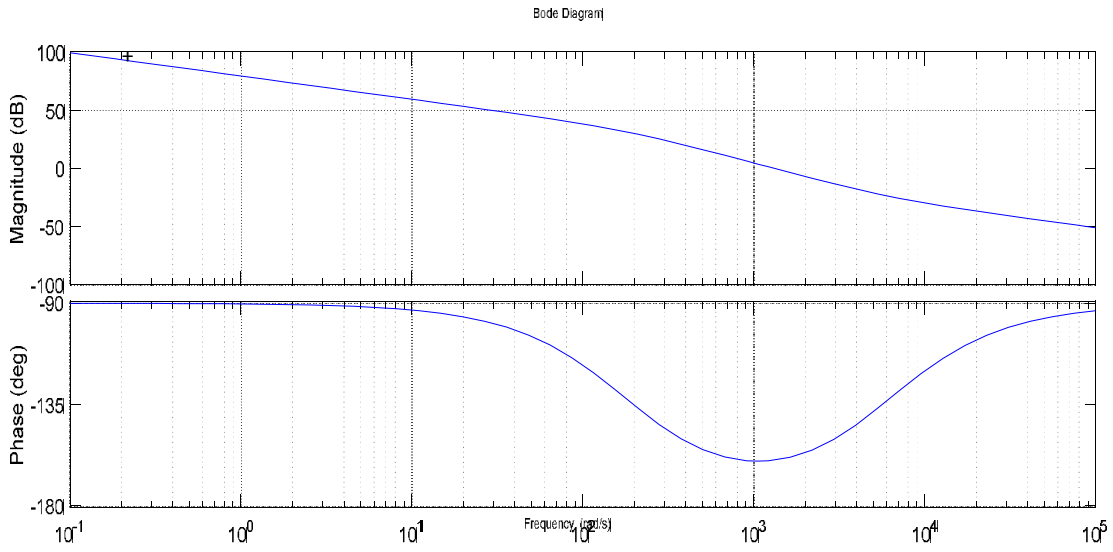

Fig.5. 40: Bode plot of transfer function in (5.20).

$$T_{c1}(s) = \frac{v_o(s)}{i_L(s)} = \frac{(1-D)}{\left(Cs + \frac{1}{R}\right)} \tag{5.17}$$

$$T_c(s) = K_p + \frac{K_i}{s} = \frac{K_p\left(s + \frac{K_i}{K_p}\right)}{s} \tag{5.18}$$

From random search method optimal values of K_p and K_i are found to be 0.0833 and 180.43.

The transfer function of outer loop is given by

$$T_{OL}(s) = T_c(s)T_{pv}(s)H(s) \tag{5.19}$$

$$T_{OL}(s) = \frac{285.3s + 1.718\times10^6}{s^2 + 185.2s} \tag{5.20}$$

From the bode plot of equation (5.20) as shown in Fig. 5.40, it is observed that the "phase margin" has reduced to 20^o and "gain cross over frequency" is 1216 rad/s. RSM based PI controller chosen here reduced the steady-state error improves the low frequency gain maintaining a "positive phase margin" and satisfying the stability criteria. Compared with other the techniques which involves computational delay and complex calculation using RSM techniques the optimal values of K_p and K_i are found accurately for a linear PI controller on real time.

5.7. Summary

This chapter focuses on DC grid integration of solar PV system, for which three different configurations are proposed. These configurations are proposed to address two major challenges faced during DC grid integration of PV system i.e. MPP extraction for varying input and stable DC grid voltage during grid side disturbances. The performance of the proposed configurations is evaluated under different combinations of input and

output variations. It has been observed that the configuration 3 performance is efficient. Consequently the hybrid controller proposed in chapter 4 is used in configuration 3.

From the results and analyses it is observed that the third configuration with proposed hybrid controller performs well under different climatic conditions and varying load conditions. The hybrid controller used here performs dual tasks of harnessing maximum power and regulating DC output. RSM based MPPT controller used here extracts the MPP accurately and efficiently; a stable and steady DC grid side response according to the grid requirement is being fed using RSM based two loop average current control technique. But it has drawback that if one of the subsystem fails to operate then the desired DC grid voltage is maintained by improving the voltage feeding capability of the rest of the subsystems which might exceed the converter capability. To overcome this drawback a novel topology is proposed in chapter 6 to integrate PV and wind farms to high voltage DC grid.

Second major work done in this chapter is, stability analysis of TLAC controlled DC-DC boost converter. From the stability analysis it is observed that the proposed controller produces a stable DC output voltage according to the grid needs with no delay in response.

Chapter 6

Performance Evaluation of High Voltage DC Grid Connected Solar PV and Wind Farms Using Hybrid Controller with FRT Protection

6.1. Introduction

In the previous chapter performance of DC grid connected solar PV system using hybrid controller is evaluated. In this chapter both solar PV and wind farms are connected to DC grid using hybrid controller. The specifications of the proposed topology are attained using Nanhui wind project, in China. The hybrid controller used here extracts the maximum power operating point from PV and wind in addition to achieving stable DC output voltage at low voltage DC grid. To maintain constant voltage in HVDC link during unsymmetrical faults on the AC grid side and also to satisfy grid codes an efficient fault ride through (FRT) protection scheme is implemented using chopper protection circuit. Simulation studies are performed to demonstrate the performance of the proposed configuration under varying weather conditions and grid side disturbances, using MATLAB/Simulink.

6.2. Description of Proposed Topology

The conventional topology for connecting offshore wind energy conversion systems (WECS) and large solar farms to DC grid using AC collection systems is shown in Fig. 6.1, it consists of rectifiers, inverters, transformers, DC cables to collect energy from the wind farm to offshore converter station. But this topology faces challenges like, moderate efficiency, larger size and weight, contributing higher installation and maintenance costs [123-125].

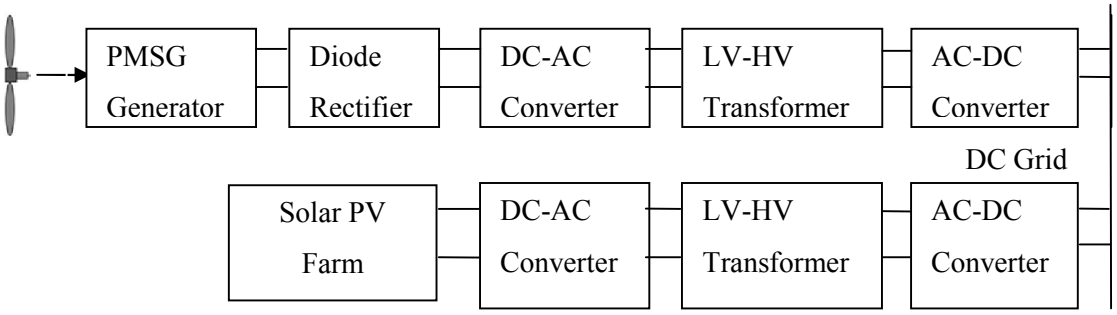

Fig.6. 1: Conventional topology for DC grid connected PV and Wind farms using AC collection systems.

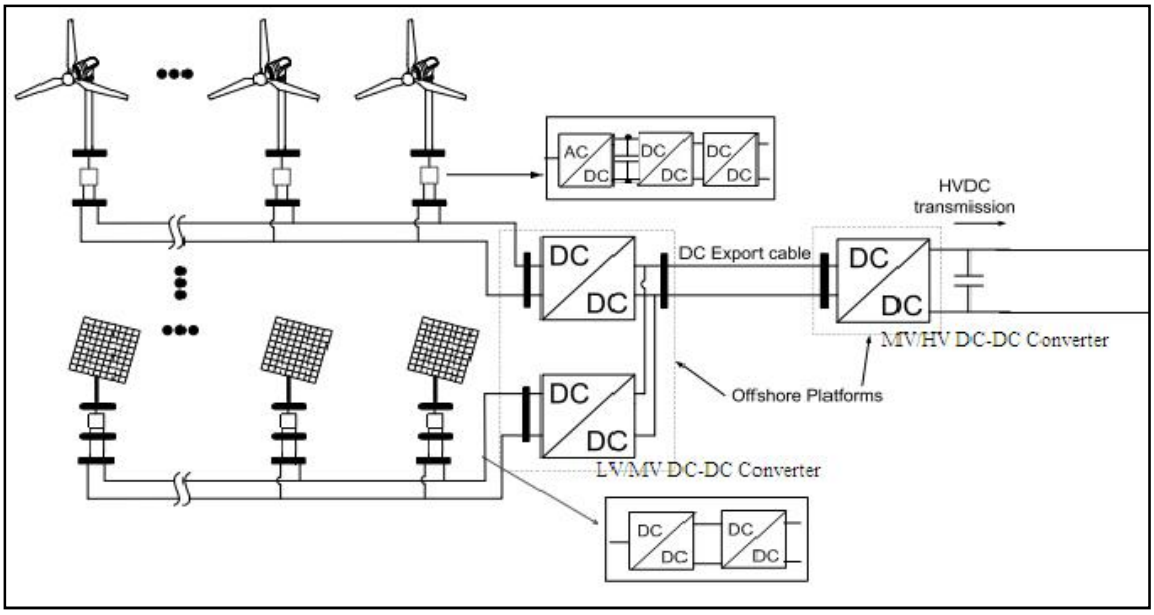

Fig.6. 2: Proposed topology for DC grid connected PV and Wind farms using DC collection systems.

The schematic diagram of the proposed system for connecting offshore WECS and solar PV farms to DC grid using DC Collection system is shown in Fig. 6.2. Nanhui wind project in China is considered as reference for constructing the proposed topology. It consists of a string of PV and Wind farms connected to low voltage DC grid of 1000V. Each PV string consists of solar PV farm of 100 kW power rating connected to low voltage DC grid using two series connected DC-DC converters where as in offshore wind farm string consists of wind turbine fed PMSG of

rating 200 kW connected to low voltage DC Grid using rectifier and two series connected DC-DC converters as shown in Fig. 6.3. Each of hundred such PV and wind farms are connected to low voltage DC grid to generate a power output of 30 MW.

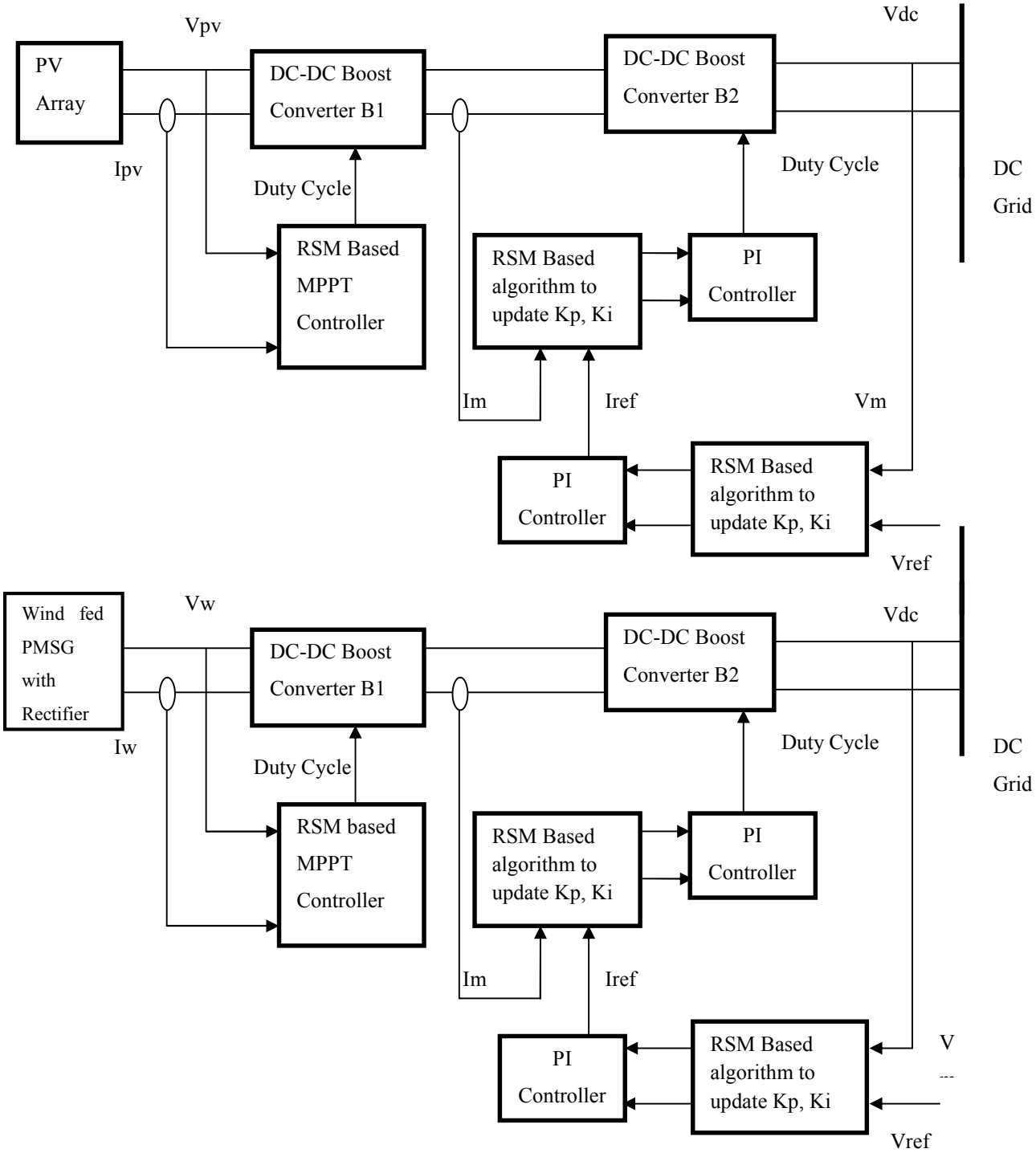

Fig.6. 3: Proposed Topology for DC grid connected PV and PMSG based WECS.

To track maximum power at fluctuating wind speeds and at variable irradiations MPPT controller using random search method is considered, it adjusts the duty cycle of converter-1 for maximum power extraction, while DC-DC boost converter-2 along with random search method based TLAC voltage regulator is used to maintain the stable DC output considering grid side and input side nonlinearities. In addition to that they will improve the voltage profile and helps in delivering the power to the offshore grid.

Many such strings consisting of PV and wind farms are connected to low voltage DC grid, which is connected to DC collection platform using MLBC circuit that steps up the voltage from 1k V to 10 kV. To achieve the high voltage gain and to transmit the power through HVDC transmission LCC coupled step-up DC-DC Converter is installed at offshore platform. It will step up the voltage from 10kV to 30kV.The proposed system eliminates inverters, heavy AC transformers and use of large filters, thus increasing overall conversion efficiency.

6.3. Modeling of Wind Energy Conversion System

In recent years, there is increase in research in the area of wind energy generation due to its advantages like inexhaustible potential, rise in competitive cost and environmental friendly nature [126]. Wind turbine transforms wind energy into mechanical energy. Wind turbine system usually consists of a gearbox that helps in matching the turbine low speed to speed of the generator which is rated for higher speeds, a blade pitch angle control for controlling the amount of power to be transformed.

The output of wind turbine system is coupled to the electrical generator which generates electrical energy from mechanical energy. At present, the wind generators used for commercial applications are squirrel cage induction generator (SCIG), wound field synchronous generator

(WFSG), and doubly fed induction generator (DFIG) and permanent magnet synchronous generator (PMSG) [127-130]. Considering the speed at which they rotate the wind turbine generators are classified into: fixed speed wind energy generation and variable speed wind energy generation.

Compared to fixed speed wind energy generation variable speed wind energy generation is more attractive due to improved energy generation and reduced flicker problem [131]. By operating wind turbine at wide range of wind speeds large amount of energy can be captured enabling the power coefficient to its maximum value in variable-speed wind turbines. At varying wind speeds, the wind turbine can be operated at MPP by maintaining the shaft speed optimally to achieve maximum efficiency at all wind velocities [132].

One of the major problems offered by variable-speed wind generation systems are the presence of the gearbox coupling, which increases the size of the plant, creates wear and tear as well as noise and reduces the efficiency [133]. Recently, there is increase in research interest on PMSG due to its advantages; the desirable features offered by PMSG are high air–gap flux density, compact size and structure due to the absence of external DC excitation, no gear box requirement, improved power density, high torque producing capability and large torque-to-inertia ratio [134]. PMSG when compared with an induction generator offers advantages like better efficiency as there are no rotor losses, reduced no-load current for speeds less than the rated speed and less sensitive to parameter variation of generator due to decoupling control [135]. Therefore, high performance variable-speed generation with better efficiency and great controllability is offered by PMSG based wind generation system.

6.3.1. WindTurbine modeling

The wind turbine will convert the associated kinetic energy of wind into mechanical energy. The kinetic energy associated with wind is given by, [133],

$$E_{kin} = \frac{1}{2} mv^2 \tag{6.1}$$

Where,

m is air mass and

v is velocity of wind

and the mass '*m'* can be expressed as

$m = \rho(Ad)$ (6.2)

Where,

ρ is density of air particles

A is area swept by the blades of the rotor

D is the distance travelled by the wind

Under ideal condition the mechanical power developed by the turbine is given by,

$$P_w = \frac{E_{kin}}{t} = \frac{\frac{1}{2}\rho A d v^2}{t} = \frac{1}{2}\rho A v^3 \tag{6.3}$$

where the actual power captured by the turbine always relies on efficiency of wind turbine, *Cp(λ, β)* which depends on two factors namely tip speed ratio (λ) and pitch angle (β)

Tip speed ratio, λ is turbine to the wind speed ratio, [133] and is given by,

$$\lambda = \frac{\omega R}{v} \tag{6.4}$$

Where ω is the angular speed of the turbine measured in rad/s, and R is the radius of the turbine in m. The actual power captured by the turbine is

$$P = \frac{1}{2} C_p(\lambda, \beta)\rho A v^3 \tag{6.5}$$

The torque developed by the wind turbine *T* is

$$T = \frac{1}{2} C_t(\lambda, \beta) \rho A R v^2 \tag{6.6}$$

where $C_t(\lambda, \beta)$ represents the torque coefficient of the turbine and $C_p(\lambda, \beta)$ is a nonlinear function

$$C_t(\lambda, \beta) = \frac{C_p(\lambda, \beta)}{\lambda} \tag{6.7}$$

The characteristics of the power conversion coefficient $C_p(\lambda, \beta)$ of the turbine aerodynamics can be estimated by the non-linear functions. The Cp-λ characteristics of wind turbine for different pitch angles are shown in Fig. 6.4, [135]. The speed-power characteristics of wind turbine at different wind speeds are shown in Fig. 6.5 [135].

$$C_p(\lambda, \beta) = c_1 \left(\frac{c_2}{\lambda_i} - c_3 \beta - c_4 \right) e^{-c_5 / \lambda i} - c_6 \lambda \tag{6.8}$$

Where

$$\lambda_i = \left[\frac{1}{\lambda + 0.08\beta} - \frac{0.035}{\beta^3 + 1} \right]^{-1} \tag{6.9}$$

The coefficients c_1 to c_6 are 0.5176,116, 0.4,5,21 and-0.0068

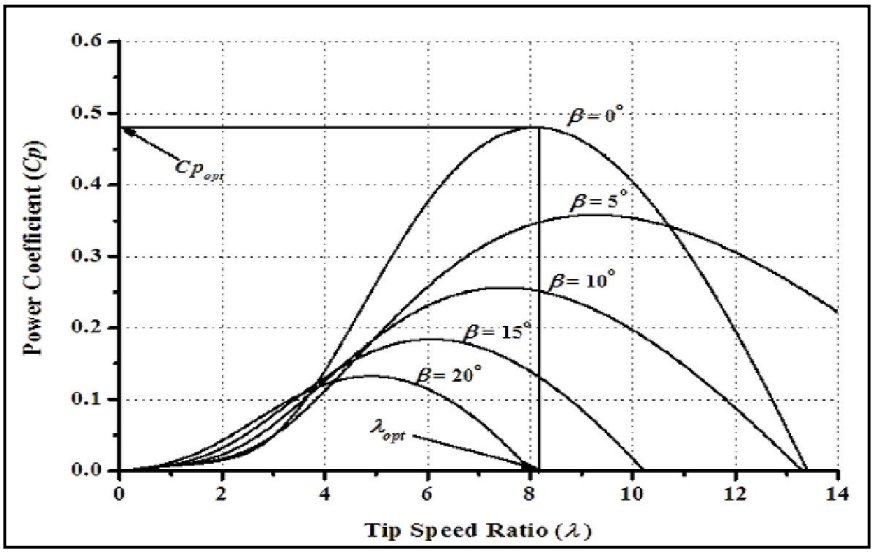

Fig.6. 4: *Cp-λ* characteristics of wind turbine

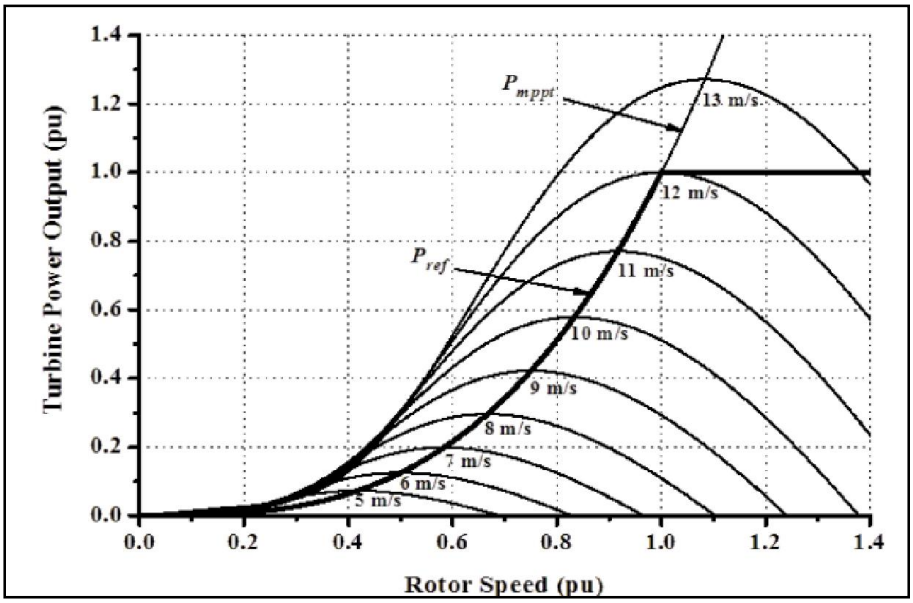

Fig.6. 5: Turbine Speed Characteristics

6.3.2. Drive Train Model

The shaft system of wind turbine coupled to generator can be represented in two different ways one is lumped mass system and the other one is two mass system [136]. It is more accurate to represent the shaft in two mass system model that considers the impact of grid side disturbances that leads to shaft oscillations in wind turbine generator. In two mass model, two separate masses are used to indicate the "low speed turbine, damper, high speed generator and spring".

The model of the drive train is shown in Fig. 6.6.

The differential equations representing electromechanical parameters of wind turbine and generator are given by,

$$2H_{tur}\frac{d\omega_{tur}}{dt} = P_m - K_s\theta_s - D_{tur}\Delta\omega_{tur} \tag{6.10}$$

$$2H_{gen}\frac{d\omega_{gen}}{dt} = K_{sh}\theta_{sh} - P_{el} - D_{gen}\Delta\omega_{gen} \tag{6.11}$$

$$\frac{d\theta_{sh}}{dt} = \omega_b(\omega_{tur} - \omega_{gen}) \tag{6.12}$$

Where,

H_{tur} is inertia constant of turbine

$H\text{-}_{gen}$ is inertia constant of generator

D_{tur} is damping coefficient of turbine

D_{gen} is damping coefficient of generator

K_{sh} is shaft stiffness coefficient

Θ_{sh} is Torsion angle of the shaft connecting the turbine

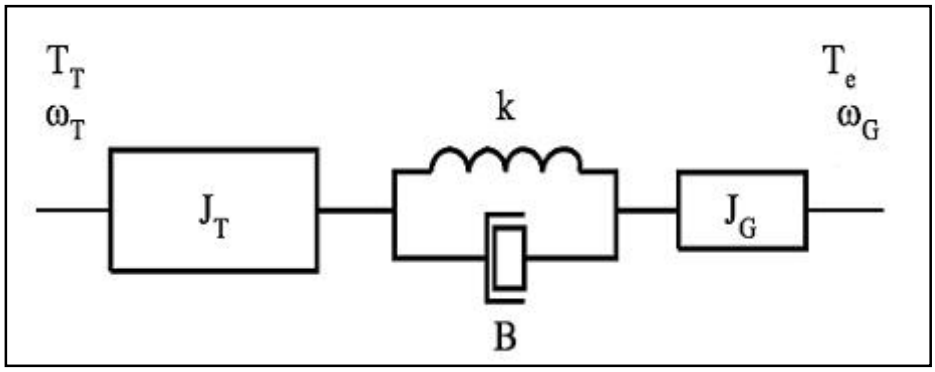

Fig.6. 6: Drive train model.

6.3.3. Permanent Magnet Synchronous Generator

Out of all Wind Energy Conversion Systems (WECS) available in literature for commercial power generation PMSG based variable speed WECS has accelerated growth due to its advantages like simple in structure, smaller in size and weight, lesser maintenance cost due to absence of gear box, slip rings and brushes, higher conversion efficiency and good controllability due to lesser sensitivity to the parameter variations [137]. So, PMSG based WECS is chosen for DC grid integration.

The dynamic model of PMSG is derived using two phase synchronous rotating reference frame in which the direct axis lags the quadrature axis by 90^o with respect to direction in which the rotor rotates. The equivalent circuit of PMSG in synchronous rotating reference frame for both quadrature and direct axis are given in Fig. 6.7 and 6.8.

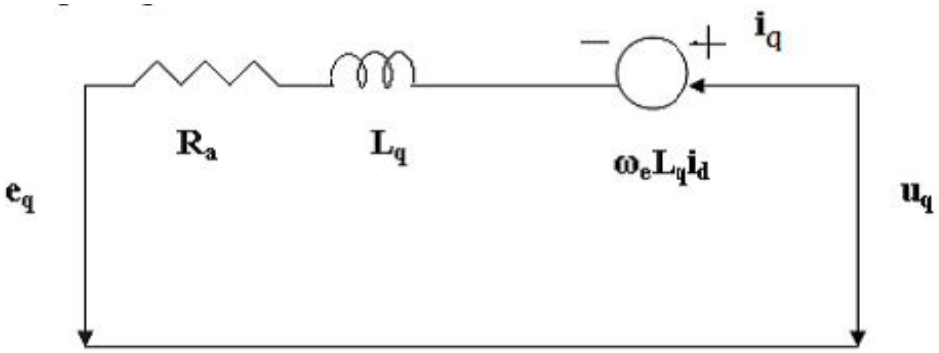

Fig.6. 7: Equivalent circuit of PMSG on quadrature axis.

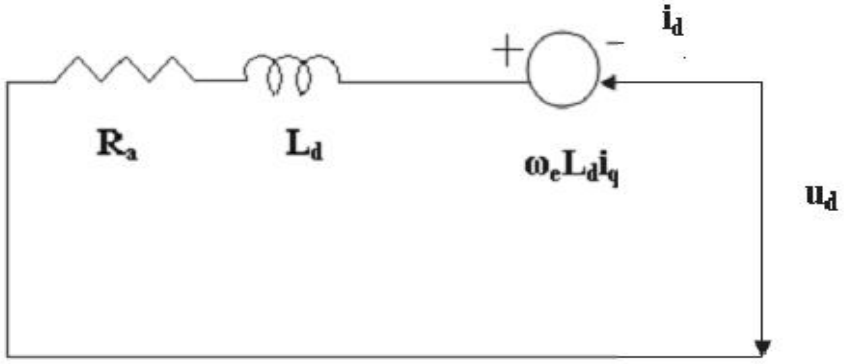

Fig.6. 8: Equivalent circuit of PMSG on direct axis.

The electrical representation of permanent magnet synchronous generator in synchronous reference frame is given by [136],

$$\frac{di_d}{dt} = -\frac{R_a}{L_d} i_d + \omega_e \frac{L_q}{L_d} i_q + \frac{1}{L_d} u_d \tag{6.13}$$

$$\frac{di_q}{dt} = -\frac{R_a}{L_d} i_q - \omega_e \left(\frac{L_d}{L_q} i_d + \frac{1}{L_d} \lambda_o \right) + \frac{1}{L_d} u_d \tag{6.14}$$

$$\omega_e = P\omega_g \tag{6.15}$$

$$e_q = \omega_e \lambda_o \tag{6.16}$$

$$T_e = 1.5P[(L_d - L_q) i_d i_q + i_q \lambda_o] \tag{6.17}$$

where,

R_e is winding resistance of the stator

ω_e is electrical rotational speed

ω_g is the mechanical rotational speed

λ_o is flux generated by the permanent magnets

P is number of poles

u_d is direct axis voltage and

u_q is quadrature axis voltage

L_d is inductance offered in direct axis

L_q is inductance offered in quadrature axis and

Te is electromagnetic torque developed

e_q is quadrature axis electromagnetic potential offered

Table 6. 1: Parameters of single solar PV module

S.No	Parameters	Rating
1	Maximum power	305.3 W
2	Voltage under open circuit	64.2 V
3	Voltage at maximum power	54.7 V
4	Current under short circuit	5.96 A
5	Current at maximum power	5.58 A
6	Number of PV cells per module	66

Table 6. 2: Specifications of Boost converter-1 and 2

S.No	Parameters	Rating
1	Inductance of converter-1	5mH
2	Capacitance of converter-1	0.006 F
3	Switching Frequency of converter-1	5000 Hz
4	Input Voltage of converter-1	256.8
5	Output Voltage of converter-1	550 V
6.	Output Current of converter-1	5.58 A
7	Inductance of converter-2	1 mH
8	Capacitance of converter-2	8 mF
9	Switching Frequency of converter-2	5000 Hz
10	Input Voltage of converter-2	550 V
11	Output Voltage of converter-2	1000 V

6.4. Results and discussion

In this work an efficient way to integrate large solar PV and wind farms to DC grid is proposed. In addition to it, the impact of DC chopper protection circuit on high voltage DC link over voltages caused during grid side faults is evaluated in the later section. The proposed system consists of DC grid connected solar PV and wind farms and intermediate DC-DC converter circuits (LV-MV and MV-HV converters). DC Grid connected PV farm consists of PV array, two DC-DC converters and a hybrid controller, each PV array consists of five series connected modules per string and sixty six strings in parallel. The specifications of each PV module are given in Table 1. The specifications of converter 1 and 2 are given in Table 2. Wind farm topology consists of wind turbine fed PMSG connected to low voltage DC grid, using diode

rectifier and series connected boost converters 1 and 2 along with hybrid controller. The specifications of wind turbine, PMSG and converters 1 and 2 are given in Table 3.

The performance of the system under different test conditions namely, at constant input with fixed load, at varying input with fixed load and at varying input with load disturbance are studied.

Case A: At constant input and fixed load

In solar PV system, for a constant input irradiation of 1000W/m^2, the output voltage response of converter B_1 and B_2 are shown in Fig. 6.9 and 6.10. It is observed that converter 1 and 2 produces a stable DC voltage of 500 V and 1000 V and an output current of 200A and 100A respectively, as shown in Fig. 6.11. The output power delivered to the low voltage DC grid at constant irradiation of 1000 W/m^2 is nearly 100 kW.

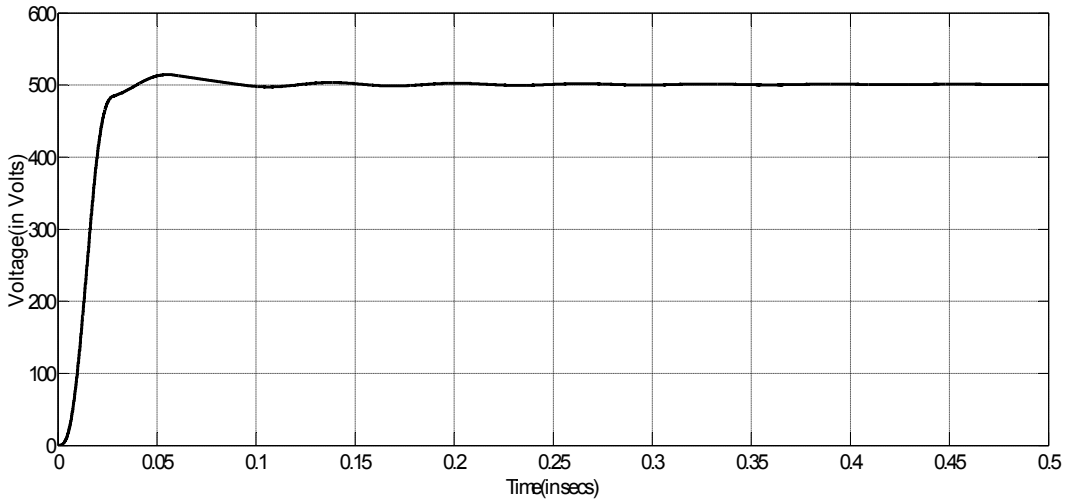

Fig.6. 9: Output voltage response of converter 1.

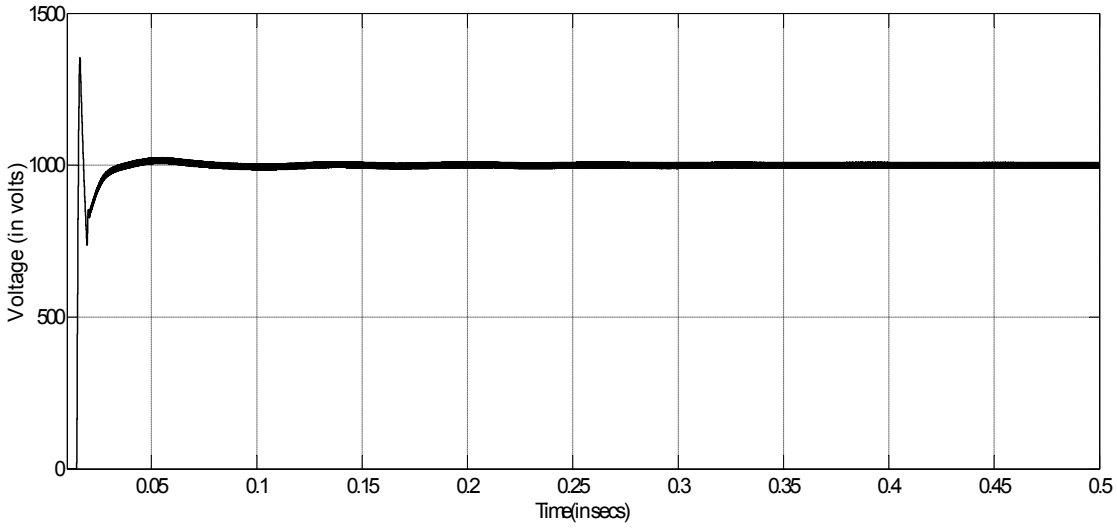

Fig.6. 10: Output voltage response of converter 2.

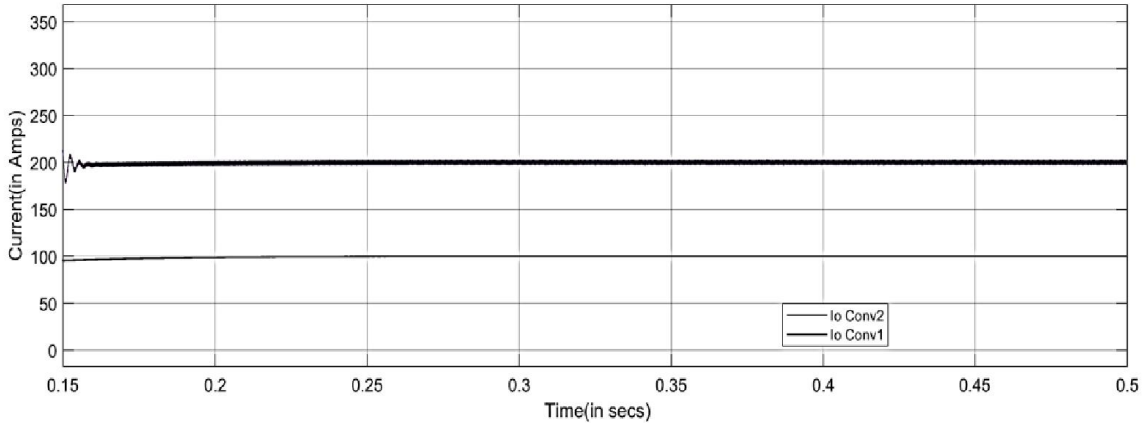

Fig.6. 11: Output current response of converter 1 and 2.

At constant wind speed of 12m/s, the performance of wind farm connected to low voltage DC grid is evaluated. The speed of the rotor, torque developed and generated output voltage of PMSG at 12m/s wind speed are shown in Fig. 6.12 and 6.13. The input voltage to the coverter-1 at constant wind speed is 250 V. The voltage and current response of converter 2 connected to DC grid are shown in Fig. 6.14, it is shown that the magnitude of voltage and current are 1000 V and 200A respectively generating a power output of 200 kW.

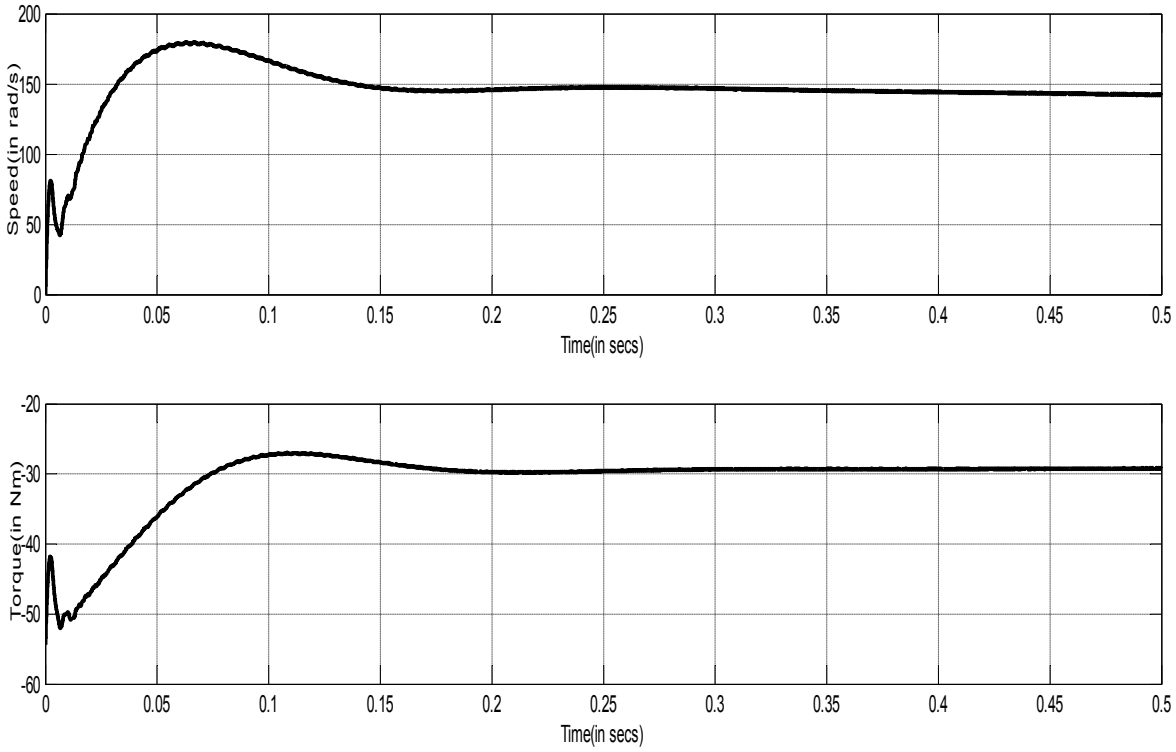

Fig.6. 12: Speed and torque developed by wind turbine.

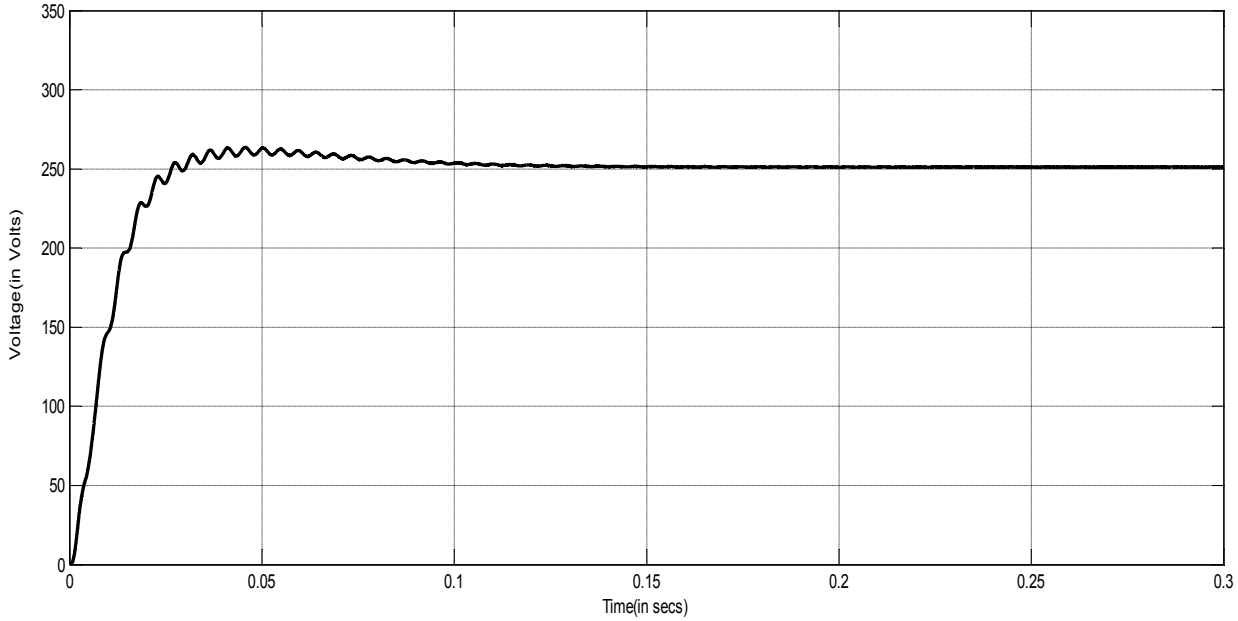

Fig.6. 13: Input voltage to DC-DC converter1 at constant wind speed.

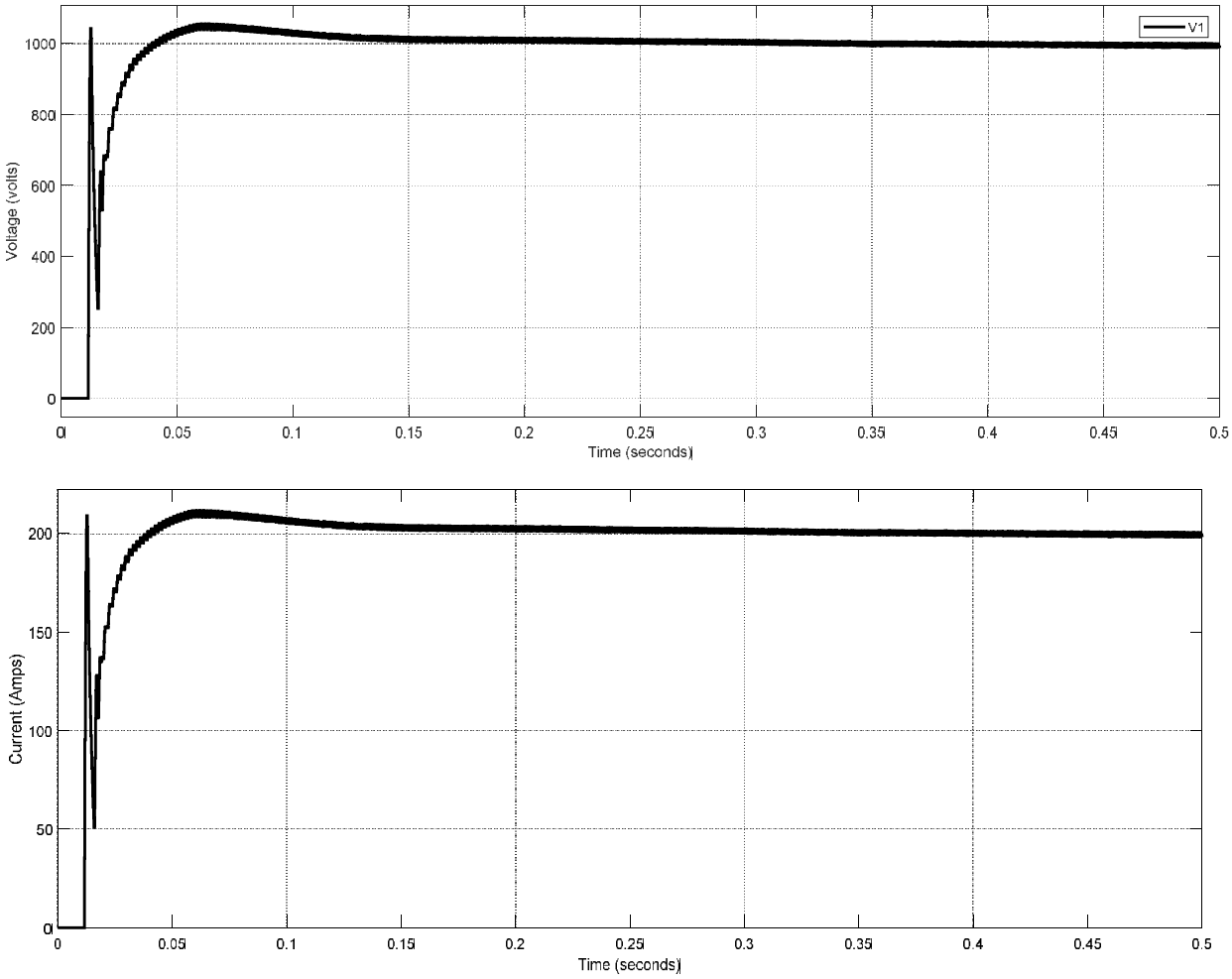

Fig.6. 14: Output voltage and current response of converter-2 using hybrid controller at constant wind speed

Table 6. 3:Wind Turbine, PMSG And Converters Specifications

Parameter	Rating
Mechanical power output	200 kW
Base wind speed	12 m/s
Stator phase resistance Rs	0.4578
Armature Inductance	3.34 mH
Voltage Constant (L-L)/rpm	248.12 V/rpm
Flux established by magnets (V.s)	0.17099 Vs
Inductance of converter-1	3mH
Capacitance of converter-1	0.005 F

Switching Frequency of converter-1	5000 Hz
Input Voltage of converter-1	250 V
Inductance of converter-2	1 mH
Capacitance of converter-2	10 mF
Switching Frequency of converter-2	5000 Hz
Input Voltage of converter-2	500 V
Output Voltage of converter-2	1000 V

Table 6. 4: MLBC Specifications

Parameter	**Rating**
Power	30 MW
Input Voltage	1 kV
Output Voltage	10 kV
Capacitances	50 μF
Inductances	30 mH
Switching Frequency	5 kHz

Case B: At varying input irradiation and wind speed with fixed load

As the input irradiation to PV system varies as given in Fig.6.15, the output voltage and current response of converter-1 with RSM based MPPT technique is shown in Fig. 6.16. The maximum power extracted by converter-1 with MPPT controller is shown in Fig. 6.17. From the response it is observed that random search method is able to extract the maximum power by controlling the duty cycle and hence the output voltage of converter-1.The output voltage response of converter-2 with fixed load on DC grid with and without voltage regulator are shown in Fig.6.18 and Fig. 6.19. From the voltage response of converter-2 it is observed that though there are input side perturbations the output voltage is still maintained at 1000 V due to RSM based TLAC voltage controller.

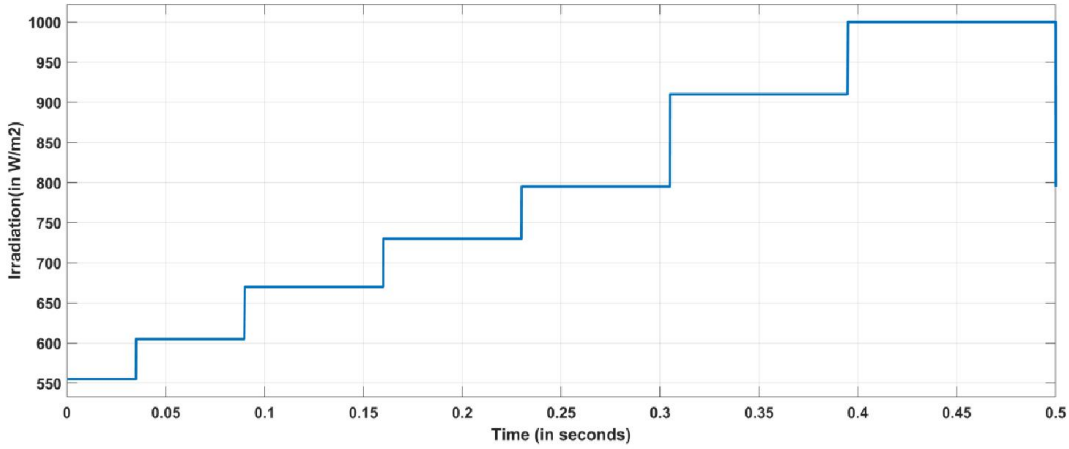

Fig.6. 15: Input irradiation to PV array of 100 kW rating.

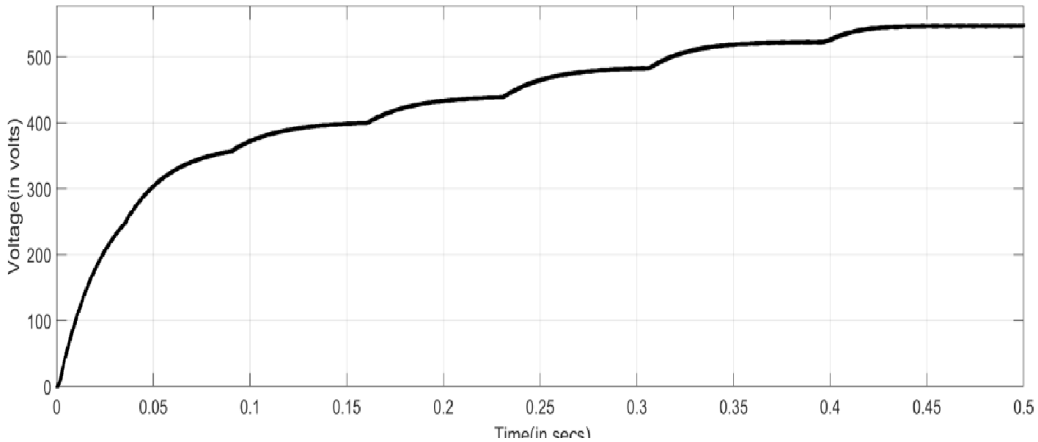

Fig.6. 16: Output voltage of converter 1 at variable irradiation.

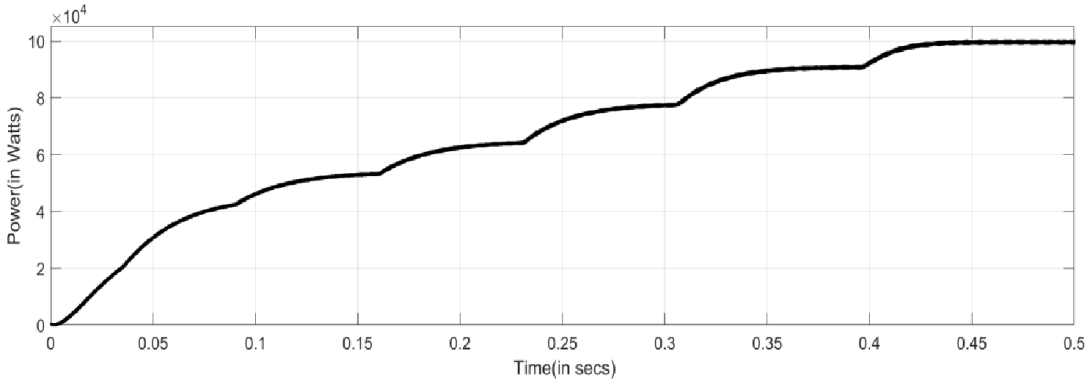

Fig.6. 17: Maximum power extracted by converter1 with RSM based MPPT controller.

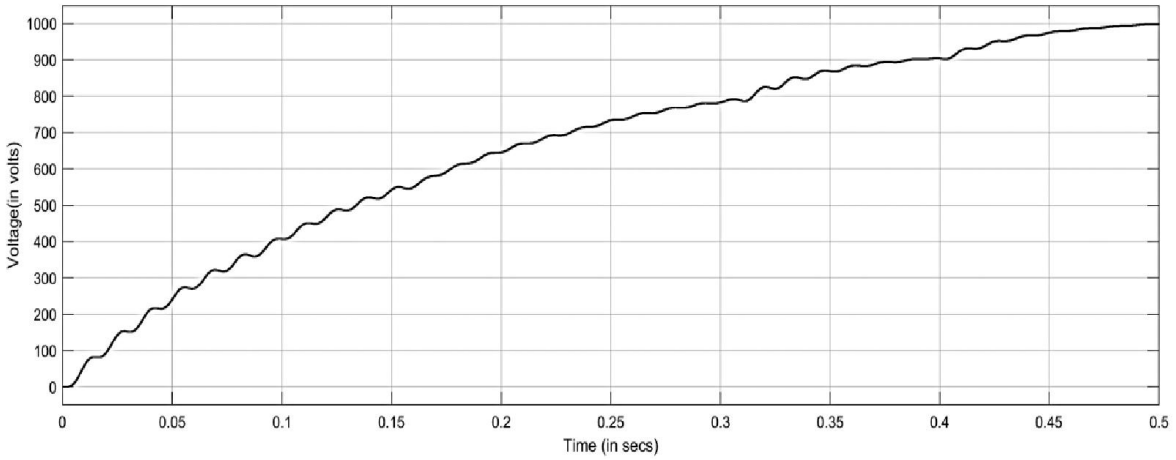

Fig.6. 18: Output voltage of converter-2 at variable irradiation and fixed load without voltage regulator.

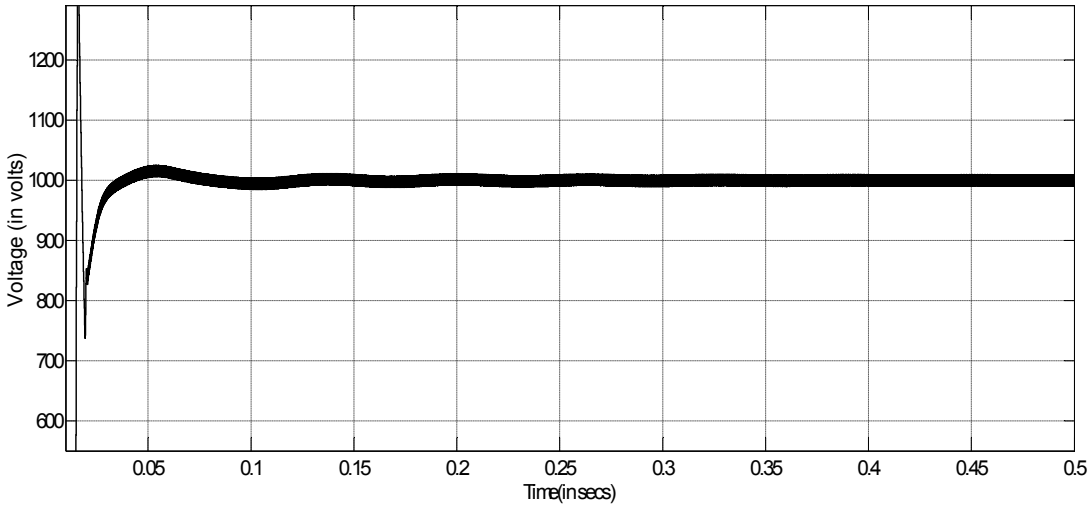

Fig.6. 19: Output voltage of converter-2 at variable irradiation and fixed load with voltage regulator.

At varying wind speed as shown in Fig. 6.20, the output response of converter-1 is shown in Fig. 6.21. RSM based MPPT technique is implemented here as it offers good tracking efficiency and extracts the maximum power. At varying wind speed the output response of converter-2 is shown in Fig. 6.22. The output voltage is maintained at 1000 V due to the presence of RSM based TLAC voltage controller.

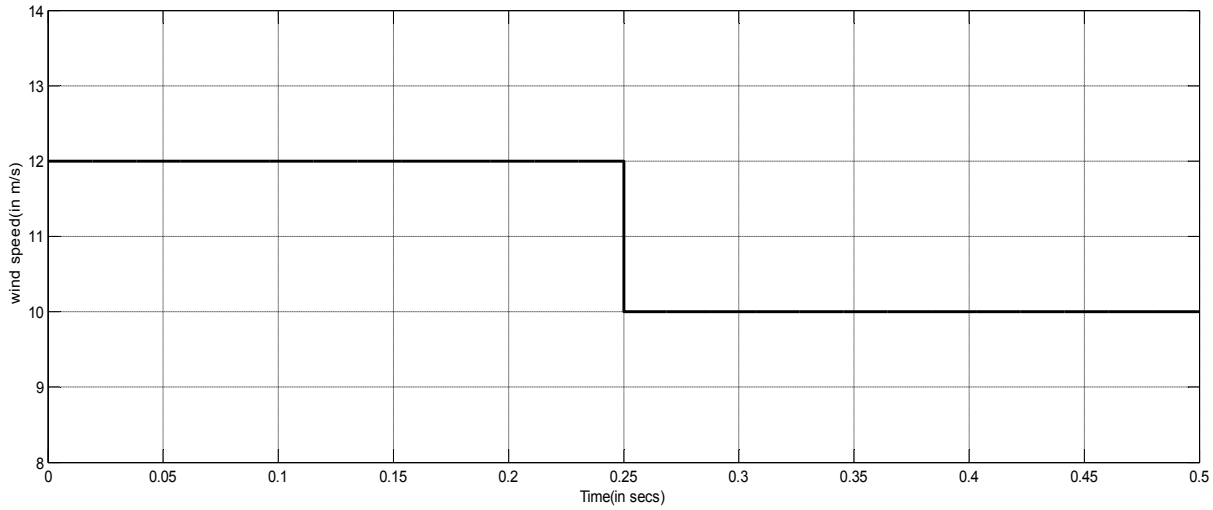

Fig.6. 20: Variable wind speed.

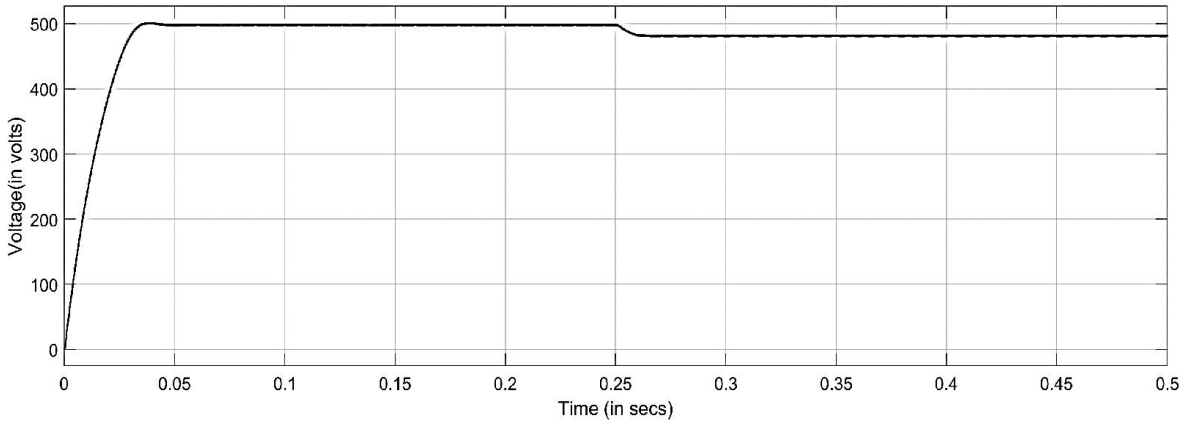

Fig.6. 21: Output voltage response of converter-1 using MPPT controller at variable wind speed

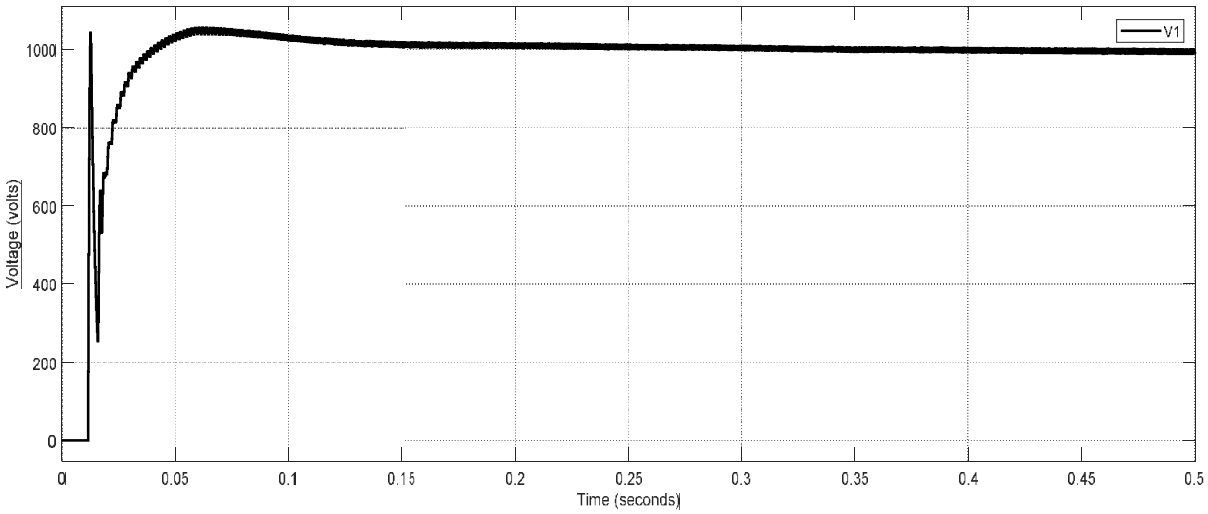

(a)

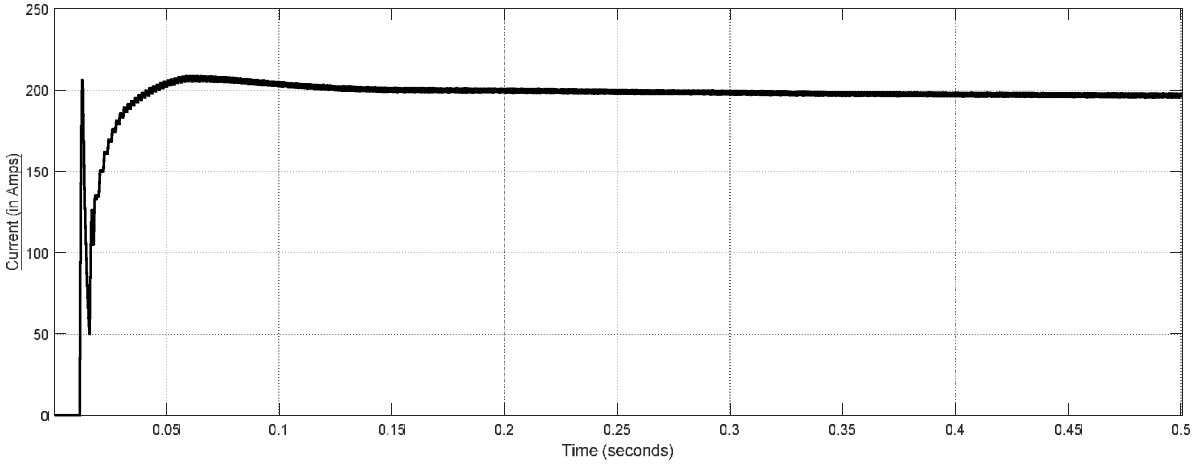

(b)

Fig.6. 22: Output(a) voltage and(b) current response of converter-2 using hybrid controller.

Case C: Variable input with grid side disturbance:

The performance of the proposed PV system at variable input irradiation and with disturbances at load end is analyzed in this section. If the input irradiation varies as shown in Fig.6.15 and LV grid side voltage is changed from 1000 to 1050 V then the output voltage response of converter-2 is shown in Fig. 6.23. From the voltage response it is identified that DC voltage of 1050 V, is fed to low voltage DC grid as the grid demands using proposed voltage controller.

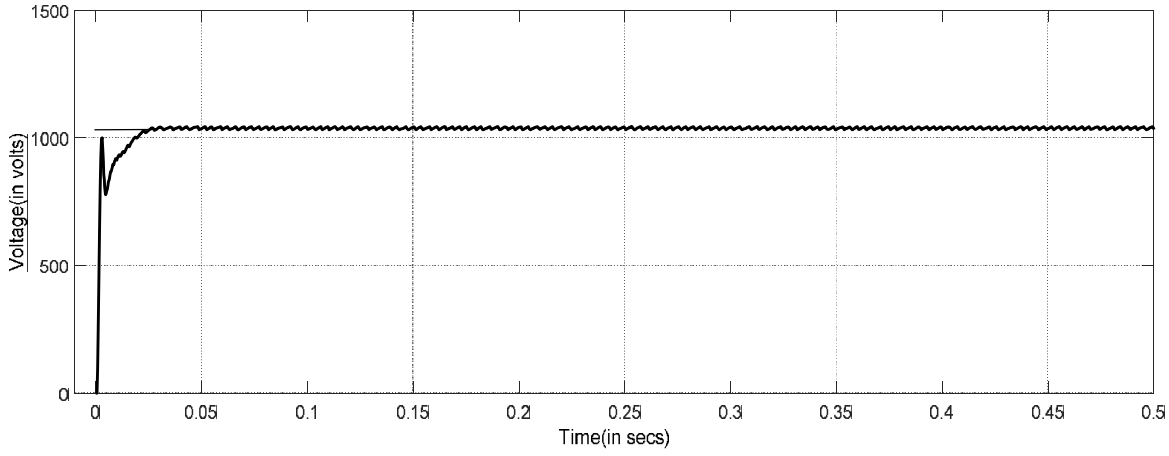

Fig.6. 23: Output voltage fed by solar PV farm to DC grid at variable load using proposed voltage regulating technique

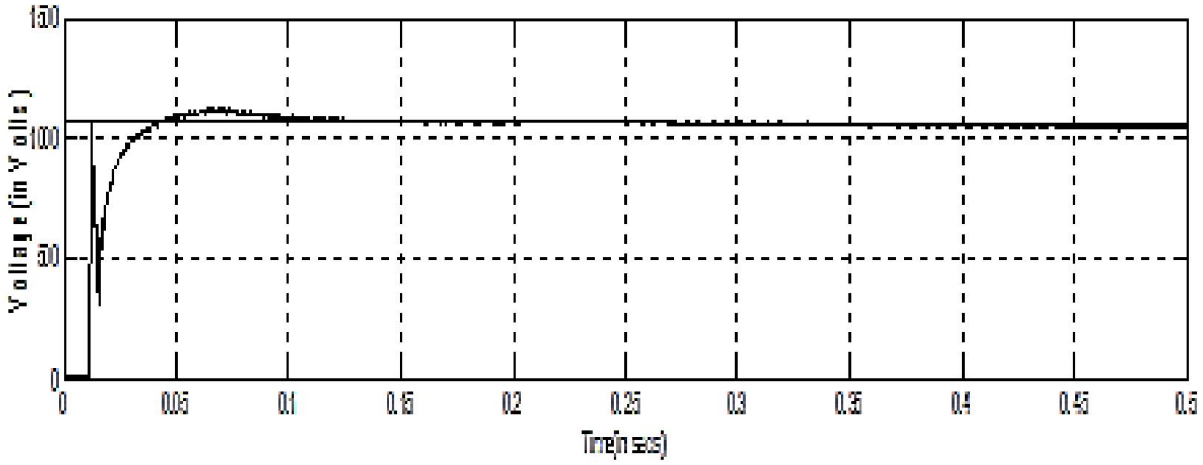

Fig.6. 24: Output response of converter-2 of wind topology during grid side voltage fluctuations.

Likewise, when the wind speed changes as shown in Fig. 6.20 and grid voltage changes from 1000 to 1050 V the voltage response of wind farm connected to low voltage DC grid is shown in Fig. 6.24. From the response of proposed system it is observed that the output voltage is stable and same as desired DC grid voltage.

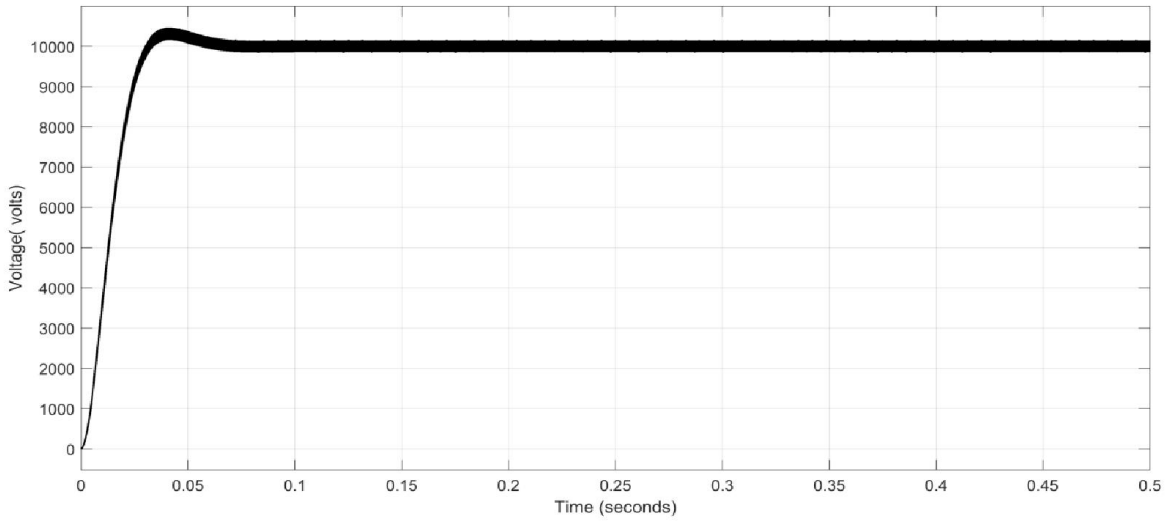

(a)

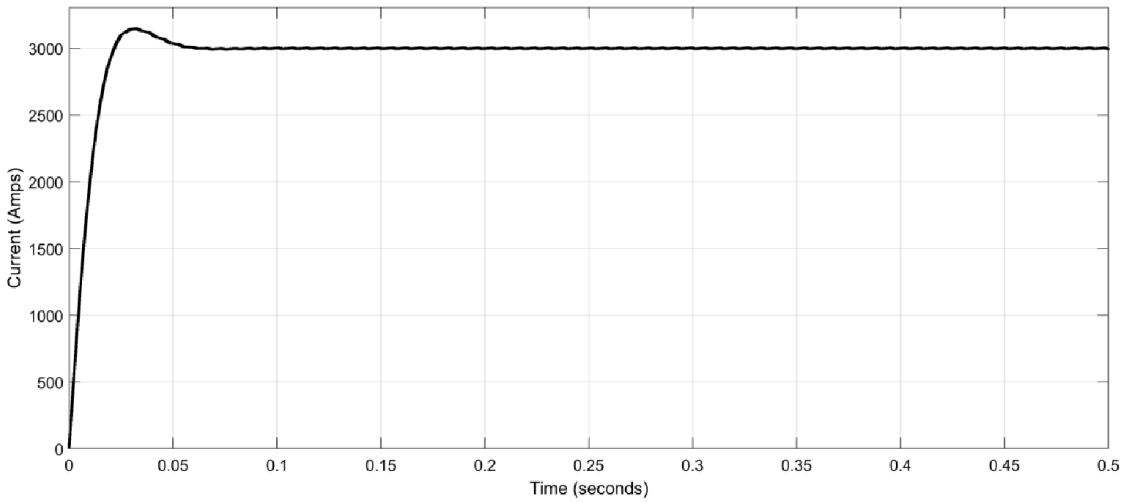

(b)

Fig.6. 25: MLBC (a)output voltage and (b) output current response.`

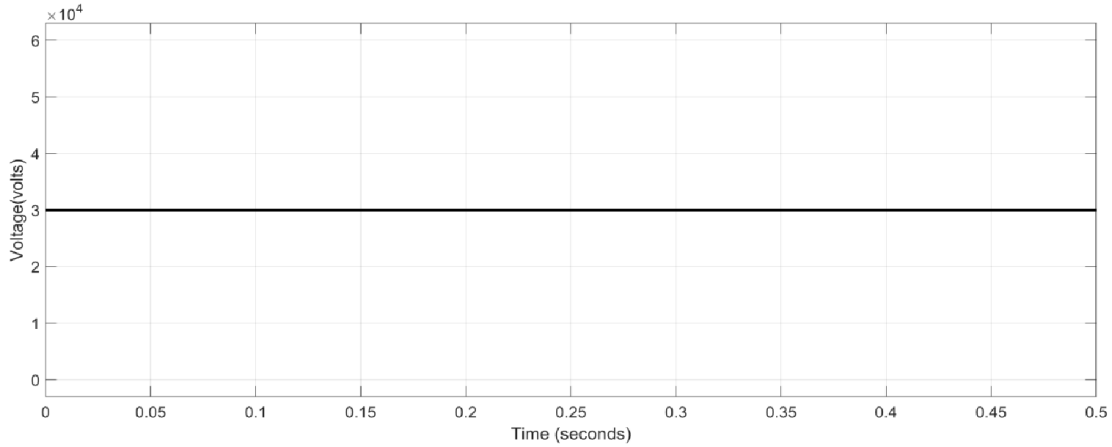

Fig.6. 26: LCL boost converter output voltage response.

Low voltage DC grid side voltage of 1000 V is stepped up to 10 kV using MLBC circuit. The output voltage and current response of MLBC circuit is shown in Fig. 6.25. At DC collection platform the DC voltage is stepped up from 10 kV to 30 kV using LCL boost converter circuit. The specifications of LCL boost converter and MLBC are given in Table 6.4 and 6.5. The output voltage and current response of LCL Boost converter are shown in Fig. 6.26 and 6.27. The output voltage of LCL boost converter is 30kV, which is the voltage rating of HVDC transmission link. The output current of LCL converter is 1 kA. The power transferred by HVDC transmission link is 30 MW.

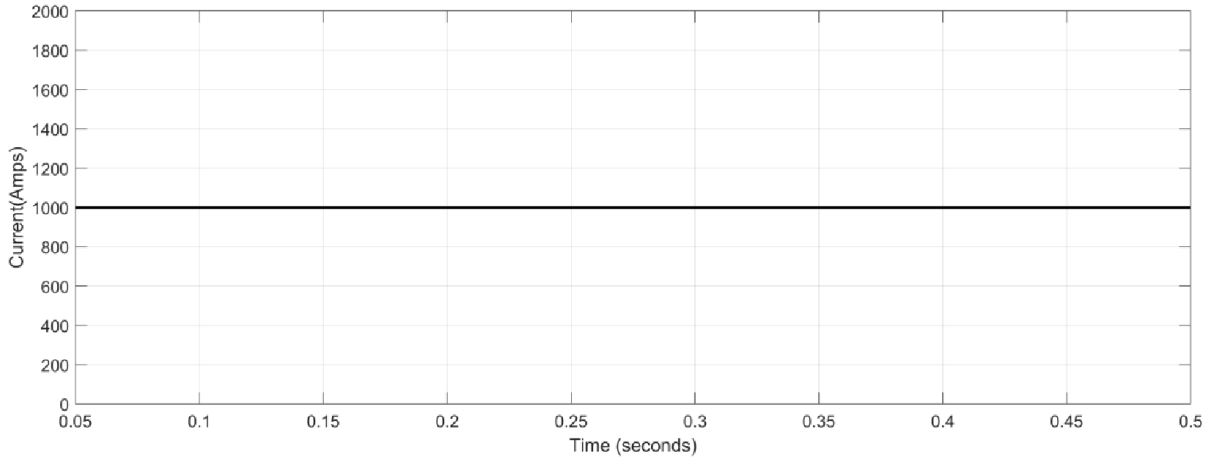

Fig.6. 27: LCL boost converter output current response.

Table 6. 5:LCL Boost Converter Specifications

Power	30 MW
Input Voltage	10 kV
Output Voltage	30 kV
Capacitances C_1, C_2	120 µF, 10 µF
Inductances L_1, L_2	10.67 mH and 43 mH
Switching Frequency	1.5 kHz

6.5. Fault Ride Through Protection

6.5.1. Introduction

According to TenneT Grid Codes, it is needed that a wind farm should stay connected to the grid when fault occurs on grid [139]. Even if the voltage dip is maximum at AC grid during fault period that should not disconnect the wind or solar PV farm from grid for a fault-clearing period of up to 150 ms as shown in Fig. 6.28. In the area above the limit line 1, instability of the wind or solar PV farm and disconnection from the grid are not permitted. Above limit line 2, if there are any technical problems like instability etc. exists then the wind or solar PV farm is allowed to disconnect from the grid.

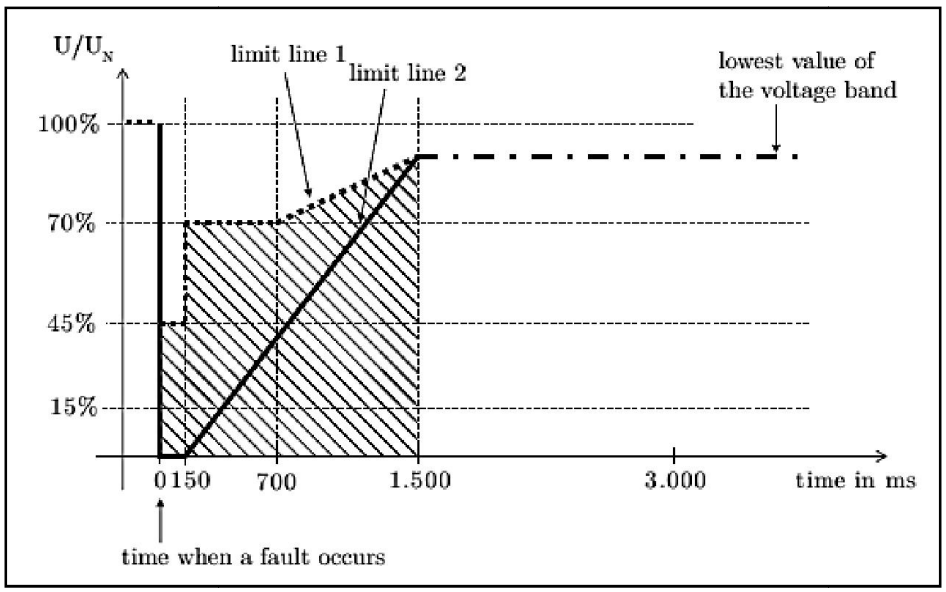

Fig.6. 28: TenneT GC fault Ride-through point of common coupling voltage limit lines [138].

In the proposed system, the other end of HVDC transmission is connected to AC grid using inverter to covert DC power to AC, since the consumption of electricity is in AC. In case, if three phase short circuit fault occurs near to AC grid side converter then the total power transfer capability of the converter will be limited due to voltage dip at PCC, AC grid side voltage drops will create a sudden rise in the DC link voltage causing damage to the equipment nearby. The energy supplied by the wind farms during this fault period creates an imbalance in power, which charges the capacitance in DC link. The DC system responds to this imbalance with a short time constant leading to over-voltages that could create a potential damage to the DC equipment. There are many techniques proposed in literature to limit this overvoltage. Controlled resistors, crowbar protection circuit, DC snubber circuit, series dynamic resistor circuit, Series Fault Current Limiter and DC Chopper protection circuits are proposed that will dissipate excess energy in the DC link in order to maintain the voltage with in safe margins [139-143]. For the present study DC Chopper FRT protection circuit is chosen to protect HVDC link from over voltages, because of its simplicity in construction and efficient operation.

6.5.2. DC Chopper FRT Protection circuit

The DC chopper circuit is shown in Fig. 6.29. It consists of power resistor in series with MOSFET switch, if the voltage in DC link goes beyond the set value, the chopper protection circuit will be turned on, protecting the DC link capacitor, equipment in DC link and IGBTs under AC grid side faults. The wind and solar PV farm are still connected to grid without interrupting its operation. Under steady state, when the DC link voltage is within the safe limit the chopper circuit will be inactive. Fig.6.30 indicates the HVDC link with DC chopper protection circuit.

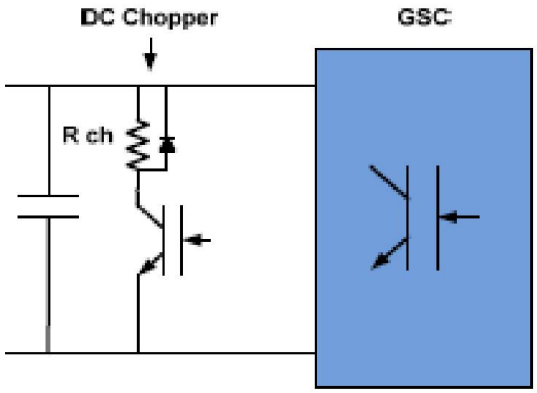

Fig.6. 29: DC Chopper protection circuit in DC link. [142]

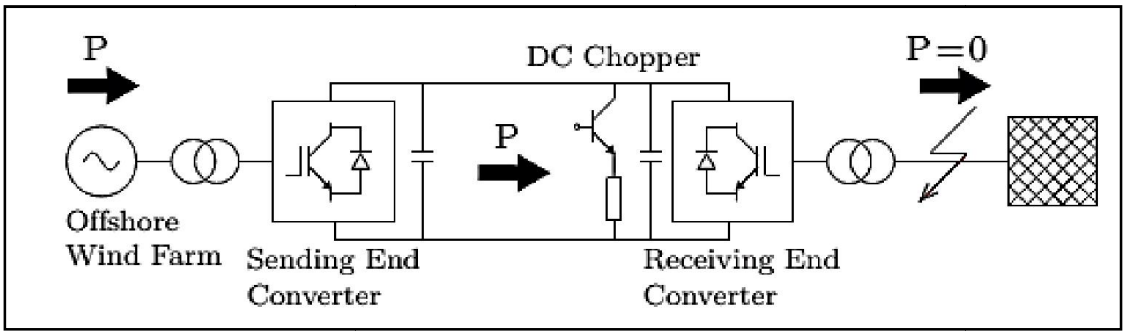

Fig.6. 30: DC Chopper protection circuit in PCC coupled VSC HVDC transmission, [142].

6.5.3. DC Chopper Design

The DC chopper circuit is designed considering the worst case scenario where the export of power is completely diminished when the wind farm is generating its maximum power. Therefore, the DC chopper is designed for rating equal to the wind farms rating.

The active power transferred to the grid from the converter is [142].

$$P_g = \frac{V_g V_c \sin(\delta_C)}{X_p}$$

Where, *Pg* is active power injected into the grid

Xp is the reactance offered between the grid and converter

$Vc = Vc\angle\delta c$ is the voltage at converter and

$Vg = Vg\angle 0$ is the grid side voltage.

As discussed earlier, the grid fault could create a voltage dip of up to 0 % of the nominal steady state grid voltage. Then the subsequent rise in DC link voltage is given by:

$$V_{dc} = \sqrt{\frac{2}{C_{eq}} \int (P_w - P_c) dt}$$

where Pw is active power of the wind farm injected into the DC link, and

Ceq is the equivalent capacitance offered by the capacitors and DC line neglecting the others.

If the excess power, i.e. ($Pw - Pc$) is dissipated by resistor in DC chopper circuit then DC voltage balance can be maintained in the DC link.

Considering 1.05 pu and 1.1 pu as current and voltage limits, the resistance offered by DC chopper and current required can be calculated as given below,

$$R_{ch} = \frac{(1.1 V_{rated})^2}{P_{rated}}$$

$$I_{chop} = \frac{(1.05V_{rated})}{R_{ch}} = \frac{(1.05P_{rated})}{V_{rated}} = 1.05\ I_{rated}$$

Using hysteresis controller the chopper control is implemented. The valve creating the chopper circuit is controlled based on voltage in the DC link. The DC valve is closed when the difference in voltage exceeds the threshold limit, making the resistor in chopper circuit to dissipate the excess energy. The DC valve is blocks the chopper circuit if the voltage in the DC link is below the predefined minimum limit. In general, this method of controlling the chopper circuit is considered simple, fast and robust and it doesn't need any fast communication channel for its operation [143].

$$signal = \begin{cases} 1 & V_{DC} > V_{max} \\ 0 & V_{DC} > V_{max} \\ hold\ V_{min} < V_{DC} < V_{max} \end{cases}$$

Those voltage limits always depend upon the design of the system.

6.6. Fault Ride Through Results

To analyze the performance of the proposed system under the influence of fault, a three phase short circuit fault is created near to the AC grid, between the instants 0.1 s and 0.25 s.

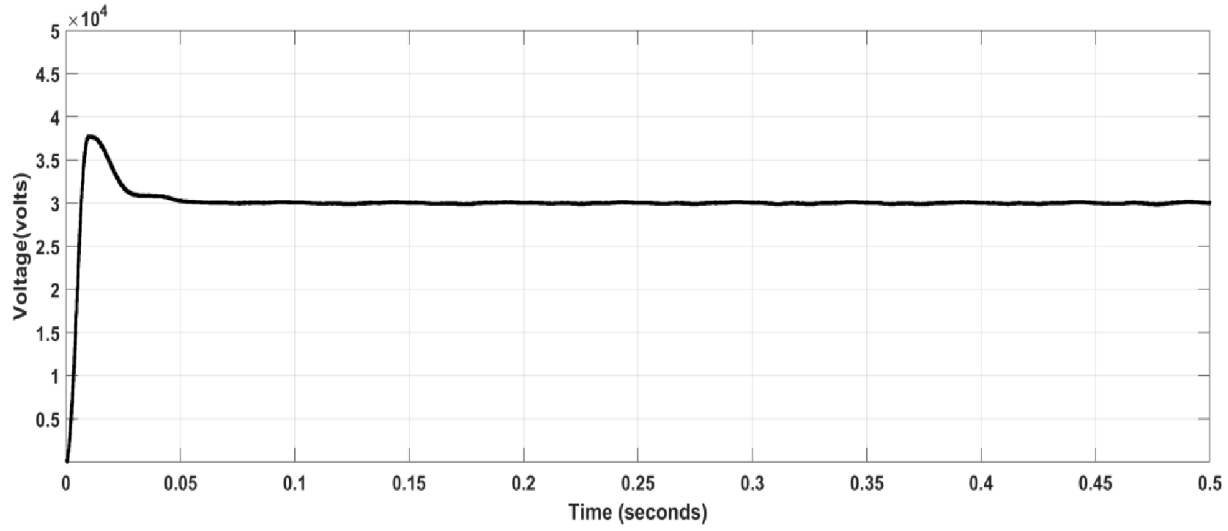

Fig.6. 31: DC link voltage before three phase fault.

The DC link voltage before the fault is shown in Fig. 6.31. When three phase fault occurs near to the grid, between the instants 0.1s and 0.25s, the DC link voltage during the period of fault is shown in Fig. 6.32. It is observed that during fault period there is an over voltage in DC link.

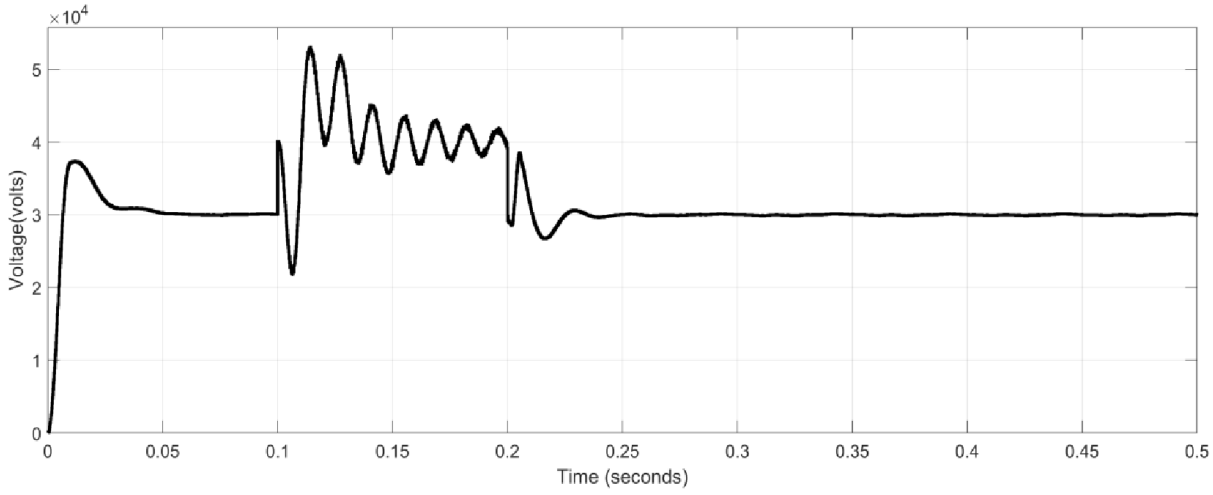

Fig.6. 32: DC link voltage before and during three phase fault, without fault ride through.

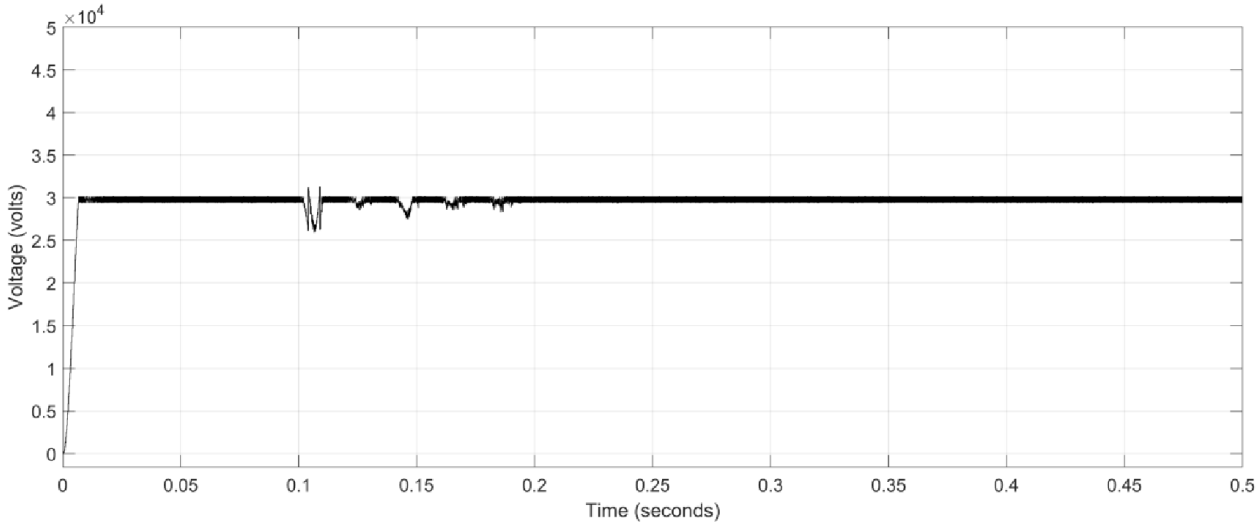

Fig.6. 33: DC link voltage during three phase fault, with fault ride through.

To protect the equipment near to DC link against this over voltages FRT protection circuit namely DC chopper circuit is inserted in DC link. Due to the presence of DC Chopper circuit the DC link voltage is maintained constant as shown in Fig. 6.33. The power is dissipated

in the resistor connected across the chopper protecting the equipment against external faults. From Fig. 6.33 it is examined that the DC chopper protection circuit provides efficient FRT protection diverting the excess power to the resistor present in the circuit and limiting the voltage in DC link. Under normal operation the FRT circuit is turned off without affecting its steady state operation.

6.7. Summary

The major work done in this chapter is, the performance of DC grid connected solar PV and wind farms (taking reference as Nanhui project, China) is evaluated using proposed hybrid controller under varying weather and load disturbances.

From the simulation results it is observed that the proposed system performs well under different climatic conditions and varying load conditions the hybrid controller used here performs dual tasks of harnessing maximum power and regulating DC output. The proposed system offers good flexibility and reliability in its operation under maintenance or failure of any of the system in addition to that it provides fault ride through protection against different faults. DC chopper protection circuit gives efficient FRT protection to the proposed system under fault condition diverting the fault current through resistor.

CHAPTER-7

Conclusions and Future Scope

7.1 Conclusions

Due to increase in the potential market for solar and wind energy generation, their penetration into the AC grid is increasing with time. Due to which the present AC grid faces technical challenges like voltage and frequency instability, operational instability, dynamic reactive power support etc. Majority of these issues can be overcome by integrating to DC grid and it is considered as a promising solution, when compared to AC grid due to its technical and economical benefits.

To integrate large solar PV and wind farms to DC grid, different DC collection topologies are proposed in literature for high voltage DC grid integration. A new topology for integrating RES to high voltage DC grid is proposed in this work. The proposed topology in comparison with the previous topologies offers better reliability and flexibility, as there are two different sources there is continuity in power supply and efficient when compared to AC collection system.

RES like photovoltaic cells, fuel cells and wind will be at a low voltage level, they must be stepped up considerably for DC grid integration, for which we need a high voltage gain DC-DC boost converters. The open loop and closed loop operation of conventional DC-DC boost converter is analyzed using small signal mathematical modeling. From the simulation results it is observed that using fuzzy controller in closed loop operation, the performance of the system has improved the over shoot, steady state error, settling time, rise time, delay time are reduced. To step up voltage from low voltage to medium voltage, multilevel boost converter (MLBC) is chosen. The performance of MLBC is compared with transformerless high gain DC-

DC boost converter for medium voltage applications. It is shown that MLBC offers low voltage stress, low ripple current, better efficiency, etc. compared to transformer-less high gain boost DC-DC Converter.

One of the major contributions in this work is, a hybrid controller proposed to address two challenges faced during DC grid integration i.e. extracting the maximum power from the variable input and regulating DC voltage according to the grid requirement. For efficient MPPT tracking a comparative study is performed among different MPPT control techniques like incremental conductance, perturb and observe, fuzzy logic and random search method. From the results it is observed that RSM based MPPT controller performs well under varying weather conditions and is able to track the maximum power from the source with good tracking efficiency and less oscillations.

RSM based two loop average current controlled voltage regulator is proposed to provide stable DC output at low voltage DC grid, considering grid side and input side perturbations. It is observed from the simulations that when compared to linear PI controller the proposed RSM based TLAC voltage regulator provides stable DC output at varying load conditions where as optimal tuning is needed for PI controller for different load conditions.

The performance of DC grid connected solar PV system consisting of hybrid controller is evaluated under different weather conditions and grid side disturbances. From the results and analyses it is observed that the proposed system performs well under different climatic conditions and varying load conditions the hybrid controller used here performs dual tasks of harnessing maximum power and regulating DC output. Performed stability analysis on TLAC controlled DC-DC boost converter. From the stability analysis it is observed that the proposed

controller produces a stable DC output voltage according to the grid needs with no delay in response.

The performance of proposed topology consisting of PV and wind farm connected to DC grid is evaluated under different weather conditions, load disturbances and fault conditions. From the simulation results it is observed that the proposed system performs well under different climatic conditions and varying load conditions the hybrid controller used here performs dual tasks of harnessing maximum power and regulating DC output. The proposed system offers good flexibility and reliability in its operation under maintenance or failure of any of the system. The DC chopper protection circuit used in high voltage DC link gives efficient FRT protection to the proposed system under fault condition diverting the fault current through resistor.

7.2 Future Scope:

- To improve overall efficiency of the DC grid connected renewable energy topology further, there is a need for design of efficient high voltage gain DC-DC Boost converter with improved voltage and power levels.
- The hardware prototype of the proposed hybrid controller for DC Microgrid connected applications can be implemented as a future work.
- Considering that most of the RES generate either DC or can be easily interfaced to DC grid using efficient power electronic interface. Like DC transmission, to improve efficiency in utilization of energy the present AC distribution can be replaced with DC, significant energy saving can be done as there is no DC-AC-DC Converter.

Bibliography

[1]. Keyhani, A., Marwal, M.N. and Dai, M, “Integration of Green and Renewable Energy in Electric Power Systems”, John Wiley and Sons, Hoboken 2010.

[2]. Renewables 2017 Global Status Report-http://www.ren21.net/wp-content/uploads/2017/06/17-652_GSR2018_FullReport_web_final_.pdf

[3]. Hannah Ritchie and Max Roser (2018)- "Renewables". *Published online at OurWorldInData.org.* Retrieved from: 'https://ourworldindata.org/renewables’.

[4]. Molina, Marcelo G., Euzeli C. dos Santos, and Mario Pacas. "Improved power conditioning system for grid integration of photovoltaic solar energy conversion systems", 2010 IEEE/PES Transmission and Distribution Conference and Exposition Latin America (T&D-LA), 2010.

[5]. Annual Report 2017-18, https://mnre.gov.in/file-manager/annual-report/2017-2018/EN/index.html.

[6]. Chakraborty S, Kramer SB, KroposkiB, “ A review of power electronics interfaces for distributed energy systems towards achieving low-cost modular design”, Renewable Sustainable Energy Reviews, 2009, Vol. 13, PP. No 2323–2335.

[7]. Piwko, R, “Grid Integration of Large-Capacity Renewable Energy Sources and Use of Large-Capacity Electrical Energy Storage”, White Paper, IEC 2012.

[8]. M. Prodanovic, K. De Brabandere, J. Van den Keybus, T. Green and J. Driesen,” Harmonic and reactive power compensation as ancillary services in inverter-based distributed generation”, IETGener. Transm. Distrib., 2007.

[9]. Josep M. Guerrero, Poh Chiang Loh, , Tzung-Lin Lee,and Mukul Chandorkar, "Advanced Control Architectures for Intelligent Microgrids—Part II: Power Quality, Energy Storage, and AC/DC Microgrids", IEEE Transactions On Industrial Electronics, Vol. 60, No. 4, April 2013.

[10]. Alba Colet-Subirachs, Albert Ruiz´ Alvarez, Oriol GomisBellmunt, Felipe Alvarez-Cuevas-Figuerola, and Antoni Sudri aAndreu, "Centralized and Distributed Active and Reactive Power Control of a Utility Connected Microgrid Using IEC61850", IEEE Systems Journal, Vol. 6, No. 1, March 2012.

[11]. N. Phuangpornpitak and S. Tia, "Opportunities and Challenges of Integrating Renewable Energy in Smart Grid System," vol. 34, pp. 282–290, 2013.

[12]. B. N. Stram, "Key challenges to expanding renewable energy," Energy Policy, vol. 96, pp. 728–734, 2016.

[13]. M. Dreidy, H. Mokhlis, and S. Mekhilef, "Inertia response and frequency control techniques for renewable energy sources : A review," Renew. Sustain. Energy Rev., vol. 69, no. November 2016, pp. 144–155, 2017.

[14]. Ministry of Power, "Report of the Technical Committee on Large Scale Integration of Renewable Energy, Need for Balancing, Deviation Settlement Mechanism (DSM) and associated issues," Apr. 2016.

[15]. G. Mondal, J. Bamberger, M. B. Buhl, and S. Nielebock, "Voltage Source Operation of Parallel PV / Wind inverters-stabilized Hybrid Power Plants in ' Diesel off- Mode ' - An experimental verification," 2017.

[16]. Sethuraman Ganesan, Technology Head, Power Grids division, ABB India Ltd "Digitalisation Should Unleash Huge Value for Utilities", http://www.powertoday.in/News/Giving-grids-the-green-edge-/74791.

[17]. V. Khare, S. Nema, and P. Baredar, "Solar – wind hybrid renewable energy system : A review," Renew. Sustain. Energy Rev., vol. 58, pp. 23–33, 2016.

[18]. M. Yu, W. Huang, N. Tai, X. Zheng, P. Wu, and W. Chen, "Transient stability mechanism of grid-connected inverter-interfaced distributed generators using droop control strategy," Appl. Energy, vol. 210, no. March 2017, pp. 737–747, 2018.

[19]. E. Bitar, P. P. Khargonekar, and K. Poolla, Systems and control opportunities in the integration of renewable energy into the Smart Grid, vol. 18, no. PART 1. IFAC, 2011.

[20]. A. K. Alsaif, "Challenges and Benefits of Integrating the Renewable Energy Technologies into the AC Power System Grid," Am. J. Eng. Res., no. 4, pp. 95–100, 2017.

[21]. O. Alsayegh, S. Alhajraf, and H. Albusairi, "Grid-connected renewable energy source systems : Challenges and proposed management schemes," Energy Convers. Manag., vol. 51, no. 8, pp. 1690–1693, 2010.

[22]. Repo S, Laaksonen H, Jarventausta P, Huhtala O, Mickelsson M., "A case study of a voltage rise problem due to a large amount of distributed generation on a weak distribution network", IEEE Power Tech Conference Proceedings, Bologna, Italy, 23–26 June, 2003, vol. 4. pp. 1–6.

[23]. L. Yang, C. Xiong, Y. Teng, Q. Hui, and Y. Zhu, "Harmonic Current Suppression of Grid-connected PV Based on PR Control Strategy," 2015 Sixth Int. Conf. Intelligient Syst. Des. Eng. Appl., pp. 2–5, 2015.

[24]. A. Chidurala et al., “Harmonic Emissions in Grid Connected PV Systems : A Case Study on a Large Scale Rooftop PV Site.”

[25]. H. Liu, X. Xie, and W. Liu, “An Oscillatory Stability Criterion based on the Unified dq - Frame Impedance Network Model for Power Systems,” IEEE, vol. 8950, 2018.

[26]. C. N. and S. K. Manjunatha, “Harmonic Current Compensation Improvement at Point of Common Coupling Using Hybrid Natural Green Sources,” IEEE 3rd Int. Conf. Adv. Electr. Electron. Information, Commun. Bio-Informatics, pp. 2–6, 2017.

[27]. H. M. Abeynayake, P.A.G.S; Attanayaka, T.L.B; Jayawardane, V.G.R.G; Alahendra, G.B; Pathiratne, K.A.M.N; Dr.Wijekoon, “Power Quality Analysis of Grid Connected Wind Power Plants in West Coast of Sri Lanka,” pp. 344–348, 2015.

[28]. D. Mascarella, S. Li, G. Joos, and P. Venne, “Reactive power coordination in DFIG based wind farms for voltage regulation & flicker mitigation,” Power Energy Soc. Gen. Meet. 2015 IEEE, pp. 1–5, 2015.

[29]. R. K. Agarwal, I. Hussain, B. Singh, A. Chandra, and K. Al-Haddad, “Improved power quality of three-phase grid connected Solar Energy Conversion System under grid voltages distortion and imbalances,” IEEE Ind. Appl. Soc. 52nd Annu. Meet. IAS 2016, pp. 2–9, 2016.

[30]. M. Rekinger, I.-T. Theologitis, G. Masson, M. Latour, D. Biancardi, A. Roesch, G. Concas, and P. Basso, “Connecting the sun: solar photovoltaics on the road to large-scale grid integration,” European Photovoltaic Industry Association, Brussels, Belgium, Full report, Sep. 2012.

[31]. D. Mende, Y. T. Fawzy, D. Premm, and S. Stevens, “Increasing the Hosting Capacity of Distribution Networks for Distributed Generation Utilizing Reactive Power Control -

Potentials and Limits," presented at the 2nd International Workshop on Integration of Solar Power into Power Systems, Lisbon, Portugal, 2012.

[32]. V. Musolino, P. Alet, E. Perret-aebi, C. Ballif, and L. Piegari, "Alleviating Power Quality Issues When Integrating PV Into Built Areas : Design and Control of DC Microgrids," pp. 102–107, 2015.

[33]. M. Braun, T. Stetz, T. Reimann, B. Valov, and G. Arnold, "Optimal Reactive Power Supply in Distribution Networks - Technological and Economic Assessment for PV-Systems," presented at the 24th European Photovoltaic Solar Energy Conference, Hamburg, Germany, 2009, pp. 3872 – 3881.

[34]. H. Holttinen, P. Meibom, A. Orths, B. Lange, M. O'Malley, J. O. Tande, A. Estanqueiro, E. Gomez, L. Söder, G. Strbac, J. C. Smith, and F. van Hulle, "Impacts of large amounts of wind power on design and operation of power systems, results of IEA collaboration," Wind Energy, vol. 14, no. 2, pp. 179–192, Mar. 2011.

[35]. R. Perez, E. Lorenz, S. Pelland, M. Beauharnois, G. Van Knowe, K. Hemker Jr., D. Heinemann, J. Remund, S. C. Müller, W. Traunmüller, G. Steinmauer, D. Pozo, J. A. RuizArias, V. Lara-Fanego, L. Ramirez-Santigosa, M. GastonRomero, and L. M. Pomares, "Comparison of numerical weather prediction solar irradiance forecasts in the US, Canada and Europe," Sol. Energy, vol. 94, pp. 305–326, Aug. 2013.

[36]. W. Katzenstein and J. Apt, "The cost of wind power variability," Energy Policy, vol. 51, pp. 233–243, Dec. 2012.

[37]. J. Nikoletatos and S. Tselepis, "Renewable Integration in Power Grids," IEA Energy Technology Systems Analysis Programme (ETSAP), Technology Brief E15, Dec. 2013.

[38]. M. Milligan, E. Ela, B.-M. Hodge, B. Kirby, D. Lew, C. Clark, J. DeCesaro, and K. Lynn, "Integration of Variable Generation, Cost-Causation, and Integration Costs," Electr. J., vol. 24, no. 9, pp. 51–63, Nov. 2011.

[39]. T. Stetz, K. Diwold, M. Kraiczy, D. Geibel, S. Schmidt, and M. Braun, "Techno-Economic Assessment of Voltage Control Strategies in Low Voltage Grids," IEEE Trans. Smart Grid, vol. 5, no. 4, pp. 2125–2132, Jul. 2014.

[40]. C. G. K. Vanchinathan, "Novel Voltage Stability analysis of a grid connected-photovoltaic system," vol. 3, no. 7, pp. 38–43, 2012.

[41]. G. Mondal, J. Bamberger, M. B. Buhl, and S. Nielebock, "Voltage Source Operation of Parallel PV / Wind inverters-stabilized Hybrid Power Plants in ' Diesel off- Mode ' - An experimental verification," 2017.

[42]. K. S. Reddy, M. Kumar, T. K. Mallick, H. Sharon, and S. Lokeswaran, "A review of Integration, Control, Communication and Metering (ICCM) of renewable energy based smart grid," Renew. Sustain. Energy Rev., vol. 38, pp. 180–192, 2014.

[43]. A. Gupta, R. P. Saini, and M. P. Sharma, "Steady-state modelling of hybrid energy system for off grid electrification of cluster of villages," Renew. Energy, vol. 35, no. 2, pp. 520–535, 2010.

[44]. J. H. Eto, J. Undrill, P. Mackin, R. Daschmans, B. Williams, B. Haney, R. Hunt, J. Ellis, H. Illian, C. Martinez, M. O'Malley, K. Coughlin, and K. H. LaCommare, "Use of Frequency Response Metrics to Assess the Planning and Operating Requirements for Reliable Integration of Variable Renewable Generation," Lawrence Berkeley National Laboratory, Berkeley, California, USA, LBNL-4142E, Dec. 2010.

[45]. International Energy Agency, “The Power of Transformation: Wind, Sun and the Economics of Flexible Power Systems,” International Energy Agency, Paris, France, ISBN 978-92-64-20802-5, 2014.

[46]. B. Bletterie, A. Gorsek, B. Uljanic, B. Blazic, A. Woyte, T. Vu Van, F. Truyens, and J. Jahn, “Enhancement of the Network Hosting Capacity – Clearing Space for/with PV,” presented at the 25th European Photovoltaic Solar Energy Conference and Exhibition / 5th World Conference on Photovoltaic Energy Conversion, Valencia, Spain, 2010, pp. 4828 – 4834.

[47]. Forum Netztechnik Netzbetrieb, “Power generation systems connected to the low-voltage distribution network: Technical minimum requirements for the connection to and parallel operation with low-voltage distribution networks,” VDE, Berlin, Germany, Application Guide VDE-AR-N 4105:2011-08, Aug. 2011.

[48]. T. Stetz, “Autonomous Voltage Control Strategies in Distribution Grids with Photovoltaic Systems: Technical and Economic Assessment,” PhD thesis, Universität Kassel, 2013.

[49]. A. B. Attya, J. L. Domínguez-garcía, F. D. Bianchi, and O. Anaya lara,“Electrical Power and Energy Systems Enhancing frequency stability by integrating non-conventional power sources through multi-terminal HVDC grid,” Int. J. Electr. Power Energy Syst., vol. 95, pp. 128–136, 2018.

[50]. S. Lu and L. Wang, “Integration of Wind-Power and Wave-Power Generation Systems Using a DC Micro Grid,” pp. 1–8, 2014.

[51]. Hafiz Abu Bakar Siddique, Syed Mansoor Ali, Rik W. De Doncker. "DC collector grid configurations for large photovoltaic parks", 2013 15th European Conference on Power Electronics and Applications (EPE), 2013.

[52]. Torres-Olguin RE, Garces A, Molinas M, Undeland T, " Integration of offshore wind farm using a hybrid HVDC transmission composed by the PWM current-source converter and line-commutated converter", IEEE Trans Energy Convers 2013;28:125–34.

[53]. Chen X, Sun H, Wen J, Lee WJ, Yuan X, Li N, et al, "Integrating wind farm to the grid using hybrid multiterminal HVDC technology", IEEE Trans Ind Appl 2011;47:965–72.

[54]. M. Patsalides, V. Efthymiou, A. Stavrou, and G. E. Georghiou, "Simplified distribution grid model for power quality studies in the presence of photovoltaic generators," IET Renew. Power Gener., pp. 1–11, 2015.

[55]. S. Nguefeu, C. Finck, F. Sultanem, J. P. Taisne, J. B. Curis, and A. M. Denis, "Accomodation of offshore wind farms: an opportunity for the development of HVDC grids," in Proc. 4th European Conference on HV and MV Substation Equipment, 2011.

[56]. N. Flourentzou, V. G. Agelidis, and G. D. Demetriades, "VSC-Based HVDC Power Transmission Systems: An Overview," IEEE Transactions on Power Electronics, vol. 24, no. 3, pp. 592–602, 2009.

[57]. T. M. Haileselassie and T. Undeland, "Multiterminal HVDC for Offshore Windfarms - Control Strategy," Wind Power to the Grid-EPE Wind Energy Chapter-2nd Seminar, 2009.

[58]. B. Silva, C. L. Moreira, L. Seca, Y. Phulpin, and J. a. Pecas Lopes, "Provision of Inertial and Primary Frequency Control Services Using Offshore Multiterminal HVDC Networks," IEEE Transactions on Sustainable Energy, vol. 3, no. 4, pp. 800–808, Oct. 2012.

[59]. M. Callavik, A. Blomberg, J. Haefner, and B. Jaconson, "The hybrid HVDC breaker: An innovation breakthrough enabling reliable HVDC grids," Nov. 2012.

[60]. Shen J-M, Jou H-L, Wu J-C, " Transformer-less three-port grid-connected power converter for distribution power generation system with dual renewable energy sources", IET Power Electron 2012, Vol. 5:501.

[61]. Jovcic D., "Interconnecting offshore wind farms using multiterminal VSC-based HVDC", Power Eng Soc Gen Meet 2006 IEEE 2006:7.

[62]. C. Bucher, G. Andersson, and L. Küng, "Increasing the PV Hosting Capacity of Distribution Power Grids – A Comparison of Seven Methods," presented at the 28th European Photovoltaic Solar Energy Conference and Exhibition, Paris, France, 2013, pp. 4231 – 4235.

[63]. Fernando Martinez-Rodrigo, Dionisio Ramirez, Alexis B. Rey-Boue, Santiago de Pablo, Luis Carlos Herrero-de Lucas, "Modular Multilevel Converters: Control and Applications", Energies 2017, 10(11).

[64]. S. Lundberg, "Wind Farm Configuration and Energy Efficiency Studies - Series DC versus AC Layouts", Ph.D. dissertation, Chalmers Univ. Technol., G¨ oteborg, Sweden, 2006.

[65]. Y. Jin, J. Fletcher, and J. O'Reilly, "Multi-terminal DC wind farm collection and transmission system internal fault analysis," in Proc. IEEE Int. Symp. Ind. Electron., 2010, pp. 2437–2442.

[66]. Gomis-Bellmunt O, Liang J, Ekanayake J, King R, Jenkins N, " Topologies of multiterminal HVDC-VSC transmission for large offshore wind farms", Electr Power Syst Res 2011;81:271–81.

[67]. G. Stamatiou, K. Srivastava, M. Reza, and P. Zanchetta, " Economics of DC wind collection grid as affected by cost of key components," inProc. World Renew. Energy Congr., 2011, pp. 4177–4184.

[68]. Rault, P., X. Guillaud, F. Colas, and S. Nguefeu. "Investigation on interactions between AC and DC grids", 2013 IEEE Grenoble Conference, 2013.

[69]. Monjean P, Robyns B, “DC grid architectures to improve the integration of wind farms into electricity transmission and distribution networks”, Eco-friendly Innov. Electr. Transm. Distrib. Networks, 2014, p. 291–311. doi:10.1016/B978-1-78242-010-1.00014-8.

[70]. Torres-Olguin RE, Garces A, Molinas M, Undeland T, "Integration of offshore wind farm using a hybrid HVDC transmission composed by the PWM current-source converter and line-commutated converter", IEEE Trans Energy Convers 2013, vol 28, pp 125–34.

[71]. R. W. Erickson, “DC-DC power converters,” in Wiley Encyclopedia of Electrical and Electronics Engineering. Hoboken, NJ, USA: Wiley,1999.

[72]. M. P Kazimierkowski, F. Blaabjerg and R. Krishnan, “Control in Power Electronics: Selected Problems”, Academic Press, 2002.

[73]. R. D. Middlebrook, “Transformerless DC-to-DC converters with large conversion ratios,” IEEE Trans. Power Electron., vol. 3, no. 4, pp. 484–488, Oct. 1988.

[74]. F. L. Tofoli, D. de Castro Pereira, W. J. de Paula, and D. de Sousa Oliveira J´ unior, “Survey on non-isolated high-voltage step-up DC-DC topologies based on the boost converter,” IET Power Electron., vol. 8, no. 10, pp. 2044–2057, 2015.

[75]. Wuhua Li, Yi Zhao, Yan Deng and Xiangning He, “Interleaved Converter with Voltage Multiplier Cell for High step-up and High efficiency Conversion”, IEEE Trans. Power Electron., Vol. 25, No. 9,September 2010.

[76]. Shih-Ming Chen, Tsorng-Juu Liang, Lung-Sheng Yang, Jiann-Fuh Chen, “ A Cascaded High Step-Up DC-DC Converter With Single Switch for Microsource Applications”, IEEE Trans. Power Electron.,Vol.26, No.4, April 2011.

[77]. Yi-Ping Hsieh, Jiann-Fuh Chen, Tsorng-Juu Liang, Lung-Sheng Yang, “Novel High step up DC-DC Converter with Coupled-Inductor and Switched-Capacitor Techniques for a Sustainable Energy System”, IEEE Trans. Power Elect tron. Vol. 26, No. 12, December 2011.

[78]. Yi-Ping Hsieh, Jiann-Fuh Chen, Tsorng-Juu Liang, Lung-ShengYang, “Novel High Step-Up DC-DC Converter With Coupled-Inductor and Switched-Capacitor Techniques”, IEEE Trans. Ind.Electron. Vol. 59, No. 2, February 2012.

[79]. Ti-Ping Hsieh, Hiann-Fuh Chen, Tsorng-Juu Liang, Lung-Sheng Yang. “Novel High Step-Up DC-DC Converter With Coupled- Inductor and Switched-Capacitor Techniques”, IEEE Trans. Ind. Electron., Vol. 59, No.2, February 2012.

[80]. Mahajan Sagar Bhaskar, Sanjeevikumar Padmanaban, Frede Blaabjerg , Patrick William Wheeler , “An Improved Multistage Switched Inductor Boost Converter (Improved M-SIBC) for Renewable Energy Applications: A key to Enhance Conversion Ratio”, IEEE 19th Workshop on Control and Modeling for Power Electronics(COMPEL), pp. 1-6, 2018.

[81]. S.K. Changchien, T.J Liang, J.F. Chen, L.S. Yang, “Step-up DC-DC converter by coupled inductor and voltage-lift technique” , IET Power Electron.2010 Vol. 3, Iss. 3, pp. 369-378.

[82]. Stefan P. Engel, Marco Stieneker, Nils Soltau; Sedigheh Rabiee, Hanno Stagge, Rik W. De Doncker, "Comparison of the Modular Multilevel DC Converter and the Dual-Active Bridge Converter for Power Conversion in HVDC and MVDC Grids”, IEEE Transactions on Power Electronics, Volume: 30, Issue: 1, pp.124-137, 2015.

[83]. Hugo Rolando Estofanero Larico, Ivo Barbi, "Three-Phase Flyback Push–Pull DC–DC Converter: Analysis, Design, and Experimentation”, IEEE Transactions on Power Electronics, Volume: 28, Issue: 4,pp.1961-1970, 2013.

[84]. Shih-Ming Chen, Tsorng-Juu Lian ng, Lung-Sheng Yang, Jiann-FuhChen, “A Safety Enhanced, High Step-Up DC-DC Converter for AC Photovoltaic Module Application, IEEE Trans. Power Electron. Vol 27, No.4 April 2012.

[85]. Theodore Soong, Peter Lehn, “A Transformerless High Boost DC-DC Converter for use in Medium / High Voltage Applications”, IECON 2012 - 38th Annual Conference on IEEE Industrial Electronics Society, pp, 174-179.

[86]. Miaosen Shen, Fang Zheng Peng, Leon M. Tolbert, “Multilevel DC-DC Power Conversion System With Multiple DC Source”, IEEE Trans. Power Electron. Vol.23, No1. January 2008.

[87]. Jovcic D, Zhang L., Hajian M.,"LCL VSC converter for high-power applications", IEEE Trans Power Deliv 2013; vol. 28, pp. 137–44.

[88]. A.W.N. Husna, S.F. Siraj, M.Z.AbMuin, “Modelling of DC-DC Converter for Solar Energy System Applications”, IEEE Symposium on Computers & Informatics, pp. 125-129, Mar. 2012.

[89]. N. F Nik Ismail ; I. Musirin ; R. Baharom ; D. Johari, “Fuzzy logic controller on DC/DC boost converter”, 2010 IEEE International Conference on Power and Energy, pp. 1-6, Dec 2010.

[90]. Julio C. Rosas-Caro, Juan M. Ramírez, Pedro Martín García-Vite, “Novel DC-DC Multilevel Boost Converter”, Proc. Power Electron. Specialists Conference, PESC 2008, pages 2146-2151.

[91]. Jovcic D, Zhang L., "LCL DC/DC converter for DC grids", IEEE Trans Power Delivery 2013; vol. 28, pp. 2071–2079.

[92]. Lin, C.-H., Huang, C.-H., Du, Y.-C., Chen, J.-L.: “Maximum photovoltaic power tracking for the Pv array using the fractional-order incremental conductance method”, Appl. Energy., vol. 88, no. 12, pp. 4840-4847, 2011.

[93]. Subudhi, B., Pradhan, R.: ‘A comparative study on maximum power point tracking techniques for photovoltaic power systems’, IEEE Trans. Sustain. Energy, vol. 4, no. 1, pp. 89–98, 2013.

[94]. Ronn Raedani, Moin Hanif, “Design, Testing and Comparison of P&O, IC and VSSIR MPPT Techniques”, Proceedings of Third International Conference on Renewable Energy Research and Applications , pp-322-328, 2014.

[95]. W. Xiao A. Elnosh V. Khadkikar H. Zeineldin "Overview of maximum power point tracking technologies for photovoltaic power systems" Proc. 37th Annual Conf. on IEEE Industrial Electronics Society (IECON) pp. 3900-3905 2011.

[96]. Kish, G., Lee, J., Lehn, P. “Modelling and control of photovoltaic panels utilising the incremental conductance method for maximum power point tracking”, IET Renew. Power Gener. 2012, vol. 6, no. 4, pp. 259-266, 2012.

[97]. M. Alqarni M.K. Darwish "Maximum power point tracking for photovoltaic system: modified perturb and observe algorithm" Proc. 47th Int. Universities Power Engineering Conf. (UPEC) pp. 1-4 2012.

[98]. L. Piegari ; R. Rizzo, “Adaptive perturb and observe algorithm for photovoltaic maximum power point tracking”, IET Renewable Power Generation, vol. 4, isssue 4, pp. 317-328, 2014.

[99]. N. Femia G. Petrone G. Spagnuolo M. Vitelli "Increasing the efficiency of P&O MPPT by converter dynamic matching" Int. Symp. on Industrial Electronics vol. 2, pp. 1017-1021 , 2004 .

[100]. Hiyama, T., Kitabayashi, K.: 'Neural network based estimation of maximum power generation from PV module using environmental information', IEEE Trans. Energy Convers., vol. 12, no. 3, pp. 241–247, 1997.

[101]. Veerachary, M., Senjyu, T., Uezato, K.: 'Feedforward maximum power point tracking of PV systems using fuzzy controller', IEEE Trans. Aerosp. Electron. Syst., vol. 38, no. 3, pp. 969–981, 2002.

[102]. Chekired, F., Larbes, C., Mellit, A., "Comparative study between two intelligent Mppt-controllers implemented on Fpga: application for photovoltaic systems", Int. J. Sustain. Energy, vol. 31, pp. 1-17, 2012.

[103]. Muhammad Ammirrul Atiqi Mohd Zainuri, Mohd Amran Mohd Radzi, Azura Che Soh, Nasrudin Abd Rahim, "Development of adaptive perturb and observe-fuzzy control maximum power point tracking for photovoltaic boost dc–dc converter," IET Renewable Power Generation, vol. 8, no 2, pp. 183–194, May 2013.

[104]. Hugues Renaudineau, Fabrizio Donatantonio, Julien Fontchastagner, Giovanni Petrone, Giovanni Spagnuolo, Jean-Philippe Martin, and Serge Pierfederici, "A PSO-Based Global MPPT Technique for Distributed PV Power Generation," IEEE Transactions on Industrial Electronics, Vol. 62, No. 2, Feb 2015.

[105]. Liu, Y.-H., Huang, S.-C., Huang, J.-W., Liang,W.-C.: 'A particle swarm optimization-based maximum power point tracking algorithm for PV systems operating under partially shaded conditions', IEEE Trans. Energy Convers., vol. 27, no. 4, pp. 1027–1035, 2012.

[106]. Mellit, A., Rezzouk, H., Messai, A., Medjahed, B.: “Fpga-based real time implementation of Mpptcontroller for photovoltaic systems”, Renew. Energy, vol.36,no. 5, pp. 1652-1661, 2011.

[107]. Abou Soufyane Benyoucef , Aissa Chouder , Kamel Kara , Santigo Silvestre and Oussama Ait Sahed, “DSP Implementation of a novel artificial bee colony optimization-based MPPT for photovoltaic systems subject to in homogeneous insolation by using direct control”, Applied Soft Computing, vol 32, July 2015.

[108]. Kinattingal Sundareswaran1, Sankar Peddapati1, S. Palani, “Application of random search method for maximum power point tracking in partially shaded photovoltaic systems,” IET Renew. Power Gener., vol. 8, no. 6, pp. 670–678, 2014.

[109]. Baba, N.: ‘Convergence of a random optimization method for constrained optimization problems’, J. Optim. Theory Appl., vol. 33, no. 4, pp. 451–461, 1981.

[110]. Ishaque, Kashif, and Zainal Salam. "A review of maximum power point tracking techniques of PV system for uniform insolation and partial shading condition", Renewable and Sustainable Energy Reviews, 2013.

[111]. S. C. Raviraj P. C. Sen "Comparative Study of Proportional-Integral Sliding Mode and Fuzzy Logic Controllers for Power Converters" IEEE Transactions on Industry Applications vol. 33 no. 2 March/April 1997.

[112]. Leedy, A.W., Guo, L., Aganah, K.A. “A constant voltage Mppt method for a solar powered boost converter with dc motor load”, Proc. of IEEE Southeastcon, pp. 22-28, 2012.

[113]. H. Renaudineau et al., “Efficiency optimization through current-sharing for paralleled dc-dc boost converters with parameter estimation,” IEEE Trans. Power Electron., vol. 29, no. 2, pp. 759–767, Feb. 2014.

[114]. Hussein, K.H., Muta, I.: 'Maximum photovoltaic power tracking: an algorithm for rapidly changing atmospheric conditions', Proc. Inst. Electr. Eng.—Gener. Transm. Distrib., vol. 142, no. 1, pp. 59–64, 1995.

[115]. M.G.Villalva, J.R.Gazoli, and E.R.Filho, "Comprehensive approach to modeling and simulation of photovoltaic arrays," IEEE Trans. Power Electron., vol. 24, no. 5, pp. 1198-1208, May 2009.

[116]. Kish, G., Lee, J., Lehn, P. "Modelling and control of photovoltaic panels utilising the incremental conductance method for maximum power point tracking", IET Renew. Power Gener. 2012, 6(4), pp. 259-266.

[117]. S.Saravanan, and N.Ramesh Babu, "Performance Analysis of Boost and Cuk Converter in MPPT based PV System," IEEE Int. Conf. on Circuit, Power and Computer Technology (ICCPCT), 2015.

[118]. Abdel-Gawad H, Sood VK (2014), "Small-signal analyses of boost converter, including parasitics operating in CCM", 6th IEEE power India international conference (PIICON), pp 1–6.

[119]. Prasanna & Rathore, Akshay, "Two loop average current control implementation using cypress PSoC with closed loop experimental results", IEEE Energy Conversion Congress and Exposition, ECCE, pp. 1-6, 2013.

[120]. F. Delfino, R. Procopio1 M. Rossi and G. Ronda, Integration of large-size photovoltaic systems into the distribution grids: a P–Q chart approach to assess reactive support capability, IET Renewable Power Generation, Sept 2010, Vol. 4, Issue 4, pp. 329–340.

[121]. Athula D. Rajapakse and DharshanaMuthumuni, Simulation Tools for Photovoltaic System GridIntegration Studies, IEEE Electrical Power & Energy Conf., Oct 2009, pp. 1-5.

[122]. Chijioke Joe-Uzuegbu and Gloria Chukwudebe, “High Voltage Direct Current (HVDC) Technology: An Alternative Means Of Power Transmission”, 3rd IEEE International Conference on Adaptive Science and Technology, Nov 2011, pp. 1-5.

[123]. Nikolas Flourentzou, Vassilios G. Agelidis and Georgios D. Demetriades, “VSC-Based HVDC Power Transmission Systems: An Overview”, IEEE Transactions on Power Electronics, March 2009, Vol. 24, No. 3, pp. 121–125.

[124]. MihaelaAlbu, Elias Kyriakides, Gianfranco Chiccoa, MihailPopa, and Alexandru Nechi, “Online Monitoring of the Power Transfer in a DC Test Grid”, IEEE Transactions On Instrumentation And Measurement, May 2010, Vol. 59, No. 5, pp. 360- 390.

[125]. M. Chinchilla, S. Arnaltes, and J. C. Burgos, “Control of permanent magnet generators applied to variable-speed wind-energy systems connected to the grid,” IEEE Trans. Energy Convers., vol. 21, no. 1, pp.130–135, Mar. 2006.

[126]. H. Li and Z. Chen, "Overview of different wind generator systems and their comparisons," Renewable Power Generation, IET, vol. 2, pp. 123-138, 2008.

[127]. V. C. Ganti, B. Singh, S. K. T. C. Aggarwal, “ DFIG Based Wind Power Conversion With Grid Power Leveling for Reduced Gusts,” IEEE Transactionon Sustainable Energy, vol. 3, no.1, pp.12-20, Jan. 2012.

[128]. H. Nian and Y. Song, “Direct Power Control of Doubly Fed Induction Generator Under Distorted Grid Voltage,” IEEE Transactions on Power Electronics, vol.29, no. 2, pp. 894-905, Feb. 2014.

[129]. C. N. Bhende, S. Mishra and S. G. Malla, “Permanent Magnet Synchronous Generator Based Standalone Wind Energy Supply System”, IEEE Transaction on Sustainable Energy, vol.2, no.4, pp. 361-373, 2011.

[130]. S. M. Deghan, M. Mohamadian and A. Y. Varjani, “A New Variable-Speed Wind Energy Conversion System Using Permanent-Magnet Synchronous Generator and Z-Source Inverter”, IEEE Transactions On Energy Conversion, vol. 24, no. 3, pp. 714-724, Sept. 2009.

[131]. S. Morimoto, H. Nakayama, M. Sanada, and Y. Takeda, “Sensorless Output Maximization Control for Variable-Speed Wind Generation System Using IPMSG”, IEEE Transaction on Industry Applications, vol. 41, no 1, pp. 60-67, Jan./Feb. 2005.

[132]. Ming Yin, Gengyin Li, Ming Zhou, Chengyong Zhao, “Modeling of the Wind turbine with a Permanent Magnet Synchronous Generator for Integration”, vol.1 2007,pp.4244-1298.

[133]. A. Miller, E. Muljadi, and D. Zinger, “A Variable Speed Wind Turbine Power Control”, IEEE Trans. on Energy Conversion, Vol. 12, No. 2, June 1997, pp. 181-186.

[134]. S. Zhang, K. J. Tseng, D. M. Vilathgamuwa, T. D. Nguyen, and X. Y. Wang, “Design of a Robust Grid Interface System for PMSG-Based Wind Turbine Generators,” IEEE Transaction on Industrial Electronics, vol. 58, no. 1, pp. 316-328, Jan. 2011.

[135]. Junfei Chen, Hongbin Wu, Ming Sun, Weinan Jiang, Liang Cai, and CaiyunGuo, ”Modeling and Simulation of Directly Driven Wind Turbine with Permanent Magnet Synchronous Generator”, in IEEE PES ISGT ASIA 2012.

[136]. Binder A., Schneider T., “Permanent magnet synchronous generators for regenerative energy conversion – a survey”, European Conference on Power Electronics and Applications, EPE 2005, 11-14 September, Dresden, Germany, 2005.

[137]. Chih-Ming Hong, Chiung-Hsing Chen, ChiaSheng Tu. "Maximum power point tracking based control algorithm for PMSG wind generation system without mechanical sensors", Energy Conversion and Management, 2013.

[138]. A. Causebrook, et al., "Fault Ride-Through of Large Wind Farms Using Series Dynamic Braking Resistors (March 2007)," Power Systems, IEEE Transactions on, vol. 22, pp. 966-975, 2007.

[139]. Christoph Nentwig et al.," Application of DC choppers in HVDC grids", in Proceedings of 2016 IEEE International Energy Conference (ENERGYCON), pp. 1-5, 2016.

[140]. Z. C. Zou, X. Y. Chen, C. S. Li, X. Y. Xiao, Y. Zhang, "Conceptual design and evaluation of a resistive-type SFCL for efficient fault ride through in a DFIG", *IEEE Trans. Appl. Supercond.*, vol. 26, no. 1, Jan. 2016.

[141]. Maoze Wang, Wei Xu, Jia Hongjie and Xinghuo Yu, "A new control system to strengthen the LVRT capacity of DFIG based on both crowbar and DC chopper circuits," *IEEE PES Innovative Smart Grid Technologies*, Tianjin, 2012, pp. 1-6

[142]. D. H. Nguyen and M. Negnevitsky, "A review of fault ride through strategies for different wind turbine systems," presented at the Universities Power Engineering Conference (AUPEC), 2010 20th Australasian 2010.

[143]. T. H. Nguyen and D. Lee, "Advanced Fault Ride-Through Technique for PMSG Wind Turbine Systems Using Line-Side Converter as STATCOM," in *IEEE Transactions on Industrial Electronics*, vol. 60, no. 7, pp. 2842-2850, July 2013.

[144]. A. Jalilian, S. B. Naderi, M. Negnevitsky, M. Tarafdar Hagh and K. M. Muttaqi, "Controllable DC-link fault current limiter augmentation with DC chopper to improve fault ride-through of DFIG," in *IET Renewable Power Generation*, vol. 11, no. 2, pp. 313-324, 8 2 2017.

Publications

Journals:

[1]. **Hari Priya, T**, Alivelu M. Parimi, "Hybrid Controller Topology for Large Solar PV Installations in High Voltage DC grid Connected Applications", Electrical Engineering Journal (Springer), vol. 100, pp. 2537–2552, 2018. (IF. 1.269)

[2]. **Hari Priya, T**, Alivelu M. Parimi, "Performance Analyses of PMSG based WECS using Hybrid Controller in DC Grid Connected Applications", International Journal of pure and Applied Mathematics, March 2018, vol.118, issue. 16, pages 903-912. (Scopus indexed).

[3]. **Hari Priya, T,** Alivelu M. Parimi, "Hybrid Control Scheme for DC grid Connected PV and Wind System with FRT Protection" (under review with EPCS, Taylor and Francis).

[4]. **Hari Priya, T**, Alivelu M. Parimi, "A Novel HVDC Topology for Integrating Large Solar and Wind Installations to High Voltage DC grid ". (under review in Ain Shams Engineering Journal, Elsevier).

Book Chapter:

[1]. **Hari Priya, T,** Alivelu M. Parimi, "Energy Management System for PV - Wind and Battery fed DC Micro Grid using Fuzzy based Proportional Integral Controller", Presented in **MARC 2018** (will be published in SPRINGER Book Chapter).

Conferences:

[1]. **Haripriya, T,** Parimi, A.M. , Rao, U.M., "Modeling of DC-DC boost converter using fuzzy logic controller for solar energy system applications" **IEEE** Asia Pacific

Conference on Postgraduate Research in Microelectronics and Electronics (PrimeAsia), pp: 147- 152, 2013.

[2]. **Hari Priya, T,** Alivelu M. Parimi , Rao, U.M, "Performance Evaluation of DC Grid Connected Solar PV System for Hybrid Control of DC-DC Boost Converter", **IEEE** 10th International Conference on Intelligent Systems and Control , Jan 2016 .

[3]. **Hari Priya, T,** Alivelu M. Parimi , Rao, U.M,"Performance Evaluation of High Voltage Gain Boost Converters for DC Grid Integration", **IEEE** International Conference on Circuit, Power and Computing Technologies, March 2016 .

[4]. **Hari Priya, T,** Alivelu M. Parimi , Rao, U.M, "Development of a Hybrid Controller for Photovoltaic Based DC-DC Boost Converter in DC Grid Connected Applications", **IEEE** International Conference on Circuit, Power and Computing Technologies, March 2016 .

[5]. **Hari Priya, T,** Alivelu M. Parimi , "Design of Adaptive Perturb and Observe –Fuzzy MPPT Controller for High Voltage Gain Multi Level Boost Converter", **IEEE** 7th Power India International Conference , Nov. 2016.

[6]. **Hari Priya, T**, Alivelu M. Parimi, "Performance Analyses of PMSG based WECS using Hybrid Controller in DC Grid Connected Applications", International Conference on Power, Circuit and Information Technologies, ICPCIT Conference Proceedings 2017.

Biography

Candidate Biography

Hari Priya T received her B.Tech degree in Electrical and Electronics Engineering from Sri Venkateswara University, India in 2008 and M.Tech degree with specialization in Power Systems in Electrical Engineering from IIT Roorkee, India in 2010. At present she is pursuing her PhD from BITS Pilani, Hyderabad Campus under the guidance of Prof. Alivelu M. Parimi. She is a student member of IEEE and IEI(India). Her current research interests include grid integrated issues of renewable energy systems, Design of controllers for MPPT and voltage regulation.

Supervisor Biography

Alivelu M. Parimi received M.E. with specialization in Control Systems in Electrical Engineering from Andhra University, Visakhapatnam, Andhra Pradesh, India in 2004. She received Ph.D. in Electrical and Electronics Engineering from, Universiti Teknologi Petronas, Tronoh, Perak, Malaysia in 2011. Currently, she is working as an Associate Professor in Department of Electrical Engineering in BITS Pilani Hyderabad Campus, Hyderabad. Her Research Interest is Application of FACTS devices to improve Power System Stability and Power Quality.